SYSTEM RELIABILITY-BASED DESIGN AND MULTIRESOLUTION TOPOLOGY OPTIMIZATION

BY

TAM HONG NGUYEN

DISSERTATION

Submitted in partial fulfillment of the requirements
for the degree of Doctor of Philosophy in Civil Engineering
in the Graduate College of the
University of Illinois at Urbana-Champaign, 2010

Urbana, Illinois

Doctoral Committee:

Professor Glaucio H. Paulino, Chair, Director of Research
Assistant Professor Junho Song, Director of Research
Professor Jerome F. Hajjar
Associate Professor C. Armando Duarte
Associate Professor Ravi C. Penmetsa, Wright State University
Alok Sutradhar, Ph.D, Ohio State University
Mr. William F. Baker, Skidmore, Owings & Merrill LLP (SOM)
Alessandro Beghini, Ph.D, Skidmore, Owings & Merrill LLP (SOM)

ABSTRACT

Structural optimization methods have been developed and applied to a variety of engineering practices. This study aims to overcome technical challenges in applying design and topology optimization techniques to large-scale structural systems with uncertainties. The specific goals of this dissertation are: (1) to develop an efficient scheme for topology optimization; (2) to introduce an efficient and accurate system reliability-based design optimization (SRBDO) procedure; and (3) to investigate the reliability-based topology optimization (RBTO) problem. First, it is noted that the material distribution method often requires a large number of design variables, especially in three-dimensional applications, which makes topology optimization computationally expensive. A multiresolution topology optimization (MTOP) scheme is thus developed to obtain high-resolution optimal topologies with relatively low computational cost by introducing distinct resolution levels to displacement, density and design variable fields: the finite element analysis is performed on a relatively coarse mesh; the optimization is performed on a moderately fine mesh for design variables; and the density is defined on a relatively fine mesh for material distribution. Second, it is challenging to deal with system events in reliability-based design optimization (RBDO) due to the complexity of system reliability analysis. A new single-loop system RBDO approach is developed by using the matrix-based system reliability (MSR) method. The SRBDO/MSR approach utilizes matrix calculations to evaluate the system failure probability and its parameter sensitivities accurately and efficiently. The approach is applicable to general system events consisting of statistically dependent component events. Third, existing RBDO approaches employing first-order reliability method (FORM) can induce significant error for highly nonlinear problems. To enhance the accuracy of component and system RBDO approaches, algorithms based on the second-order reliability method (SORM), termed as SORM-based RBDO, are proposed. These technical advances enable us to perform RBTO of large-scale structures efficiently. The proposed algorithms and approaches are tested and demonstrated by various numerical examples. The efficient and accurate approaches developed for design and topology optimization can be applied to large-scale problems in engineering design practices.

To my family

ACKNOWLEDGEMENTS

I take this opportunity to express my profound gratitude to my advisors, Professor Glaucio H. Paulino and Professor Junho Song. It is through their patience, warm encouragement, constant support, and guidance that this work can finally be accomplished. Their dedication to research, rich knowledge, high standard and great enthusiasm have been the source of motivation during my study.

I am grateful to Professor Jerome F. Hajjar, Professor C. Amando Duarte, Professor Ravi C. Penmetsa, Doctor Alok Sutradhar, Mr. William F. Baker, and Doctor Alessandro Beghini who kindly served in my dissertation committee and provided insightful suggestions and feedbacks.

I would also like to thank all my colleagues in Professor Paulino's Computational Mechanics Group and Professor Junho Song's Structural System Reliability Group. I would like to thank, especially, Chau Le, Seong-Hyeok Song, Young Joo Lee, Arun L. Gain, Won Hee Kang, Tomas Zegard, Kyoungsoo Park**,** Cameron Talischi, Hyun-woo Lim, Derya Deniz, Daniel Spring, Huiming Yin, Rodrigo Espinha, Eshan V. Dave, Bin Shen, Nolan Kurtz, Zhengyu Zhang, Sofie Leon, Lauren Stromberg, Ying Yu, and Daiane Brisotto.

I gratefully acknowledge the financial support from the Vietnam Education Foundation through the VEF fellowship. I also gratefully acknowledge the partial financial support from the National Science Foundation.

I would like to show my deepest gratefulness to my parents, Hoan Nguyen and Hong Dinh, my brother, Phuc Nguyen, my sister, Nguyet Nguyen, my niece, Minh Nguyen, and my nephew, Quang Nguyen for their love and support throughout my life. Finally, I would like to thank my lovely wife, Tram Dang, I owe the most for her endless love, understanding, support and encouragement.

TABLE OF CONTENTS

LIST OF TABLES

LIST OF FIGURES

CHAPTER 1 – INTRODUCTION

Structural design optimization is often performed in a deterministic manner, despite the existence of various uncertainties such as loads and material properties. The response of optimal designs can be fairly sensitive to these uncertainties, which may lead to failures of structures. Reliability-based design optimization (RBDO) approach has been developed to account for the uncertainties in the design process through stochastic simulation and probability analysis that are integrated with design iterations. The goal of the RBDO approach is to design the structures with safety criteria governed by extreme events; therefore, the obtained designs are better than the designs by conventional deterministic design optimization. The safety criteria can be defined as component or system events. While a significant amount of work has been done on RBDO with component events, little attention has been paid to RBDO with system events because of challenges in system reliability analyses.

This thesis investigates system reliability-based optimization and high-resolution topology optimization problems. These problems have not been well addressed in the literature yet despite their importance in practice of optimal design. In order to apply reliability-based design and topology optimization approaches to real engineering practices, the algorithms need to be improved in both accuracy and efficiency. This chapter first provides brief background information on topology optimization and reliability-based design optimization along with the limitations of existing approaches. Next, the objectives of the research and thesis organization are presented.

1.1 TOPOLOGY OPTIMIZATION

Topology optimization is a relatively new structural optimization approach that seeks for the optimal distribution of material in a specific domain under given design constraints. Different

from classical structural optimization methods, topology optimization finds the "layout" of structures that includes the information of optimal topology, shape and size of the structure (Bendsøe and Sigmund, 2003). Figure 1.1 illustrates the concepts of classical size and shape optimization in comparison to that of topology optimization approach. In a size optimization problem, the optimal thickness or section areas (sizes) of members are determined (Figure 1.1a). In a shape optimization problem, the optimal shapes of the pre-determined domains are determined (Figure 1.1b). By contrast, in a topology optimization problem (Figure 1.1c) of solid structures, the physical size, shape and connectivity are all to be determined optimally. These parameters are often expressed through the pixels/voxels of material in the domain. Therefore, a large number of material points in the domain are often employed to achieve well-defined optimal topology.

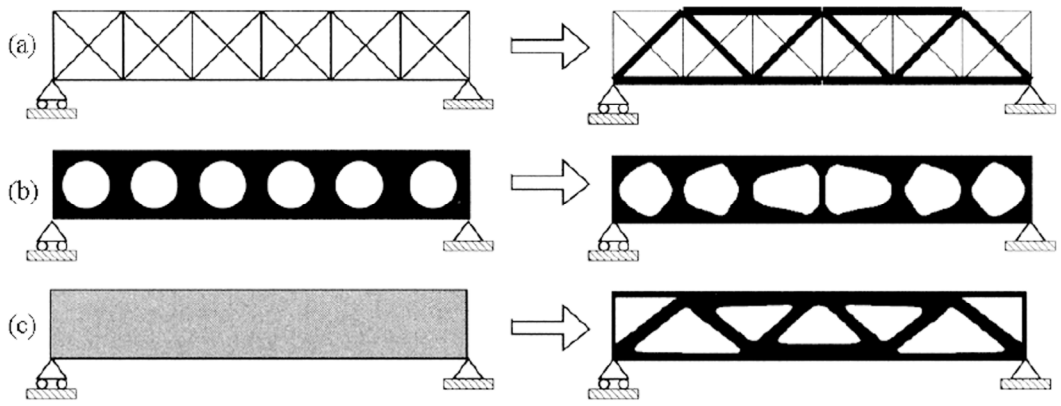

Figure 1.1: Structural optimization: (a) size optimization; (b) shape optimization; and (c) topology optimization (Bendsøe and Sigmund, 2003).

It is desirable to identify optimal distribution of solid or void regions in the given domain through topology optimization. However, it is often computationally intractable to solve such an integer optimization problem. Therefore, the material density is usually relaxed to have intermediate density between zero and full density of the material such that the objective function and the constraints become continuous and differentiable. There have been several approaches for solving topology optimization problems. In the earlier works, the homogenization method (Bendsøe and Kikuchi, 1988) used microstructures to derive the intermediate stiffness tensors. Later, an alternative approach so-called "power-law" or SIMP (Solid Isotropic Material

with Penalization) model was proposed (Bendsøe, 1989; Zhou and Rozvany, 1991; Rozvany et al., 1992; Mlejnek and Schirrmacher, 1993; Bendsøe and Sigmund, 1999). The SIMP model was criticized because of the artificial power material properties (Rozvany, 2009). However, it was later proved that the microstructures corresponding to the stiffness obtained from the SIMP model do exist as long as the penalization parameter is sufficiently large (Bendsøe and Sigmund, 1999).

Topology optimization has been applied to various engineering problems. For instance, the wing box ribs of the Airbus A380 was designed using topology optimization, which resulted in a significant weight reduction (Krog et al., 2004). In practical applications of the approach, a fine mesh is often employed in finite element simulations to obtain a well-defined design, which often makes the optimization computationally expensive or intractable. This study aims to develop an approach to obtain high-resolution optimal topology with affordable computational cost by introducing distinct levels of resolution to displacement, density and design variable fields (Chapters 2 and 3). The efficient topology optimization approach developed in this study can promote high-resolution topology optimization in various problems including biomedical problems, e.g. optimal design of craniofacial segmental bone replacements (Sutradhar et al., 2010).

1.2 RELIABILITY-BASED DESIGN OPTIMIZATION

Most of the existing design optimization studies are deterministic in nature despite various uncertainties in material properties, loads and boundary conditions, and their significant impacts on the optimal design. These studies are referred to as deterministic design optimization (DDO) in this study. Ignoring these uncertainties might result in structural designs that fail to meet important specifications or constraints. Therefore, it is critical to ensure that the optimal design has a required level of reliability through systematic treatment of uncertainties during the design optimization process. In order to address this pressing need, various reliability-based design optimization (RBDO) methods have been developed and used as powerful tools for reliable and cost-effective design, for example, see a review by Fragonpol and Maute (2005). RBDO approaches take into account the uncertainties in the design process through stochastic

simulation and probability analysis. Figure 1.2 illustrates a design optimization problem with two constraints. While the optimal design by DDO (corresponding to point A) has a significant likelihood of violating design constraints, RBDO (corresponding to point B) achieves an optimal design with the failure probability lower than the target level.

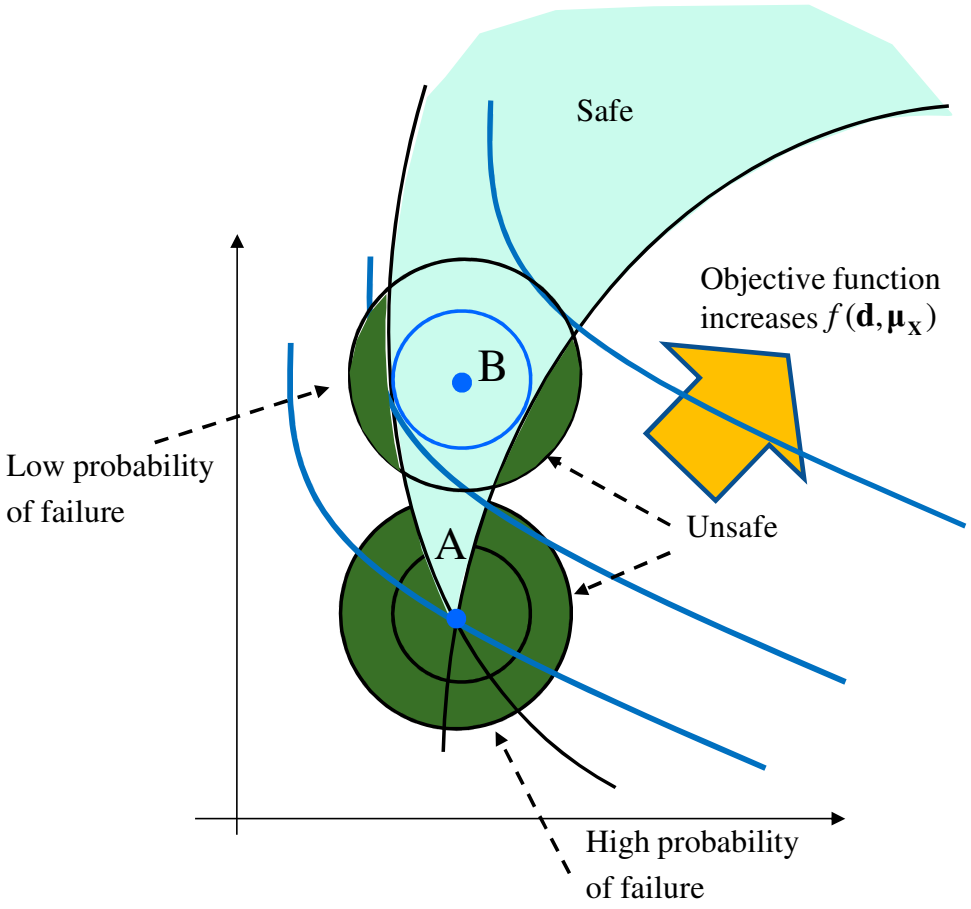

Figure 1.2: Structural optimization with uncertainty.

RBDO is a time-consuming procedure because numerical simulation of structural systems and reliability analysis are required at each step of design iterations. RBDO is particularly time-consuming and complex when the design constraint is defined as a "system" event of multiple constraints, which is termed as system reliability-based design optimization (SRBDO) problem. As an example of SRBDO, consider optimization of a structure with a high level of redundancy. The system level failure, e.g., the structural collapse is described by a complex system event

consisting of several different component failure events. However, SRBDO has received little attention in the literature compared to RBDO dealing with individual component failure events (Aoues and Chateauneuf, 2008; Valdebenito and Schuëller, 2010) in spite of significant challenges in SRBDO applications. The main challenge is the difficulty in computing system probability and its parameter sensitivities when component events are statistically dependent or the system failure event is not series or parallel system event. Recently, Song and Kang (2009) developed a matrix-based system reliability (MSR) method that computes the system failure probability and its parameter sensitivities by convenient matrix-based calculations. The MSR method is applicable to general system events including series, parallel, cut-set and link-set systems with statistical dependence between component events considered, and provides parameter sensitivities of the system failure probability, which facilitates gradient-based optimization in RBDO. In this thesis, the MSR method is used for system reliability-based optimization of structural design (Chapter 4) and topology (Chapter 5) to advance the theory and applications of system reliability-based design/topology optimization.

1.3 RESEARCH OBJECTIVES AND THESIS ORGANIZATION

The main objective of this study is to develop efficient and accurate algorithms for component and system reliability-based design and topology optimization. First, a multiresolution topology optimization approach is developed to achieve high-resolution topology optimization for large-scale problems efficiently. Second, an accurate and efficient algorithm for system reliability-based design optimization (SRBDO) is introduced. Third, the SRBDO algorithm is applied to topology optimization problem, termed as system reliability-based topology optimization (SRBTO). Topology optimization is inherently complex and time-consuming, which thus requires further improvement of SRBTO algorithms.

The thesis is organized as follows. Chapter 2 presents the multiresolution topology optimization (MTOP) approach developed to obtain high-resolution designs with relatively low computational cost in comparison to the conventional approach. The efficiency of the approach is demonstrated by solving relatively large-scale problems with a standard PC. In Chapter 3, the efficiency of the MTOP approach is further improved by using three different levels of

discretization for displacement, design and density fields. An adaptive multiresolution topology optimization scheme is also introduced in Chapter 3. Chapter 4 presents the system reliability-based design optimization algorithm using matrix-based system reliability method (SRBDO/MSR). The accuracy and efficiency of the SRBDO/MSR algorithm are demonstrated by numerical examples in the literature and by comparison with the results of Monte Carlo simulations. In Chapter 5, the component and system reliability-based *topology* optimization (CRBTO/SRBTO) problems are investigated. The accuracy and efficiency of the CRBTO and SRBTO are enhanced by using the proposed MTOP approach (Chapter 2) and RBDO algorithms that use the second-order reliability method. Finally, Chapter 6 summarizes the outcomes of the research and provides suggestions for future work.

CHAPTER 2 – MULTIRESOLUTION TOPOLOGY OPTIMIZATION

This chapter presents a multiresolution topology optimization (MTOP) scheme to obtain high-resolution optimal topology with relatively low computational cost. The scheme employs a coarser discretization for finite elements and a finer discretization for both density elements and design variables. The proposed approach is demonstrated via various two- and three-dimensional numerical examples.

2.1 INTRODUCTION

Topology optimization using the material distribution method has been well developed and applied to a variety of structural systems such as civil, mechanical and material systems (Bendsøe and Kikuchi, 1988; Bendsøe, 1989; Rozvany, 2001). The method rasterizes the domain by defining the topology via the density of pixels/voxels, and thus a large number of design variables are usually required for a well-defined design, especially in three-dimensional (3D) applications. Several studies have been devoted to developing efficient procedures to solve large-scale topology optimization problems using the material distribution method. Most of the efforts focus on the finite element analysis because the structural analysis constitutes the dominant computational cost in topology optimization. For example, Borrvall and Petersson (2001) solved 3D realistic topology optimization designs with several hundreds of thousands of finite elements using parallel computing with domain decomposition. Wang et al. (2007) introduced fast iterative solvers to reduce the computational costs associated with the finite element analysis of 3D topology optimization problems. Amir et al. (2009) proposed an approximate reanalysis procedure for the topology optimization of continuum structures. In this procedure, the finite element analysis is performed at an interval of several iterations only and approximate reanalysis is performed for other iterations to determine the displacement. The authors showed that this

rough approximation is acceptable in topology optimization. Another approach consists of using adaptive mesh refinement (AMR) to reduce the number of finite elements (Stainko, 2006; de Sturler et al., 2008). de Sturler et al. (2008) tailored the AMR method to represent void regions with fewer (coarser) elements and solid regions, especially in material surface regions, with more (finer) elements. In a topology optimization problem, where shape, size and position of the void and solid regions are unknown, the AMR method allows the finite element mesh to be refined during the optimization process.

The abovementioned studies mainly focus on reducing computational cost of structural analyses to obtain high-resolution design for large-scale problems. However, it is noted that improved resolution can be achieved by changes in mesh representations as well. Consider the existing element-based and nodal-based approaches that can be interpreted by use of a design variable mesh and a displacement mesh. In the element-based approach, the uniform density of each displacement element is considered as a design variable. By contrast, the nodal-based approach (Guest et al., 2004; Matsui and Terada, 2004; Rahmatalla and Swan, 2004) considers the densities at nodes as the design variables. The element densities are then obtained from nodal values using projection. Because the projection scheme provides control over the local gradient of material density, it imposes a minimum length scale feature and alleviates the checkerboard issue. Recently, Paulino and Le (2009) proposed to locate nodal design variables at the midpoints of the four edges of the quadrilateral elements in order to obtain higher resolution. The authors showed that these locations of the design variables result in a higher resolution topology design without increasing mesh refinement. de Ruiter and van Keulen (2004) also introduced an idea of decoupling of topology definition and the finite element mesh by using topology definition function. Wavelets were also used to obtain high-resolution optimal topology (Kim and Yoon, 2000; Poulsen, 2002a).

In this thesis, a multiresolution topology optimization (MTOP) approach is proposed to achieve high-resolution optimal topologies for large-scale problems with relatively low computational costs. This approach uses meshes with different levels of resolutions for the three fields: finite elements, density elements, and design variables to improve the efficiency. As the first step of the development, in this chapter, the same mesh is used for density elements and

design variables while the structural analysis uses a coarser finite element mesh. This is to reduce the dominant computational cost of the structural analysis, which would increase unnecessarily in a traditional approach that uses fine meshes for all three fields for high-resolution topology. Since topology is defined on the fine density element mesh, a high-resolution design is obtained despite the relatively coarse finite element mesh. In the next chapter, the MTOP approach is fully extended by using distinct meshes for all three fields.

This chapter is structured as follows: Section 2.2 provides an overview of the topology optimization formulation; Section 2.3 describes the concept and implementation of the proposed MTOP approach; Section 2.4 presents two-dimensional (2D) numerical examples, which explore conceptual aspects of the proposed approach; Section 2.5 shows 3D numerical examples, which illustrate the MTOP solution of relatively large-scale problems; and Section 2.6 provides concluding remarks.

2.2 TOPOLOGY OPTIMIZATION FORMULATION

This section reviews formulations of general topology optimization problems. The section also discusses the integration procedure of the stiffness matrix for the element-based approach, and one of the nodal-based approaches, Continuous Approximation of Material Distribution (CAMD) approach (Matsui and Terada, 2004).

2.2.1 Problem statement and formulations

For continuum structures, topology optimization aims to optimize the distribution of the material densities in a specific domain. This study considers "minimum compliance" problems in which the stiffness of the structure is maximized while satisfying a constraint given on the total volume. For a reference domain Ω in $\Re^2$ or $\Re^3$, consider the stiffness tensor $E_{ijkl}(\boldsymbol{\psi})$ defined at the position vector $\boldsymbol{\psi}$ defined over the domain. Let U denote the space of kinematically admissible displacement fields, $\mathbf{f}$ the body forces, and $\mathbf{t}$ the tractions. The equilibrium equation is then written in the weak (or variational) form (Bendsøe and Sigmund, 2003). The energy bilinear form is then determined as $a(\mathbf{u},\mathbf{v}) = \int_\Omega E_{ijkl}(\boldsymbol{\psi})\varepsilon_{ij}(\mathbf{u})\varepsilon_{kl}(\mathbf{v})d\Omega$ where the linearized strains are

determined as $\varepsilon_{ij}(\mathbf{u}) = 0.5\left(\partial u_i / \partial \psi_j + \partial u_j / \partial \psi_i\right)$. The load linear form is given by $L(\mathbf{u}) = \int_\Omega \mathbf{f}\mathbf{u} d\Omega + \int_{\Gamma_T} \mathbf{t}\mathbf{u} ds$. The basic minimum compliance problem is then expressed as

$$\begin{aligned} &\min \quad L(\mathbf{u}) \\ &s.t.: \quad a(\mathbf{u},\mathbf{v}) = L(\mathbf{v}), \text{ for all } \mathbf{v} \in U \\ &\qquad \text{volume constraint} \end{aligned} \tag{2.1}$$

Using the finite element method, the problem statement in (2.1) is discretized as follows:

$$\begin{aligned} &\min_{\rho} \quad C(\rho, \mathbf{u}_d) = \mathbf{f}^{\mathrm{T}} \mathbf{u}_d \\ &s.t.: \quad \mathbf{K}(\rho)\mathbf{u}_d = \mathbf{f} \\ &\qquad V(\rho) = \int_\Omega \rho(\boldsymbol{\psi}) dV \le V_s \end{aligned} \tag{2.2}$$

where $\rho = \rho(\boldsymbol{\psi})$ is the density at position $\boldsymbol{\psi}$, $\mathbf{f}$ and $\mathbf{u}_d$ are the global load and displacement vectors, respectively, $\mathbf{K}$ is the global stiffness matrix, C is the compliance, and V_s is the prescribed volume constraint. The optimal solution specifies whether the density at any point in the domain should be either 0 (void) or 1 (solid). However, it is impractical or computationally intractable to solve such an integer optimization problem. Therefore, in a relaxed approach, the density variables are allowed to have any value between 0 and 1. For example, in a popular approach termed as Solid Isotropic Material with Penalization (SIMP) (Bendsøe, 1989; Rozvany et al., 1992; Bendsøe and Sigmund, 1999), Young's modulus is parameterized using solid material density as follows.

$$E(\boldsymbol{\psi}) = \rho(\boldsymbol{\psi})^p E^0 \tag{2.3}$$

where E^0 is Young's modulus of the material in the solid phase, corresponding to the density $\rho = 1$, and p is the penalization parameter. To prevent singularity of the stiffness matrix, a small positive lower bound, e.g. $\rho_{\min} = 10^{-3}$, is placed on the density. Using the penalization parameter $p > 1$, the intermediate density approaches either 0 (void) or 1(solid).

$$0 < \rho_{\min} \le \rho(\boldsymbol{\psi}) \le 1 \tag{2.4}$$

In the element-based approach, the density of each element is represented by one value ρ_e and the global stiffness matrix $\mathbf{K}$ in Equation (2.2) is expressed as

$$\mathbf{K} = \sum_{e=1}^{N_{el}} \mathbf{K}_e(\rho_e) = \sum_{e=1}^{N_{el}} \int_{\Omega_e} \mathbf{B}^{\mathrm{T}} \mathbf{D}(\rho_e) \mathbf{B} d\Omega \tag{2.5}$$

where $\mathbf{K}_e(\rho_e)$ is the stiffness matrix of the element *e*, **B** is the strain-displacement matrix of shape function derivatives, and $\mathbf{D}(\rho_e)$ is the constitutive matrix which depends on the material density. For example, the formulation of the constitutive matrix for plane stress state is

$$\mathbf{D}(\rho_e) = \frac{E(\rho_e)}{1-\nu^2} \begin{bmatrix} 1 & \nu & 0 \\ \nu & 1 & 0 \\ 0 & 0 & (1-\nu)/2 \end{bmatrix} \tag{2.6}$$

The solution of the gradient-based optimization problem in Equation (2.2) requires the computation of the sensitivities of the objective function and the constraint. In the element-based approach, element density ρ_e is used as the design variable; therefore, these sensitivities can be obtained as follows.

$$\begin{aligned} \frac{\partial C}{\partial \rho_e} &= -\mathbf{u}_e^{\mathrm{T}} \frac{\partial \mathbf{K}_e}{\partial \rho_e} \mathbf{u}_e = -p\rho_e^{p-1} \mathbf{u}_e^{\mathrm{T}} \mathbf{K}_e^0 \mathbf{u}_e \\ \frac{\partial V}{\partial \rho_e} &= \int_{\Omega_e} dV \end{aligned} \tag{2.7}$$

where $\mathbf{K}_e^0$ is the element stiffness matrix of the solid material.

2.2.2 Integration of the stiffness matrix

The stiffness matrix of each element in Equation (2.5) is computed by integrating the stiffness integrand contribution over the displacement element domain. Numerical quadrature, such as Gaussian quadrature, is commonly used to reduce the integration to the summation of the stiffness integrand at specific Gauss points (Cook et al., 2002). The material density is also evaluated at the Gauss points during computation of the material property matrices.

In the element-based approach, the element density is represented by one design variable at the centroid of the element and the material densities of all the Gauss points are equal to the element density. By contrast, in the CAMD approach (Matsui and Terada, 2004), the material densities at the Gauss points are computed from the nodal design variables and the stiffness matrices are evaluated at the Gauss points, i.e.

$$\mathbf{K}_e = \int_{\Omega_e} \left(\sum_{i=1}^{N_{nod}} N_i(\boldsymbol{\psi}) \rho_i \right)^p \mathbf{B}^{\mathrm{T}} \mathbf{D}^0 \mathbf{B} \, d\Omega = \sum_{g=1}^{N_n} \left(\sum_{i=1}^{N_{nod}} N_i(\boldsymbol{\psi}) \rho_i \right)^p \mathbf{K}_g^0 \tag{2.8}$$

where N_{nod} is the number of nodes per element (e.g., $N_{nod} = 4$ for Q4 and $N_{nod} = 8$ for B8 element), N_n is the number of Gauss points for integration, $N_i(.)$ is the *i*-th shape function, $i = 1,..,N_{nod}$, $\mathbf{K}_g^0$ is the stiffness integrand at the Gauss point *g*, and $\mathbf{D}^0$ corresponds to the constitutive matrix of the solid material.

2.3 MULTIRESOLUTION SCHEME IN TOPOLOGY OPTIMIZATION

In this study, elements associated with the displacement mesh are called *finite elements* (or *displacement elements*) and elements associated with the density mesh are called *density elements*. In light of the present work, existing element-based and nodal-based approaches can be interpreted with a design variable mesh and a displacement mesh. For example, in the element-based approach using Q4 elements, a uniform density of each displacement element is considered a design variable, which is termed as a Q4/U element. Figure 2.1 shows the element-based approach using Q4/U elements with the displacement mesh, the design variable mesh, and the superposed meshes. In this section, the concept and implementation of the MTOP approach will be discussed.

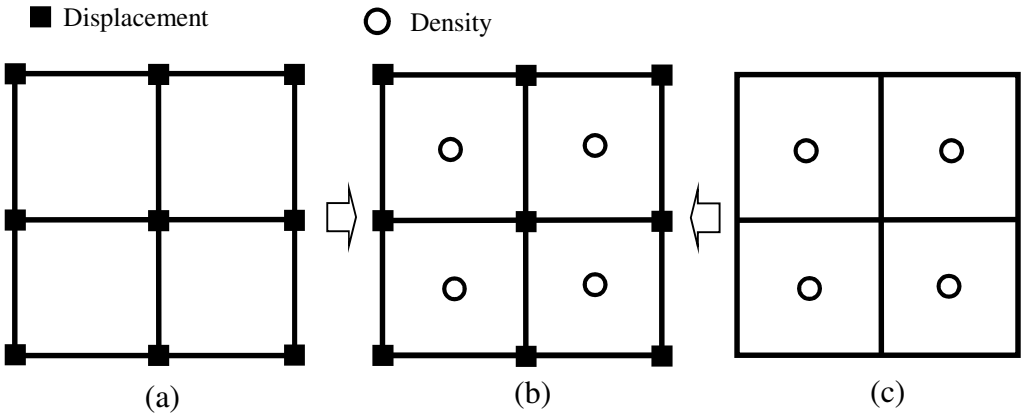

Figure 2.1: Q4/U elements: (a) displacement mesh; (b) superposed meshes; and (c) density mesh.

2.3.1 Multiresolution scheme and stiffness matrix integration

Three meshes with distinct levels of resolutions for the topology optimization problem are employed: the *displacement mesh* to perform the analysis, the *design variable mesh* to perform the optimization, and the *density mesh* to represent material distribution. For example, design variables may be defined as the material densities at the center of the density elements. However, the design variable mesh and density mesh do not need to coincide because design variables are variables used in the optimization and do not have physical meaning on their own. The design variable concept in this study is similar to the nodal design variable in the study by Guest et al. (2004). However, in their study, the design variables are associated with the nodes of the finite element mesh, while in the proposed MTOP scheme; the design variable mesh can be different from the finite element mesh. In the proposed scheme, the element densities are computed from the design variables density by projection function. The topology optimization problem definition in (2.2) is then rewritten accordingly:

$$\begin{aligned} \min_{\mathbf{d}} \quad & C(\rho, \mathbf{u}_d) = \mathbf{f}^{\mathrm{T}}\mathbf{u}_d \\ s.t.: \quad & \rho = f_p(\mathbf{d}) \\ & \mathbf{K}(\rho)\mathbf{u}_d = \mathbf{f} \\ & V(\rho) = \int_\Omega \rho dV \le V_s \end{aligned} \tag{2.9}$$

where $\mathbf{d}$ is the vector of design variables and $f_p(.)$ is the projection function.

To obtain high-resolution design, the MTOP approach employs a finer mesh for density distribution than the displacement field so that each displacement element consists of multiple density elements (sub-elements). Within each density element, the material density is assumed to be uniform. A new scheme is introduced to integrate the stiffness matrix, in which the displacement element consists of a number of different density elements. For example, Figure 2.2a shows a Q4 displacement element, Figure 2.2b presents the multiple meshes, and Figure 2.2c shows the density mesh with 25 density elements (also 25 design variables) per Q4 displacement. In the MTOP approach, this element is denoted as Q4/n25 where "n25" indicates that the number of density elements "n" per Q4 is 25. Figure 2.3 illustrates the spatial variation of the density inside a conventional element Q4/U and an MTOP element Q4/n25.

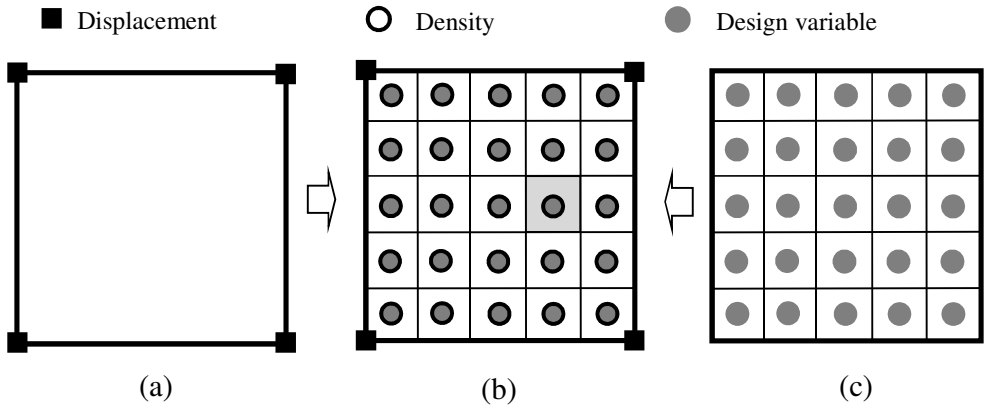

Figure 2.2: MTOP Q4/n25 element: (a) displacement mesh; (b) superposed meshes; and (c) design variable mesh.

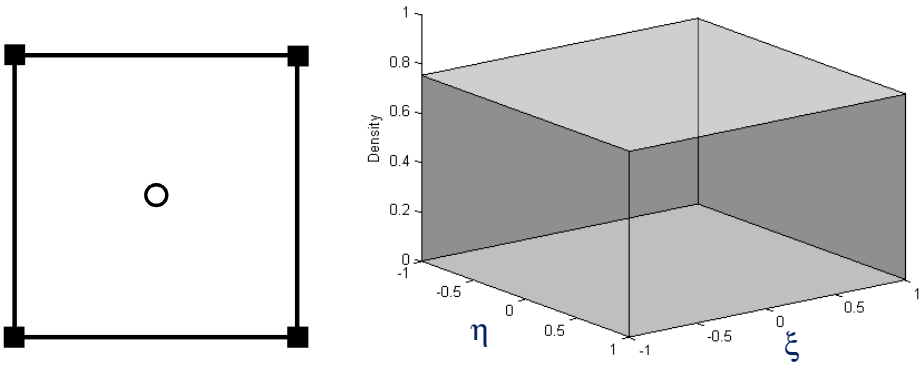

(a)

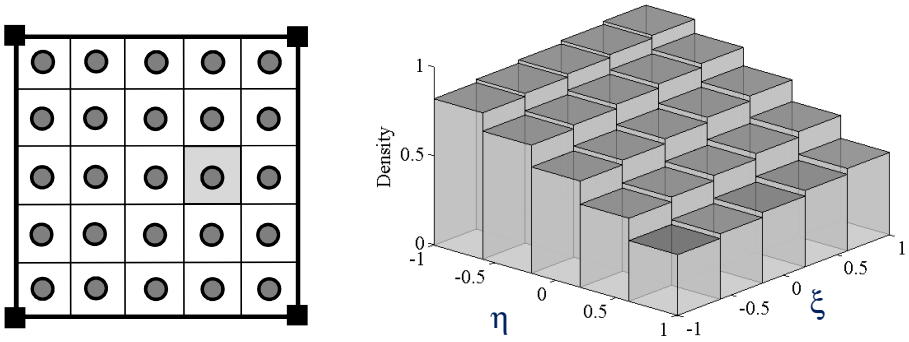

(b)

Figure 2.3: The spatial variation of the density inside a FE element: (a) Q4/U; and (b) MTOP Q4/n25.

The stiffness matrix of an MTOP element is computed by summing up the stiffness integrands over the constituent density elements. The integration procedure is expressed as

$$\mathbf{K}_e = \int_{\Omega_e} \mathbf{B}^{\mathrm{T}}\mathbf{D}\mathbf{B} d\Omega = \sum_{i=1}^{N_n} \left(\int_{\Omega_e^i} \mathbf{B}^{\mathrm{T}}\mathbf{D}\mathbf{B} d\Omega_e^i \right) \tag{2.10}$$

where Ω_e^i is the domain of the density element *i* (area A_i for 2D, and volume V_i for 3D) in the displacement element domain Ω_e, and N_n is the number of the density elements in the displacement element domain, e.g. $N_n = n$.

The SIMP interpolation model is employed to evaluate the stiffness matrix in Equation (2.10) as follows.

$$\mathbf{K}_e = \sum_{i=1}^{N_n} \left((\rho_i)^p \int_{\Omega_e^i} \mathbf{B}^{\mathrm{T}} \mathbf{D}^0 \mathbf{B} d\Omega_e^i \right) = \sum_{i=1}^{N_n} (\rho_i)^p \mathbf{I}_i \tag{2.11}$$

where $\mathbf{D}^0$ is the constitutive matrix corresponding to the solid phase, and $\mathbf{I}_i$ is computed as

$$\mathbf{I}_i = \int_{\Omega_e^i} \mathbf{B}^{\mathrm{T}} \mathbf{D}^0 \mathbf{B} d\Omega_e^i \tag{2.12}$$

When a large number of density elements are employed for each displacement element (e.g. n=25 for Q4 element, n=125 for B8 element), the integration of the stiffness matrix in (2.11) can be approximated by the summation of the integrand evaluated at the center of each density element. Thus, (2.12) can be simplified as

$$\mathbf{I}_i = \left(\mathbf{B}^{\mathrm{T}} \mathbf{D}^0 \mathbf{B} \right)\Big|_i A_i \tag{2.13}$$

Figure 2.4a shows a case in which four Gauss points are used for each density element in a Q4/n25 element for exact integration in (2.12), while Figure 2.4b shows the integration points for approximated scheme in (2.13).

In order to compute the sensitivity of the compliance, the derivative of the stiffness matrix with respect to the design variable is calculated as

$$\frac{\partial \mathbf{K}_e}{\partial d_n} = \frac{\partial \mathbf{K}_e}{\partial \rho_i} \frac{\partial \rho_i}{\partial d_n} = \frac{\partial \left(\sum_{j=1}^{N_n} (\rho_j)^p \mathbf{I}_j \right)}{\partial \rho_i} \frac{\partial \rho_i}{\partial d_n} = p \rho_i^{p-1} \mathbf{I}_i \frac{\partial \rho_i}{\partial d_n} \tag{2.14}$$

where d_n and ρ_i are the design variable and element density, respectively. The sensitivity of the constraint in Equation (2.9) is calculated similarly to Equation (2.7) as follows

$$\frac{\partial V}{\partial d_n} = \frac{\partial V}{\partial \rho_i} \frac{\partial \rho_i}{\partial d_n} \tag{2.15}$$

Equation (2.14) and (2.15) imply the summation with respect to *i*. The sensitivity $\partial \rho_i / \partial d_n$ is presented in Section 2.3.3 on projection method.

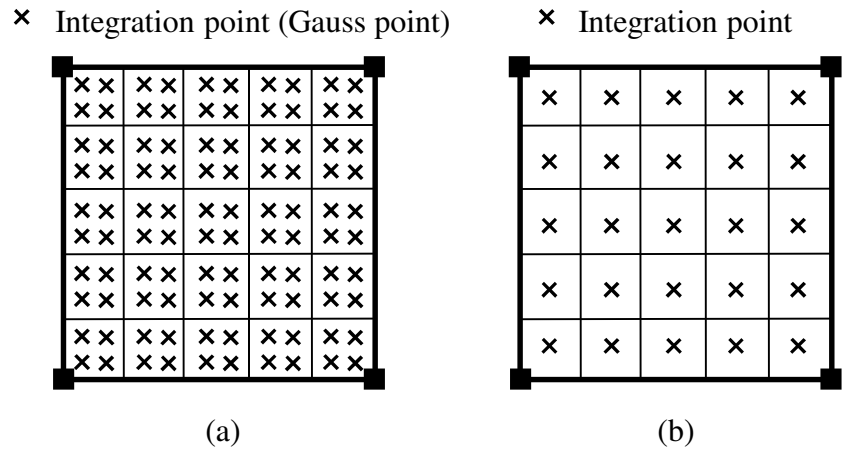

Figure 2.4: Integration points for Q4/n25 element: (a) Gauss quadrature; and (b) approximation.

2.3.2 General element types and isoparametric elements

In addition to the quadrilateral element Q4/n25 discussed in Section 2.3.1, the MTOP approach can be applied to other element types. As 2D element examples, Figure 2.5a shows a Wachspress hexagonal element (Talischi et al., 2009) with 24 density elements per displacement element (denoted by H6/n24). Figure 2.5b shows a triangular element with 16 density elements per displacement element (T3/n16). As 3D element examples, Figure 2.5c shows a brick element with 125 density elements per B8 element (B8/n125) while Figure 2.5d shows a tetrahedral element with 64 density elements (TET4/n64).

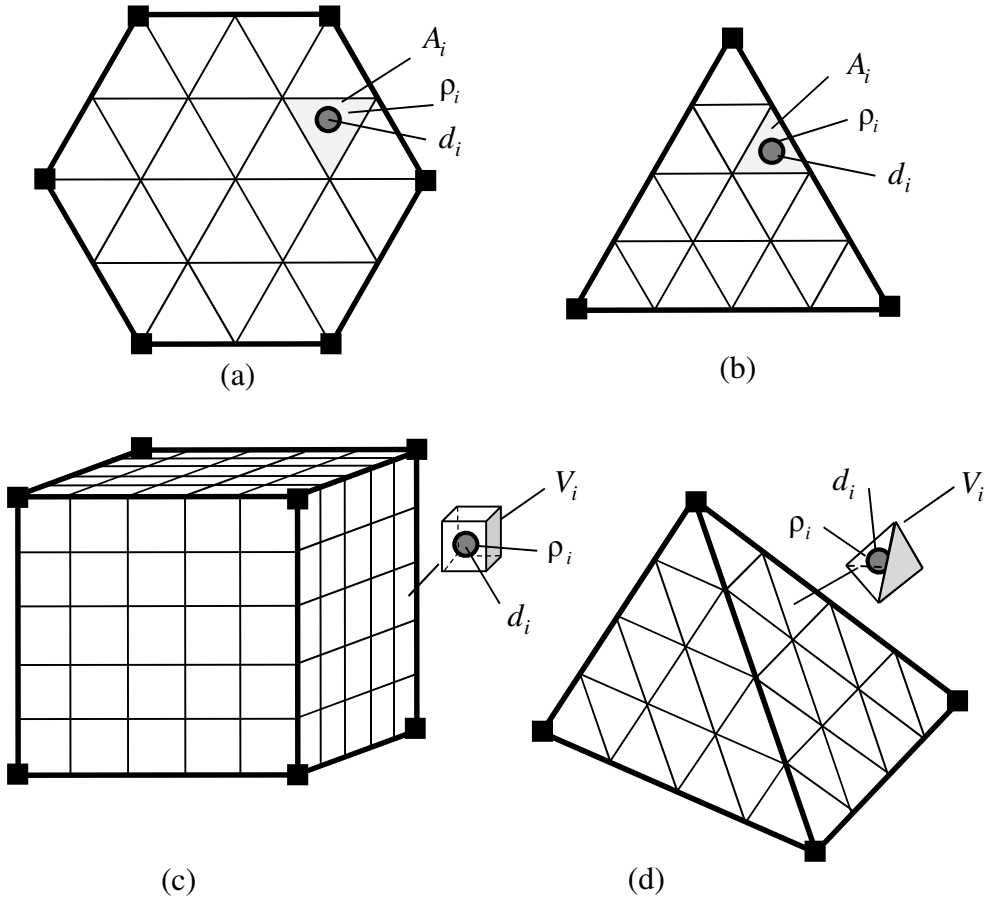

Figure 2.5: Examples of MTOP elements: (a) honeycomb Wachspress H6/n24; (b) T3/n16; (c) B8/n125; and (d) TET4/n64.

The integration technique in Equations (2.11)-(2.13) can be used for isoparametric elements as well. For example, for a Q4 element with unit thickness in Figure 2.5, the formulation to compute the stiffness matrix in the reference (parent) domain is as follows (Cook et al., 2002).

$$\mathbf{K}_e = \int_{\Omega_e} \mathbf{B}^{\mathrm{T}}\mathbf{D}\mathbf{B}d\Omega = \int_{-1}^{1}\int_{-1}^{1} \mathbf{B}^{\mathrm{T}}\mathbf{D}\mathbf{B}J d\xi d\eta \tag{2.16}$$

where (ξ, η) denote the intrinsic coordinates in the interval $[-1,1]$, J is the Jacobian, and $\mathbf{B}$ is the strain-displacement matrix in the reference (parent) domain. The standard formulation of matrix $\mathbf{B}$ in the reference domain can be found in the literature (Cook et al., 2002). The integration of (2.16) in the reference domain can be computed as follows.

$$\mathbf{K}_e = \int_{-1}^{1}\int_{-1}^{1} \mathbf{B}^{\mathrm{T}}\mathbf{D}\mathbf{B}Jd\xi d\eta = \int_{\Omega_0} \mathbf{B}^{\mathrm{T}}\mathbf{D}\mathbf{B}Jd\Omega_0 = \sum_{i=1}^{N_n}\left((\rho_i)^p \int_{\Omega_0^i} \mathbf{B}^{\mathrm{T}}\mathbf{D}^0\mathbf{B}Jd\Omega_0^i\right) \tag{2.17}$$

where Ω_0 is the reference domain, Ω_0^i is the reference domain of the density element i (A_i^0 is the area/volume of each density element i in the reference domain as shown in Figure 2.6).

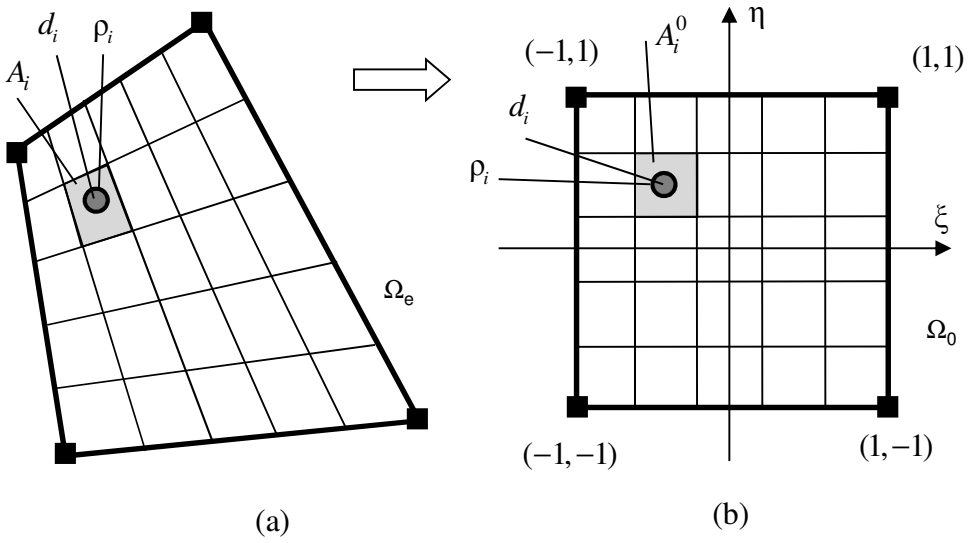

Figure 2.6: Isoparametric element: (a) initial domain; and (b) reference domain.

2.3.3 Projection method: a minimum length scale approach

Without projection, the aforementioned MTOP scheme alone does not provide mesh independency, which might lead to numerical instability and checkerboard effects (Diaz and Sigmund, 1995). Note that high-resolution design has been the objective of various studies to alleviate the checkerboard patterns (Diaz and Sigmund, 1995; Sigmund and Petersson, 1998; Poulsen, 2002a; Poulsen, 2002b; Pomezanski et al., 2005). In this study, a variation of previously reported projection method (Guest et al., 2004; Almeida et al., 2009) is employed to achieve minimum length scale and mesh independency. In the literature, the approach is also referred to as density filter (Bendsøe and Sigmund, 2003; Sigmund, 2007). The projection method uses the design variables to compute the element densities.

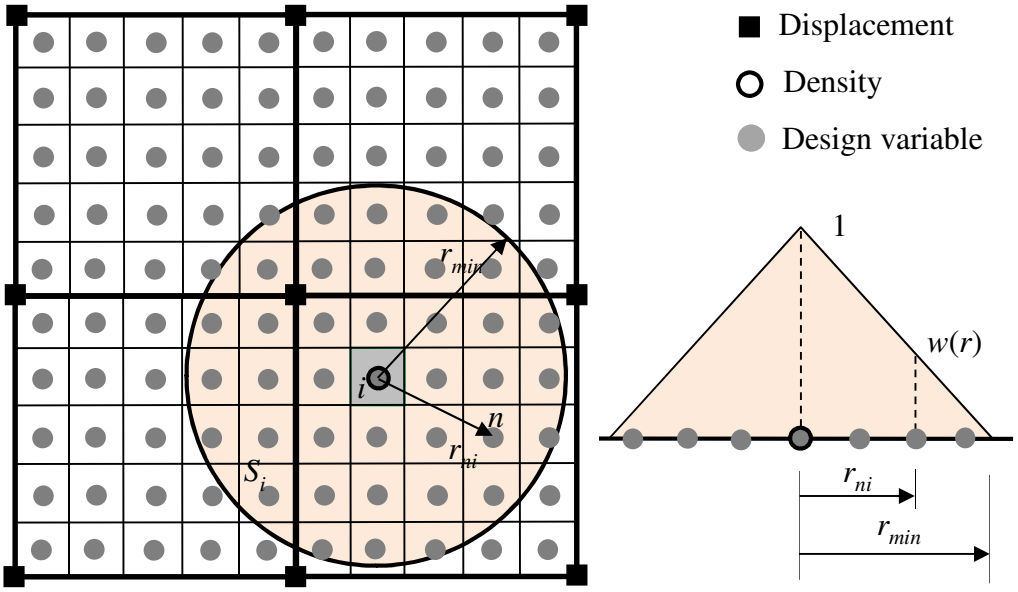

Figure 2.7: Projection function from the design variables to the density element (Q4/n25).

Here d_n denotes the design variable associated with the design variable mesh, while ρ_i represents the density of element i associated with the density element mesh. Assume that the change of material density occurs over a minimum length of $r_{\min}$, as shown in Figure 2.7. The element density ρ_i is obtained from the design variables d_n as follows.

$$\rho_i = f_p(d_n) \tag{2.18}$$

where $f_p(.)$ is the projection function. For example, if a linear projection is employed, the uniform density of a density element is computed as the weighted average of the design variables in the neighborhood as follows.

$$\rho_i = \frac{\sum_{n \in S_i} d_n w(r_{ni})}{\sum_{n \in S_i} w(r_{ni})} \tag{2.19}$$

where S_i is the sub-domain corresponding to the density element *i*. The corresponding weight function is defined as

$$w(r_{ni}) = \begin{cases} \dfrac{r_{\min} - r_{ni}}{r_{\min}} & \text{if } r_{ni} \le r_{\min} \\ 0 & \text{otherwise} \end{cases} \tag{2.20}$$

where r_{ni} is the distance from the point associated with design variable d_n to the centroid of density element i, and the physical radius $r_{\min}$ (see Figure 2.7) is independent of the mesh.

The sensitivities of the element density in Equation (2.19) with respect to design variables are derived as

$$\frac{\partial \rho_i}{\partial d_n} = \frac{w(r_{ni})}{\sum_{m \in S_i} w(r_{mi})} \tag{2.21}$$

Using the projection function with a minimum length scale, the mesh independent solution is obtained.

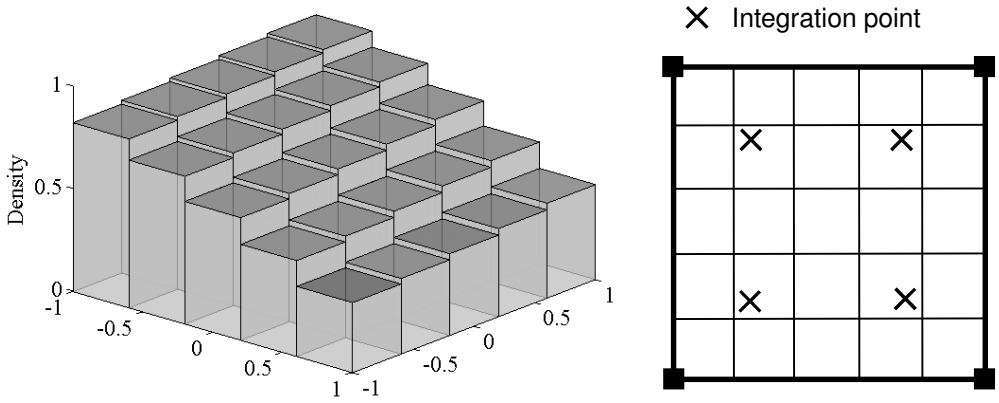

Figure 2.8: Twenty five density elements of one displacement element (Q4/n25).

2.3.4 Reduced number of integration points

During the optimization process, there may exist regions with constant material distribution, e.g., void or solid regions. For these regions, the material distribution within elements is uniform, thus the regular integration for the element stiffness can be used to further reduce the computational cost. For example, instead of using 25 integration points in a Q4/n25 element, the integration with fewer integration points such as 4 or 9 Gauss points can be employed. The

locations of the Gauss points and the corresponding weights in the integration can be found in the literature (Cook et al., 2002). Figure 2.8 shows densities inside a typical displacement element (Q4/n25) with smooth change of density. Since the stiffness matrix integrand is evaluated at the Gauss points, the densities at these Gauss points are directly computed from the design variables using projection function.

2.3.5 Selection of displacement, density, and design variable meshes

The proposed MTOP approach generalizes topology optimization methods such as the element-based approach and the super-element approach. For example, the element-based approach as shown in Figure 2.1b can be obtained using an MTOP approach with Q4/n1 elements with each element density represented by one design variable. The Q4/n1 element requires Gauss quadrature for the stiffness matrix integration in (2.10). In addition, super-element approach (Paulino et al., 2008) can be represented by the MTOP approach when special displacement, density element and design variable meshes as shown in Figure 2.9 are chosen. This mesh combination will result in the Q4/SE super-element which consists of several adjacent displacement elements having the same material density/design variable. The Q4/SE super-element also requires Gauss quadrature for the stiffness matrix integration as well.

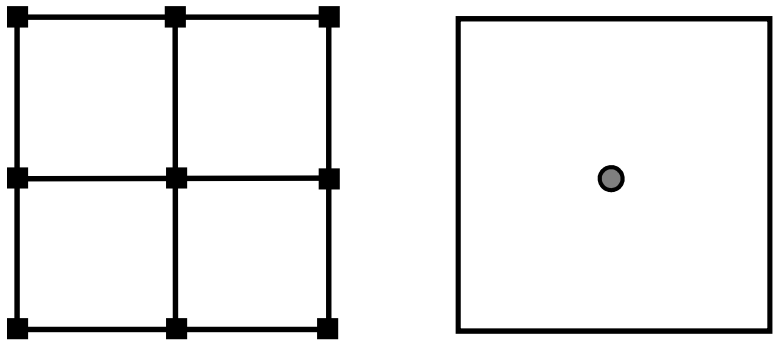

Figure 2.9: The MTOP approach for the super-element: (a) FE mesh; and (b) density/design variable mesh.

2.4 TWO-DIMENSIONAL NUMERICAL EXAMPLES

This section demonstrates the MTOP approach with 2D applications. A cantilever beam and the Michell truss benchmark examples are investigated. In all examples, SIMP model is employed to interpolate the stiffness tensor of the intermediate material density. The method of moving asymptotes (MMA) (Svanberg, 1987) is used as the optimizer throughout this thesis. More details of the MMA algorithm are presented in Appendix A. For simplicity, all the quantities are given dimensionless, e.g. Young's modulus is chosen as 1 and Poisson's ratio as 0.3 for all examples in the thesis. Instead of using prescribed volume V_s constraint in (2.2), volume fraction *volfrac*, which is defined as the ratio of the prescribed volume V_s and the total volume of the domain, is employed.

2.4.1 Cantilever beam

Figure 2.10 shows a 2D cantilever beam with a length of 48, a height of 16, and unit width. The beam is fixed at the left edge and a unit point load is applied downward at the midpoint of the right end. A volume fraction constraint *volfrac* is taken as 50%. The penalization parameter p is set equal to 4 and projection radius r_{min} of 1.2 is used for calculations. The element-based approach Matlab code (Sigmund, 2001; Bendsøe and Sigmund, 2003), modified to utilize the MMA optimizer and the projection method instead of the sensitivity filter, is used as a reference for the results of the MTOP approach.

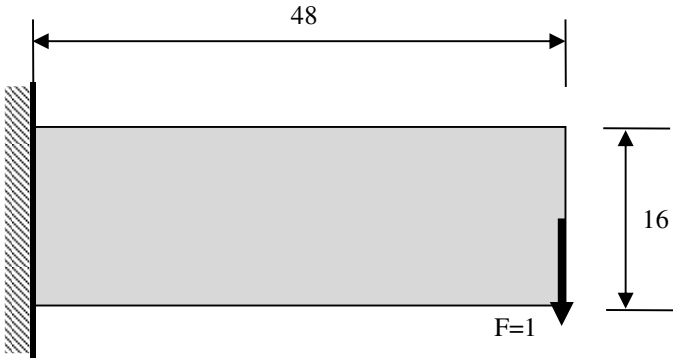

Figure 2.10: 2D cantilever beam.

(a) Two designs with the same displacement mesh size

The cantilever domain is discretized into a mesh with 768 Q4 elements (48×16) as shown in Figure 2.11a. The results obtained from the element-based and MTOP approaches are shown in Figure 2.11b and Figure 2.11c, respectively. It is shown that for the same displacement mesh size, the topology obtained by MTOP approach has a much higher resolution than that of the element-based approach.

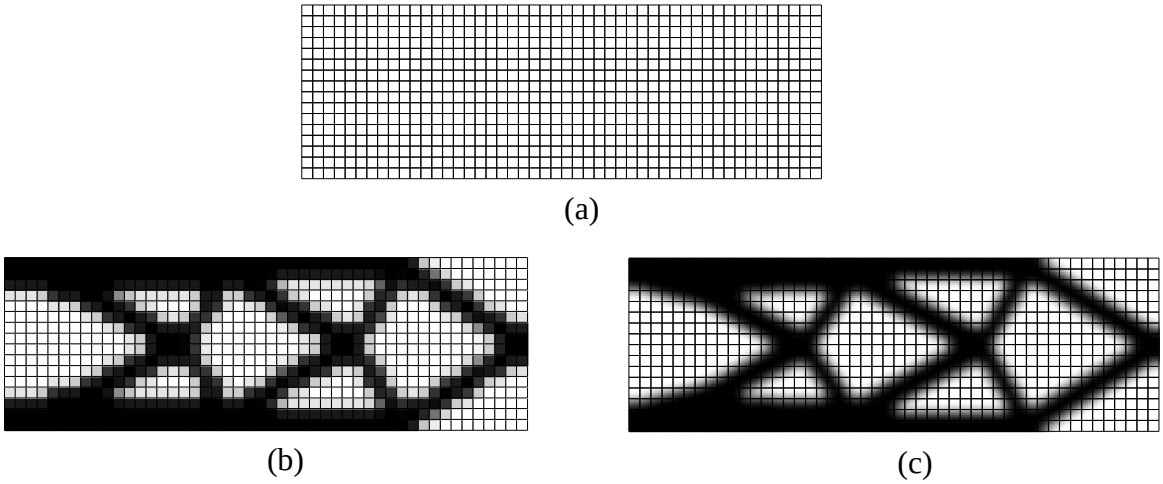

Figure 2.11: Topologies with the same FE mesh size 48×16 (*volfrac*=0.5, p=4, r_{min}=1.2): (a) FE mesh size 48×16 (for both approaches); (b) element-based approach using Q4/U elements (C=205.57); and (c) MTOP approach using Q4/n25 elements (C=208.23).

(b) Two designs with the same resolution

The finite element mesh requirement for the two abovementioned approaches to achieve topology designs with the same resolution is investigated. The element-based approach is performed on a displacement mesh of 240×80, as shown in Figure 2.12a, while the MTOP approach employs Q4/n25 elements with the coarse mesh size 48×16, as shown in Figure 2.12b. These results confirm that the topology obtained from the MTOP approach on this coarse displacement mesh has the same resolution with that obtained from the element-based approach on the fine mesh.

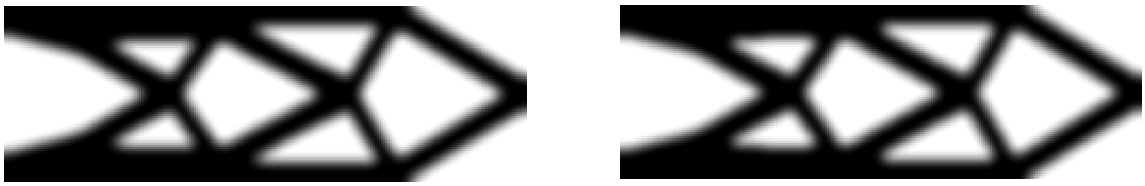

(a) (b)

Figure 2.12: Topologies with the same resolutions (*volfrac*=0.5, *p*=4, r_{min}=1.2): (a) FE mesh size 240×80, element-based approach with Q4 elements (*C*=210.68); and (b) FE mesh size 48×16, MTOP Q4/n25 elements (*C*=208.23).

(c) Accuracy of the approximated integration scheme

The integration of the stiffness matrix in (2.11) by (2.13) is an approximated scheme. In this example, the optimal topology in Figure 2.11b is obtained using MTOP Q4/n25 with 25 integration points and the corresponding optimal compliance is *C*=208.23. Finite element analysis using MTOP element is performed on the topology in Figure 2.11b using the exact integration in (2.12), four Gauss points for each density element, that is, each MTOP Q4/n25 element employs 100 Gauss points. The compliance of 207.67 is obtained which is only 0.27% different from approximation scheme in (2.13). Although more tests are needed, these results indicate that the approximation scheme in (2.13) may be used in practice for simplicity and uniform applicability.

(d) Convergence history and computational cost

The convergence histories of the MTOP and the element-based approaches are compared in Figure 2.13. During the optimization process, compliance convergence histories from the MTOP and element-based approaches for both coarse finite element mesh and fine finite element meshes are fairly similar. After 100 iterations, MTOP with a coarse mesh obtained the compliance of 208.23 while the element-based approach obtained 205.57 and 210.68 for a coarse mesh and a fine mesh, respectively.

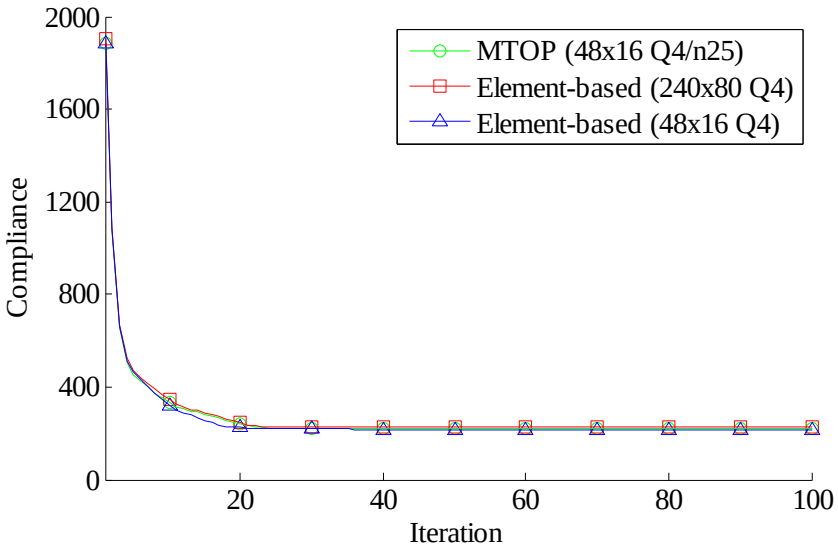

Figure 2.13: Convergence history for 100 iterations.

For optimal topologies of the same resolution, MTOP computation is much more efficient than the element-based approach. MTOP's lower computational cost is mainly attributed to a much lower number of finite elements in a coarse mesh. For example, the number of finite elements of the MTOP coarse mesh in Figure 2.12b is 25 times less than that of the fine mesh in Figure 2.12a. The efficiency of MTOP over conventional topology optimization is demonstrated more clearly when 3D large-scale problems, in which the finite element analysis cost dominant the total computational cost, are considered.

(e) Effect of number of density elements per displacement element on multiresolution design

The influence of the number of density elements per displacement element in the resolution design is further investigated. Figure 2.14 shows that the increase of the number of density elements from 4 to 16 improves the resolution of the topology design. Therefore, multiresolution designs can be obtained with the same finite element mesh. However, if the number of density elements is too large, the computational cost for optimization may increase significantly resulting in high total computational cost.

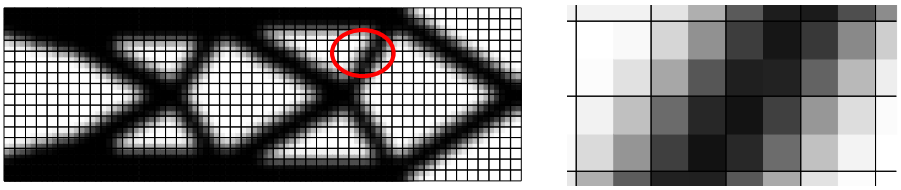

(a)

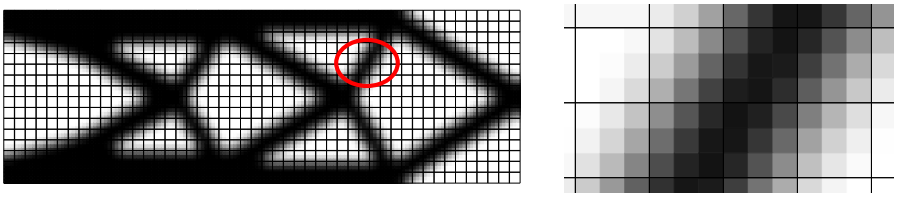

(b)

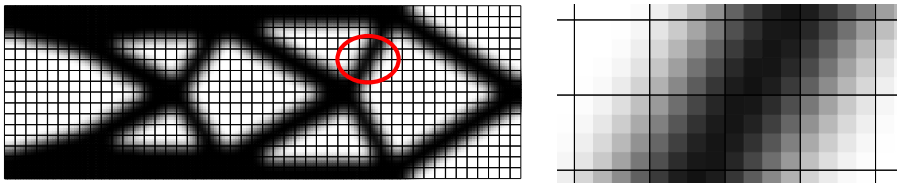

(c)

Figure 2.14: Multiresolution designs using MTOP (*volfrac*=0.5, p=4, r_{min}=1.2): (a) MTOP 48×16 Q4/n4 elements; (b) MTOP 48×16 Q4/n9 elements; and (c) MTOP 48×16 Q4/n16 elements.

(f) Influence of the minimum length scale on resolution design

To investigate the influence of length scale, the minimum length scale is varied from 1.5 to 0.75 for both element-based and MTOP approaches while keeping the displacement mesh size of 48×16. Figure 2.15 shows that for a length scale larger than the displacement element size (r_{min} > 1.0), the topology obtained from MTOP has better resolution than that from the element-based approach. When the minimum length scale is equal to or smaller than the displacement element size, the element-based approach produces checkerboard solutions. However, for MTOP approach with Q4/n25 element, instability is observed for r_{min}<0.75 only. These results indicate that the MTOP approach can utilize a length scale smaller than the element size, while the element-based approach can only employ a length scale larger than the element size.

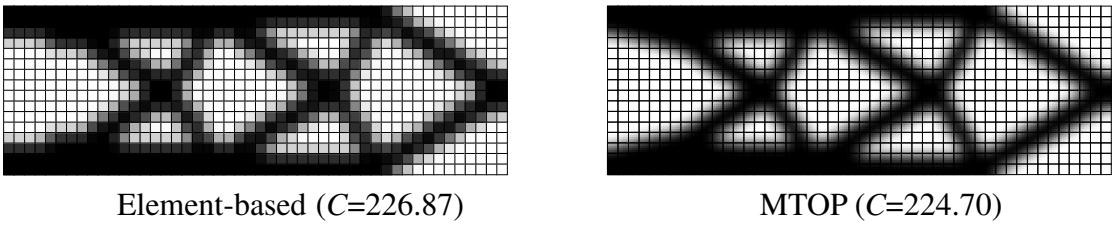

Element-based (C=226.87) MTOP (C=224.70)

(a)

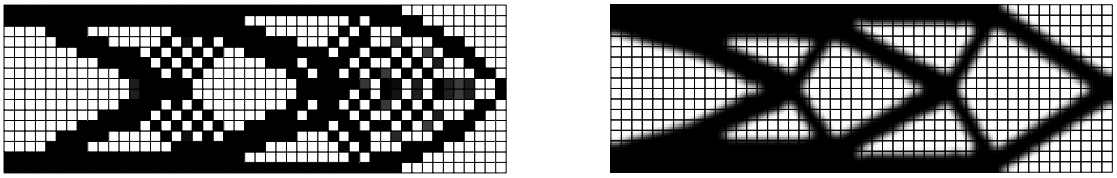

Element-based (C=199.50) MTOP (C=188.54)

(b)

Figure 2.15: Element-based approach and MTOP with different minimum length scale: (a) r_{min}=1.5; and (b) r_{min}=0.75.

(g) Discussion on the optimal topology of the cantilever beam

The topology optimization in this example is performed in a domain of continuum. However, for practical design purposes, the optimal continuum topologies may need to be transformed to corresponding discrete structures. For example, suppose the truss structure in Figure 2.16a is proposed based on the optimal topology in Figure 2.11c. This type of structural system is referred to here as TOP-form truss. The TOP-form truss is compared with other truss systems such as the K-form system on Figure 2.16b and the bracing-form system in Figure 2.16c. The performances of these truss systems are investigated as an applied load P of 1 and Young's modulus of 1000 are employed for all three systems. In each truss system, all members are assumed to have the same cross sectional areas.

First, the case in which the members in all three systems have the same area of 1 is considered. The third and fourth columns of Table 2.1 show that the TOP-form has the least compliance even though it has the least volume among the three systems. These results indicate that the TOP-form truss system based on the topology optimization in a continuum is optimal discrete topology.

Second, the cross sectional areas of the three truss systems are calibrated such that their total volumes are all equal to 100. As seen in the sixth column of Table 2.1, the TOP-form truss system results in the least compliance. This result indicates that for the same amount of material, the TOP-form truss system is more effective than other systems in minimizing the compliance of the structure.

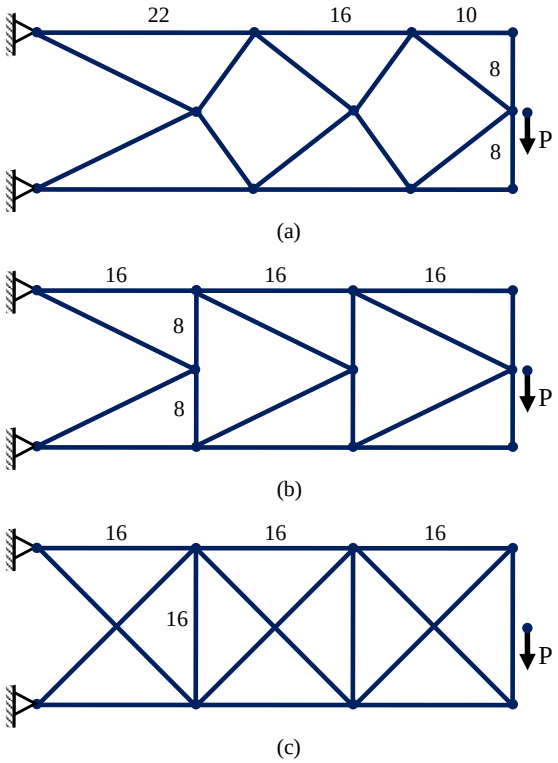

Figure 2.16: Topologies of the truss systems: (a) TOP-form; (b) K-form; and (c) bracing-form

Table 2.1: Comparison of the three truss systems

	Load P	All members have area = 1		Same total volume = 100	
		Total volume	Compliance	Member area	Compliance
TOP-form truss system	1	**239.00**	**0.301**	0.418	**0.719**
K-form truss system	1	251.33	0.302	0.398	0.759
Bracing-form truss system	1	279.76	0.348	0.357	0.973

2.4.2 Michell truss with circular support

Michell truss has been used as a verification benchmark for topology optimization (Suzuki and Kikuchi, 1991; Sigmund, 2000) because the analytical solution is available. For example, a single load transferring to a circular support was investigated by Sigmund (2000), as shown in Figure 2.17a. The theoretical optimal solution and topology optimization solution in Sigmund (2000), consisting of orthogonal curve system, are shown in Figure 2.17b and Figure 2.17c, respectively. The MTOP approach is verified by use of a Michell truss example with the domain discretization of 180×120 Q4/n25 elements. The MTOP optimal topology shown in Figure 2.17d is fairly close to the theoretical solution in Figure 2.17b and Sigmund's topology optimization solution in Figure 2.17c.

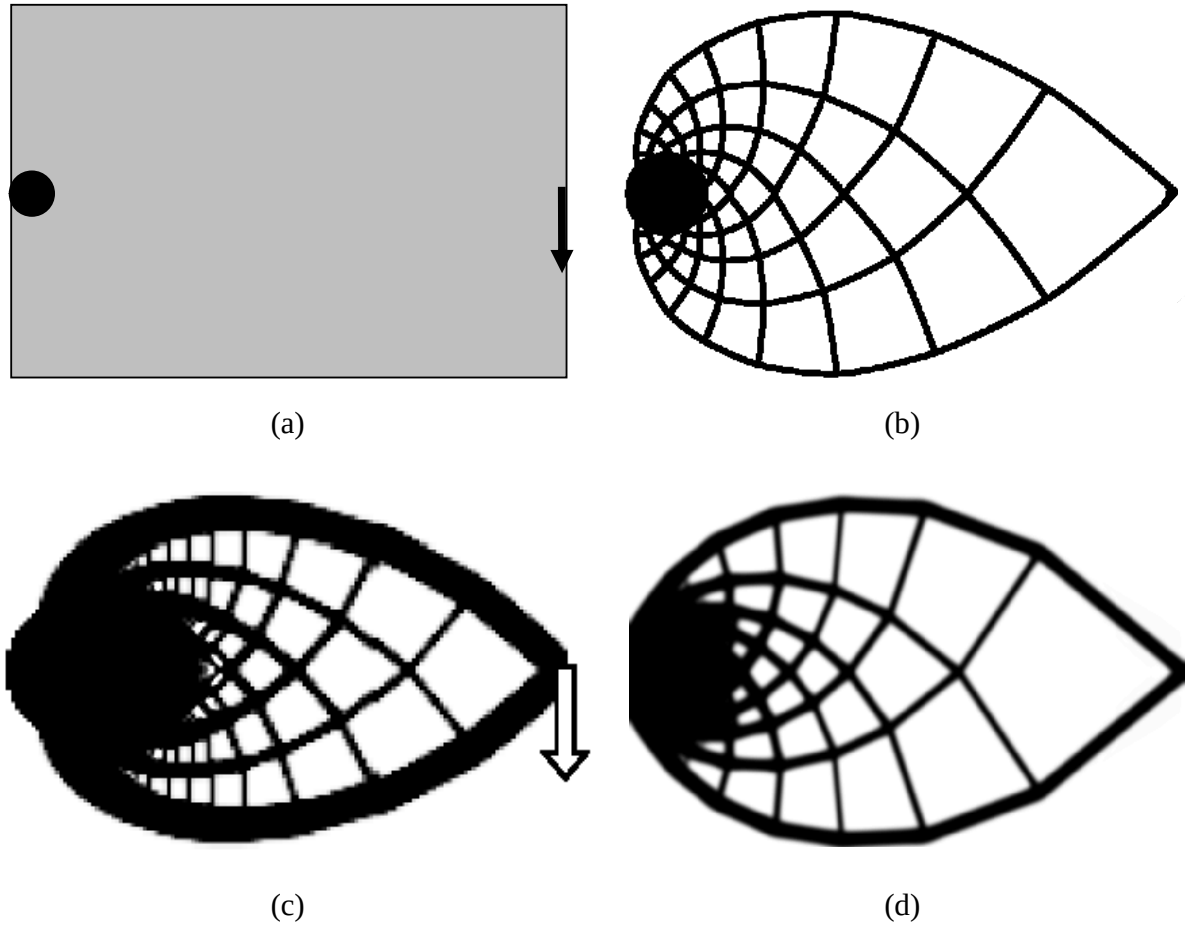

Figure 2.17: Michell truss with a circular support: (a) domain (mesh size 180×120); (b) analytical solution (taken from Sigmund 2000); (c) Sigmund's topology optimization solution (Sigmund 2000); and (d) MTOP optimal solution (*volfrac*=0.25, p=4, $r_{\min}$=1.2).

2.5 THREE-DIMENSIONAL NUMERICAL EXAMPLES

This section demonstrates the application of MTOP approach to 3D examples including a cross-shaped section, a cube, and a bridge design. The computations of these relatively large problems are performed on a single PC with an Intel® Core(TM)2 Duo 2.00 GHz 32-bit processor, 3GB RAM of memory, Windows OS, and a code developed in Matlab. Similar to the 2D examples, all quantities are dimensionless: Young's modulus of 1 and Poisson's ratio of 0.3 are employed.

2.5.1 Cross-shaped section

This example is adapted from the study by Borrvall and Petersson (2001) in which a 3D large-scale problem was solved with parallel computing. A cross-shaped domain, which has fixed boundaries on the left and right ends, is subjected to two downward loads applied on its back and front ends, as shown in Figure 2.18. The dimension of the domain is $L\times 3L\times 3L$ with $L=10$. The topology optimization problem seeks for optimal design with the volume fraction constraint of 20%. Borrvall and Petersson (2001) discretized the domain into $40\times 120\times 120$ B8 elements, which results in a total of 320,000 B8/U elements, and solved this problem with parallel computing. In this thesis, the domain is discretized into $10\times 30\times 30$ elements resulting in a total of only 5,000 B8/n125 elements. Instead of using powerful computing resources, such as parallel computing, with a large number of finite elements, a single PC is used for topology optimization using MTOP approach with only 5,000 B8/n125 elements to obtain high-resolution solution, as shown in Figure 2.19a. This optimal topology is similar to the result by Borrvall and Petersson (2001) as shown in Figure 2.19b. It is noted that Borrvall and Petersson (2001) used the sensitivity filter which is different from the projection scheme (density filter) in MTOP approach. In this study, the use of a slightly different volume fraction from Borrvall and Petersson (2001) results in a similar topology.

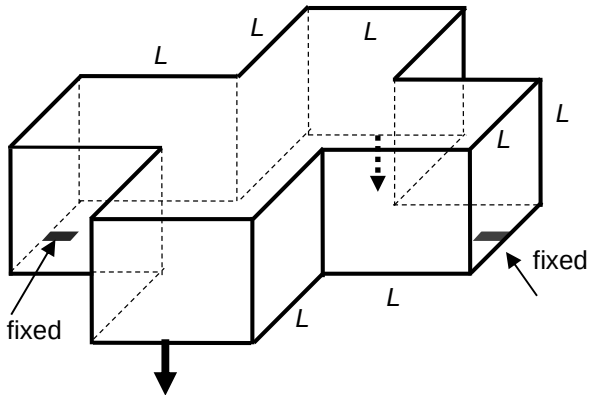

Figure 2.18: Geometry of the 3D cross-shaped section.

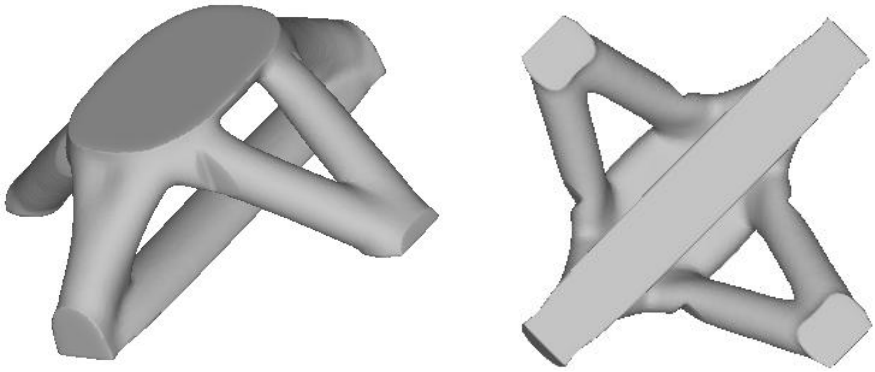

(a)

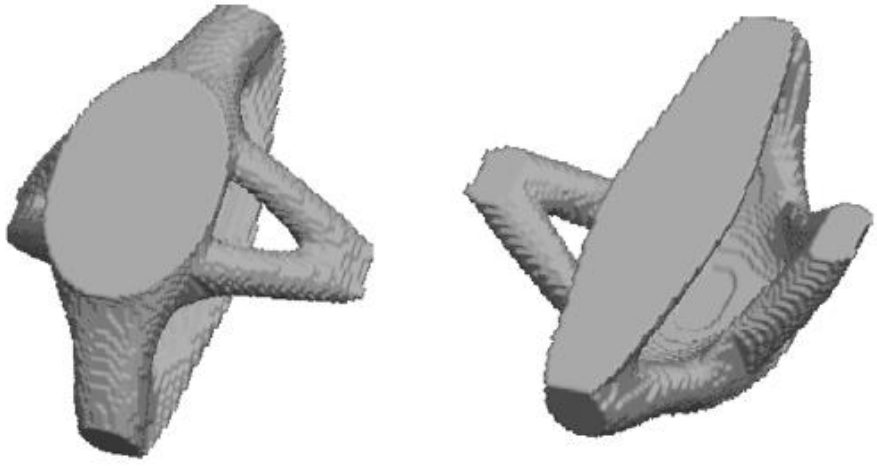

(b)

Figure 2.19: Topology optimization of the cross-shaped section: (a) MTOP using 5,000 B8/n125 elements (*volfrac*=0.2, *p*=4, r_{min}=1.0); and (b) conventional element-based approach using 320,000 B8/U elements (*volfrac*=0.25) and parallel computing (Borrvall and Petersson, 2001).

2.5.2 Cube with lateral loading

Figure 2.20 shows a 3D cube fixed at the centers of the top and bottom faces. This cube is also subjected to four tangential unit loads at the centers of the side faces. The cube domain is discretized into $20\times 20\times 20$ B8/n125 elements, which results in a total of 8,000 elements. The volume fraction constraint of 10%, minimum length scale $r_{\min}=1.0,$ and penalization parameter $p=3$ are employed. Figure 2.21 shows the optimal topology design. As shown in Figure 2.21, the topology consists of an orthogonal curve system to transfer the torsion load to the supports. It is noted that the solution of the Michell space-truss under torsion load also consists of orthogonal members as shown in Figure 2.22 (Rozvany, 1996).

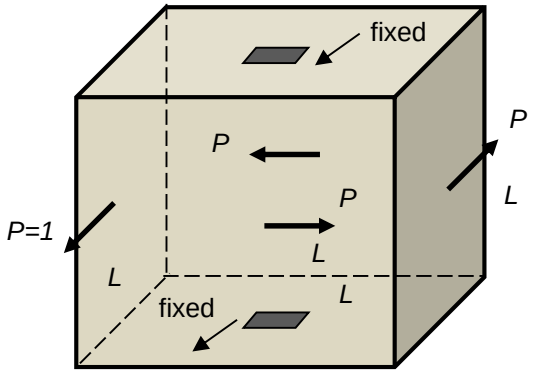

Figure 2.20: Geometry of the cube with lateral loading.

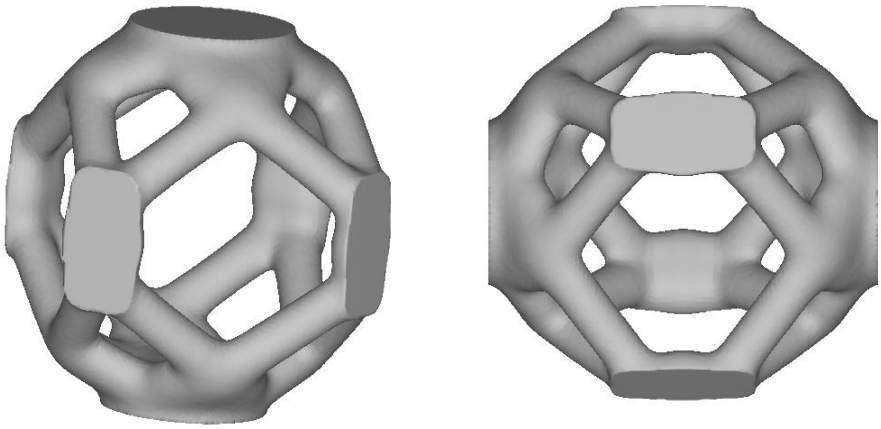

Figure 2.21: Topology of the cube using MTOP 8,000 B8/n125 elements (*volfrac*=0.1, *p*=3, $r_{\min}$=1.0).

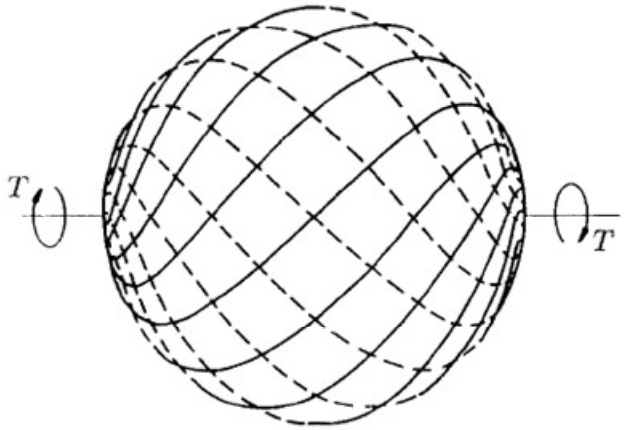

Figure 2.22: Michell space-truss under torsion loading (Rozvany, 1996).

2.5.3 Bridge design

Figure 2.23 presents a 3D bridge topology optimization example with simple supports, cantilevers and a non-designable layer at the mid-section. A deterministic unit load q is uniformly applied on the top of the non-designable layer of the bridge. The domain is discretized into $10\times120\times30$ B8/n125 elements. The non-designable layer has the unit thickness. The volume fraction constraint of 12.0%, the minimum length scale $r_{\min}=1.0,$ and penalization parameter $p=3$ are employed.

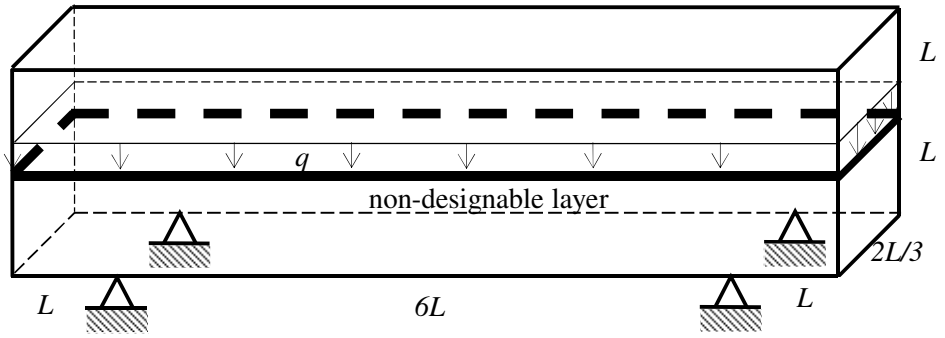

Figure 2.23: Domain for topology optimization of the bridge.

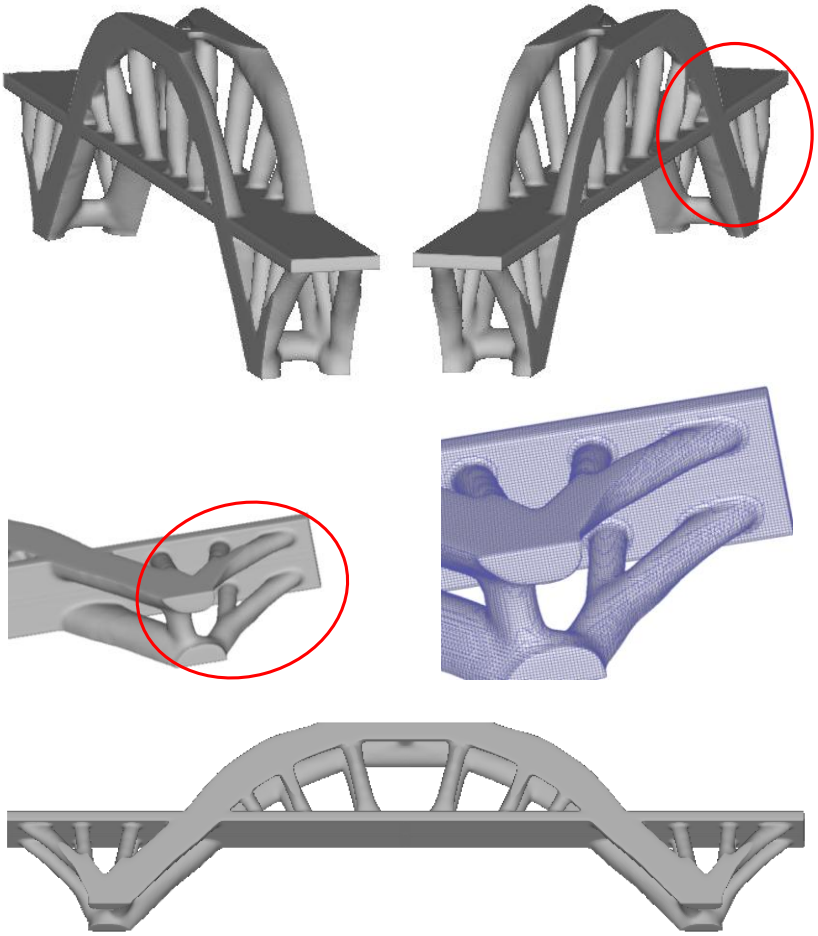

Figure 2.24: Optimal topology of the bridge by MTOP.

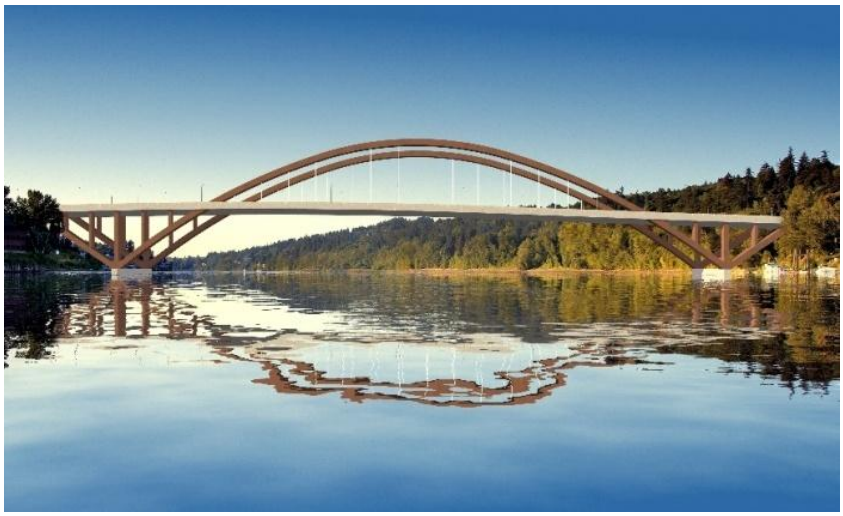

Figure 2.25: An existing bridge design (taken from http://www.sellwoodbridge.org).

The optimal topology in Figure 2.24 resembles an existing bridge design shown in Figure 2.25. However, there is a slightly difference of the two designs. Instead of the arch and vertical members of the bridge design in Figure 2.25, the optimal structure in the Figure 2.24 has flat areas at the top and non-vertical members. This is because, during the evolution of the optimal design, the diagonal members are created and compete with the formation of the arch shape to search for the load transfer points in a restricted design domain.

2.6 CONCLUDING REMARKS

In this chapter, a computational paradigm for multiresolution topology optimization (MTOP) is proposed. It leads to high-resolution designs by employing different meshes for the displacement, the density, and the design variable fields. In this chapter, the MTOP approach is explored using the same mesh for density elements and design variables and different mesh for displacement field. By using the design variable/density element mesh from coarse to fine, multiresolution designs can be obtained with the same finite element mesh. Furthermore, a projection scheme is introduced to compute element densities from design variables and to control the length scale of the density. Specifically, a coarser displacement mesh and finer density/design variable mesh are employed to obtain high-resolution designs with relatively low computational costs. The proposed MTOP approach is demonstrated by various 2D and 3D numerical examples.

CHAPTER 3 – IMPROVING MULTIRESOLUTION TOPOLOGY OPTIMIZATION

In Chapter 2, the MTOP approach is developed using the same mesh for density elements and design variables. In an attempt to improve the MTOP approach presented in Chapter 2, this chapter proposes a framework for improving multiresolution topology optimization (iMTOP) which employs fully distinct discretizations for: (1) finite elements, (2) design variables, and (3) density elements. This approach leads to high fidelity resolution with lower computational cost than the MTOP approach in Chapter 2. In addition, a heuristic adaptive multiresolution topology optimization procedure is introduced, which consists of selective adjustment and refinement of design variable and density fields.

3.1 INTRODUCTION

In general, computational cost of topology optimization mainly depends on those of the analysis and the optimization. The MTOP approach in Chapter 2 employs a coarser mesh for finite elements and a finer mesh for the density elements/design variables, therefore, the computational cost in the analysis is reduced. This chapter aims to improve the MTOP approach in Chapter 2 by further reducing the computational cost of both the analysis and the optimization while maintaining high-resolution designs. The development of this chapter includes two parts: reducing the number of design variables, and adaptively improving multiresolution topology optimization by using appropriate elements at suitable locations.

In the first part of this development, an efficient scheme for improving multiresolution topology optimization (iMTOP) is proposed by using *three* distinct discretizations: a *relatively coarse* mesh for finite elements, a *moderately fine* mesh for design variables, and a *relatively fine* mesh for density elements. Compared to the MTOP approach presented in Chapter 2, the iMTOP approach in this chapter further reduces the computational cost while maintaining the resolution

by using a *coarser* mesh for design variables. The finite element, the density element, and the design variable meshes are fully distinct in the iMTOP approach while the same mesh is used for density elements and design variables in the MTOP approach.

In the second part, an adaptive multiresolution topology optimization scheme is introduced to further increase computational efficiency. The adaptive mesh refinement approach (Costa Jr and Alves, 2003; Stainko, 2006; de Sturler et al., 2008) has been proposed to reduce the total number of finite elements by representing the void with fewer (coarser) elements and the solid with more (finer) elements. Lin and Chou (1999) proposed a two-stage approach in which the first-stage is performed with large finite elements and the optimal topology at the end of the first stage is used as the starting point for the second stage which uses a fine FE mesh. Costa and Alves (2003) employed a sequence of optimizations and mesh refinement, and used a converged solution on a coarse mesh to guide the refinement on the next refined mesh. Additionally, Stainko (2006) used a slightly different approach in which the mesh is refined only on the material boundary. Recently, de Stuler et al. (2008) refined the mesh in the solid regions and coarsened the mesh in the void regions dynamically, i.e. during the optimization process. Maute and Ramm (1995) proposed an adaptive scheme to separate the design optimization and analysis models. The authors performed shape and topology optimization separately and mapped the results to each other. They employed the adaptive mesh refinement strategy on the finite element mesh to change the design patch of the topology optimization. Kim and Yoon (2000) utilized wavelet space to perform the design optimization progressively from low to high-resolution while using the same finite element mesh. Additionally, Kim et al. (2003) developed a multiscale wavelet-Galerkin method and used it as an adaptive solver in topology optimization. The analysis and the design optimization are integrated in a multiresolution framework so that both the analysis resolution and the design resolution can be adaptively adjusted. In their approach, at all levels, the design resolution is similar or coarser than the analysis resolution. Recently, Guest and Genut (2009) used a separate design variable mesh and finite element mesh in topology optimization such that the density of the finite element is obtained by projection of the design variables. They utilized the same finite element mesh and an adaptive design variable field where the design variables can be activated and deactivated during the optimization process depending

on the structural regions. This approach provides an optimal design that has the same resolution as the finite element mesh (Guest and Genut, 2009). Essentially, the MTOP approach in Chapter 2 is opposite to the approach by (Guest and Genut, 2009). The adaptive multiresolution topology optimization approach in this chapter is based on the iMTOP scheme described in the first part. The motivation for the adaptive approach is to use iMTOP elements *where* and *when* needed only, otherwise the conventional elements are used – the finite element mesh remains the same during the optimization process.

The remainder of this chapter is structured as follows: Section 3.2 proposes an idea of using three distinct meshes for improving multiresolution approach; Section 3.3 presents the adaptive multiresolution topology optimization procedure; Section 3.4 provides two-dimensional examples; Section 3.5 provides three-dimensional examples; Section 3.6 discusses the computational cost and resolution; and Section 3.7 presents the concluding remarks.

3.2 MULTIPLE DISCRETIZATIONS FOR TOPOLOGY OPTIMIZATION

Existing topology optimization approaches such as the element-based and nodal-based approaches can be interpreted with a design variable mesh and a finite element (displacement) mesh. For example, the element-based approach considers a uniform density of each finite element as a design variable for optimization as shown in Figure 3.1a. By contrast, the nodal-based approaches (Guest et al., 2004; Matsui and Terada, 2004; Paulino and Le, 2009) consider the densities at the finite element nodes as the design variables. Another option is to locate the nodal design variables at the midpoints of the four edges of the quadrilateral elements (Paulino and Le, 2009). The design variables can be independent of the finite element mesh and can be reduced adaptively during the topology optimization process (Guest and Genut, 2009). In the abovementioned approaches, the topology design is defined via the density of the finite element mesh. Therefore, the highest level of resolution that these approaches can achieve is the resolution of the finite element mesh.

The MTOP approach in Chapter 2 uses three meshes: finite element mesh, design variable mesh, and density element mesh for multiresolution topology optimization. However, in the

MTOP approach in Chapter 2, the design variable mesh and the density mesh are coincident. For example, each Q4 element is divided into a number of density elements (e.g. n=25). The design variable is defined as the density at the center of the density element. Therefore, the number of design variables equals to the number of density elements as shown in Figure 3.1b. The uniform density of a density element is computed from the values of the design variables via a projection function.

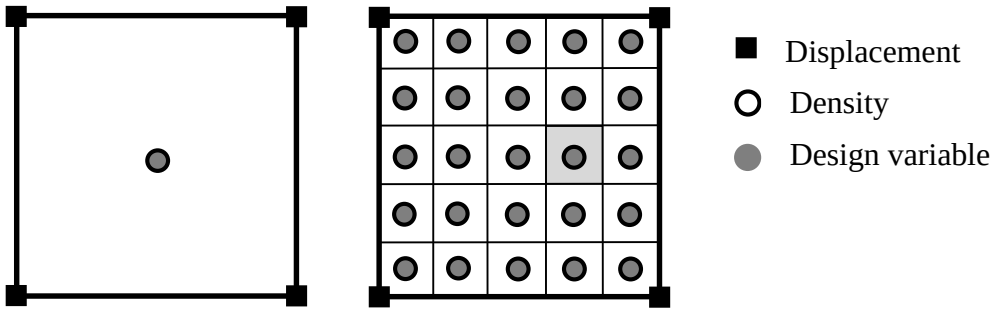

Figure 3.1: Element-based and MTOP elements (Q4/U and Q4/n25).

3.2.1 Finite element, density element and design variable meshes

This section presents an efficient procedure for improving multiresolution topology optimization (denoted as iMTOP). A *relatively coarse* mesh is employed for finite elements, a *moderately fine* mesh for design variables, and a *relatively fine* mesh for density elements. In comparison to the MTOP approach in Chapter 2, fewer design variables are employed, therefore, the computational cost can be further reduced in the optimization, sensitivity analysis and projection. For example, Figure 3.1a shows element-based approach with a Q4/U element and Figure 3.1b shows a MTOP Q4/n25 element where n=25 is the number of density elements/design variables per Q4 finite element. The proposed improvement employs fewer design variables per Q4 element than in Figure 3.1b. For instance, Figure 3.2a shows the proposed iMTOP element: Q4/n25/d9 where n=25 and d=9 are the number of density elements and design variables, respectively. The number of design variables in Q4/n25/d9 element (Figure 3.2a) is relatively smaller than that in the original Q4/n25 element (Figure 3.1b). Additionally,

Figure 3.2b and Figure 3.2c show other choices of density elements and design variables for Q4 element (Q4/n16/d5, Q4/n25/d16). Figure 3.2d shows iMTOP Q4/n25/d13 element in which the locations of design variables are unstructured. These options for density elements and design variables indicate that the three meshes are fully distinct in the iMTOP approach.

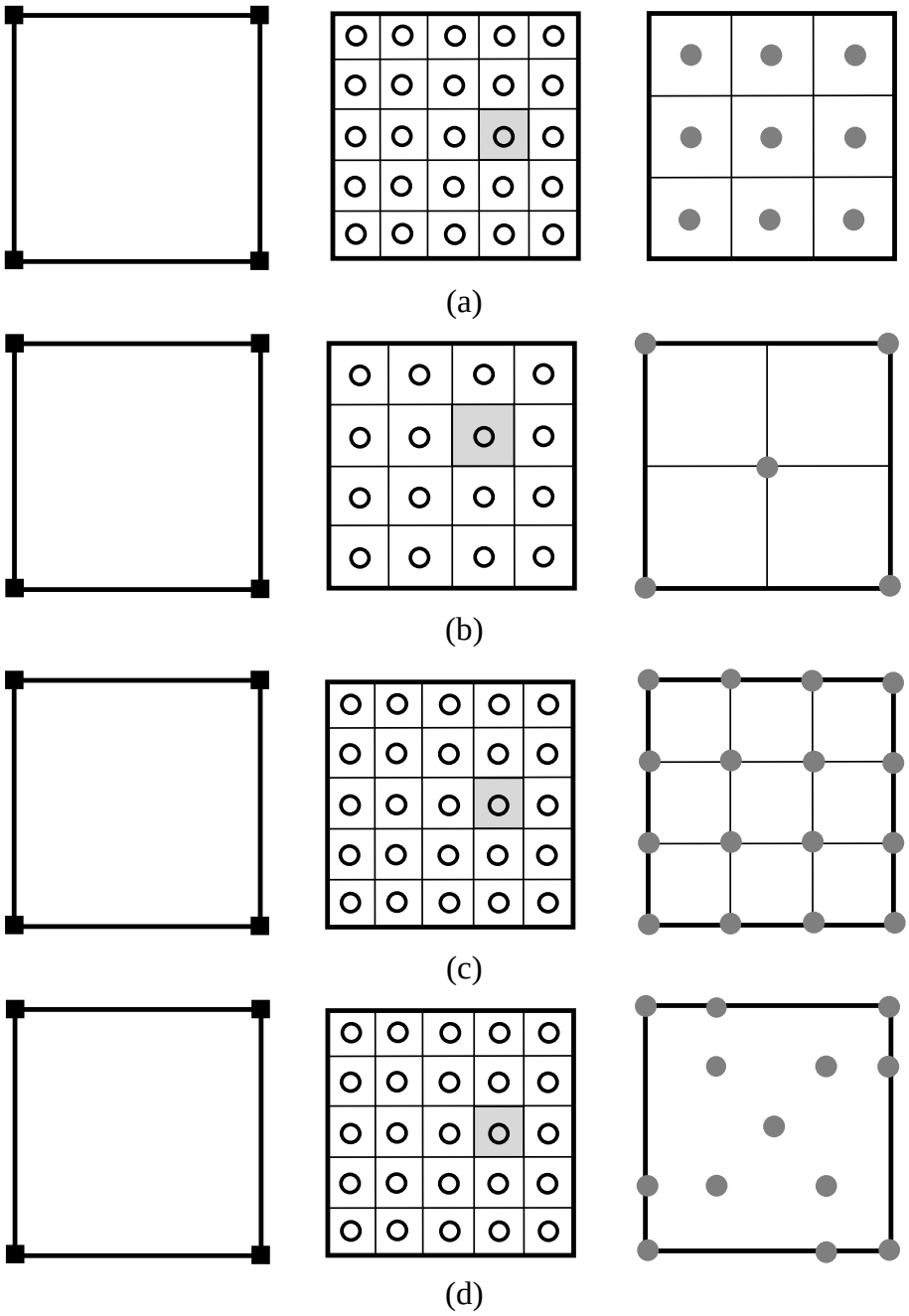

Figure 3.2: iMTOP elements: (a) Q4/n25/d9 element; (b) Q4/n16/d5 element; (c) Q4/n25/d16; and (d) Q4/n25/d13 with unstructured locations of design variables.

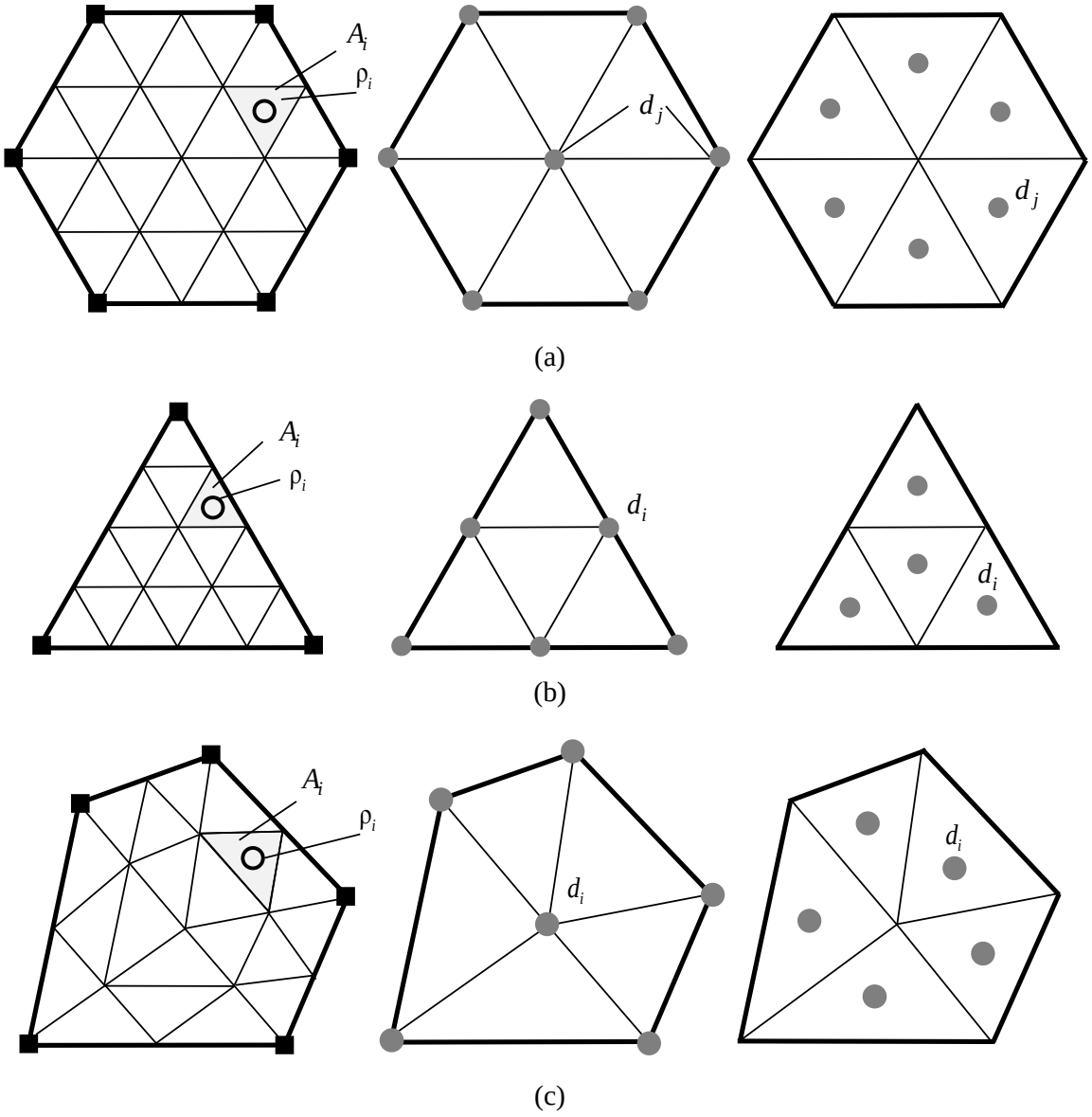

Figure 3.3: Two-dimensional iMTOP elements: (a) honeycomb Wachspress H6/n24/d7 and H6/n24/d6; (b) triangular T3/n16/d6 and T3/n16/d4; and (c) polygonal P5/n20/d6 and P5/n20/d5.

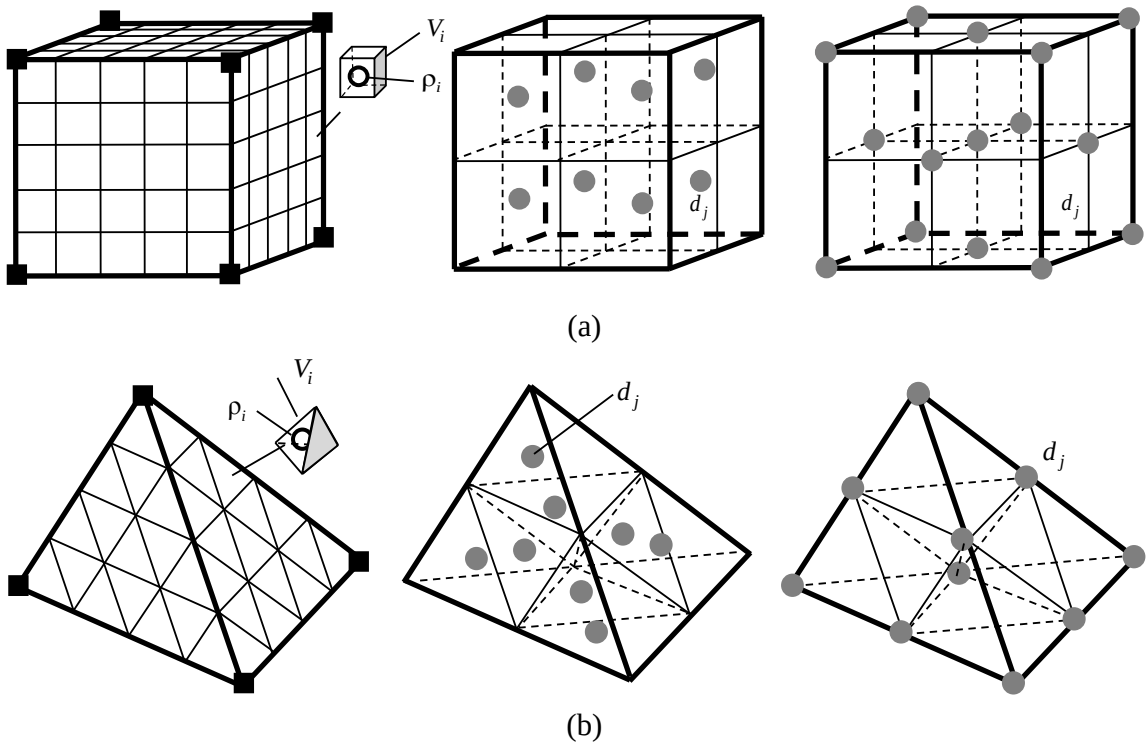

Figure 3.4: Three-dimensional iMTOP elements: (a) brick B8/n125/d8 and B8/n125/d15; and (b) tetrahedral TET4/n64/d8 and TET4/n64/d10.

3.2.2 iMTOP elements for two- and three-dimensional topology optimization

The concept of using three distinct meshes can be applied to other two- and three-dimensional element types in which the number of design variables is less than the number of density elements. For two-dimensional problems, Figure 3.3a shows a Wachspress hexagonal element (Talischi et al., 2009) with 24 density elements per finite element. Instead of using 24 design variables (H6/n24) as proposed in Chapter 2, the number of design variables can be further reduced using three distinct meshes. For example, 7 or 6 design variables can be used to create H6/n24/d7 or H6/n24/d6 elements, as shown in Figure 3.3a. Additionally, Figure 3.3b shows a triangular element with 16 density elements per finite element and 6 or 4 design variables to create T3/n16/d6 or T3/n16/d4 elements, respectively. The iMTOP approach can be applied to polygonal finite elements (Talischi et al., 2010) to improve the resolution design. For example, Figure 3.3c shows a polygonal element with 5 edges (P5) using n=20 density elements.

The P5/n20/d6 and P5/n20/d5 elements are introduced where 6 and 5 are the number of design variables per polygonal element, respectively. For three-dimensional problems, Figure 3.4a shows 125 density elements per B8 element with 8 and 15 design variables, denoted by B8/n125/d8 and B8/n125/d15; and Figure 3.4b shows a tetrahedral element with 64 density elements with 8 and 10 design variables, denoted as TET4/n64/d8 and TET4/n64/d10, respectively. It is noteworthy that the iMTOP elements in this study utilize the locations of design variables associated with the finite elements to develop systematic element types. It is actually the case that the design variables can be located at any locations in the design space, for example, as shown in Figure 3.2d. Thus, future work may seek for the optimal number and locations of the design variables.

3.2.3 iMTOP formulations and projection from design variables to density elements

The iMTOP's formulations for integration of the stiffness matrix and sensitivity is referred to Section 2.3. A variation of the previously reported projection method (Guest et al., 2004; Almeida et al., 2009) is presented here as the iMTOP's projection method to achieve minimum length scale and mesh independency. The projection method uses the design variables associated with the design variable mesh to compute the element densities which belong to the density element mesh. The formulations of projection are shown in Section 2.3.3. Figure 3.5 illustrates projection scheme of the iMTOP approach via Q4/n25/d9 elements. Using the projection function with a minimum length scale, one thus obtains a mesh independent solution for the iMTOP approach.

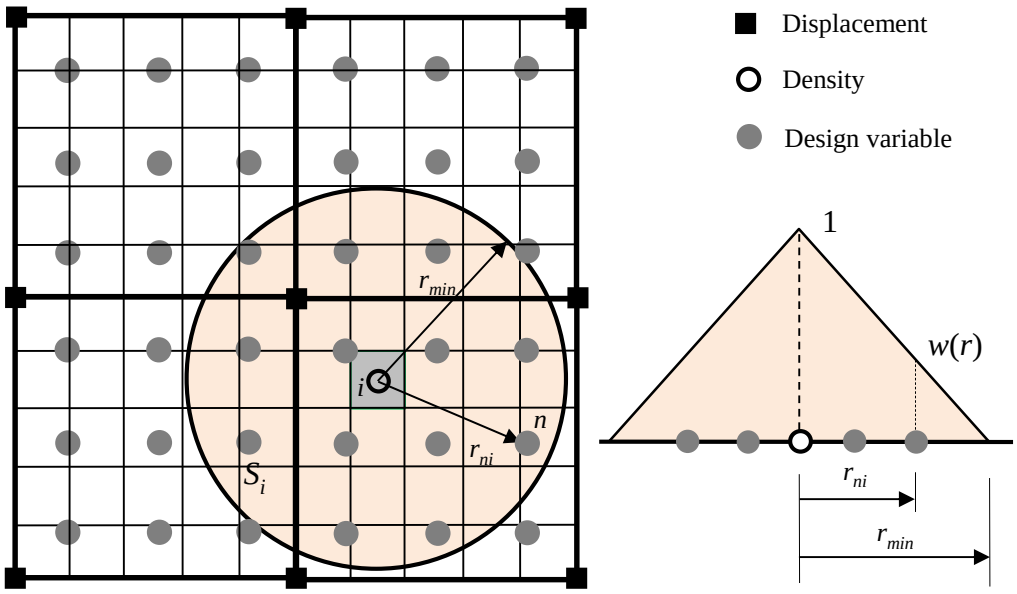

Figure 3.5: Projection function from the design variables to the density element (Q4/n25/d9).

3.3 ON ADAPTIVE MULTIRESOLUTION TOPOLOGY OPTIMIZATION

A heuristic adaptive scheme in conjunction with multiresolution topology optimization is presented. The motivation is to further reduce the number of design variables and/or density elements in the multiresolution framework. For more detailed accounts on adaptivity theory and approaches, the reader is referred to the literature (Maute and Ramm, 1995; Ainsworth and Oden; Costa Jr and Alves, 2003; Stainko, 2006; de Sturler et al., 2008). Here the proposed adaptive approach focuses on selective adjustment of the design space for topology optimization.

3.3.1 Reducing design variable and density fields

A simple and heuristic adaptive multiresolution topology optimization procedure, which is based on the scheme described in Section 3.2, is introduced. As demonstrated by numerical examples, the approach leads to high-resolution design with relatively low computational cost by using iMTOP elements (e.g. Q4/n25/d4) rather than conventional elements (e.g. Q4/U). However, iMTOP elements are used *where* and *when* needed only, otherwise conventional elements (e.g. Q4/U) are employed. During the optimization process, some regions may have uniform material

distribution such as void regions or solid regions. In the regions where material distribution is uniform, the iMTOP elements (e.g. Q4/n25/d4) are replaced by the conventional elements (e.g. Q4/U). On the other hand, the iMTOP elements are used in regions where the material density gradient is high. In these regions, structural boundaries are forming; therefore a higher resolution is needed to represent the material distribution.

3.3.2 Design space adjustment

The adaptive scheme consists of using iMTOP elements only in the regions where they are needed, otherwise conventional elements are used via a criterion based either on design variables or on density elements. The procedure is shown here in terms of density elements. For illustrative purpose, Q4/U and Q4/n25/d4 elements are used in the explanation, however more than one type of iMTOP elements can be used in a particular optimization problem. During the optimization process, element types are tracked using an "*element index"* array. Each finite element *e* is assigned an "*element index*" *ei*, where *ei*=1 indicates a conventional element (e.g. Q4/U), and *ei*=n (e.g. n=25) indicates an iMTOP element (e.g. Q4/n25/d4).

Initially, when the material distribution is uniform, all elements are assigned as conventional ones (e.g. Q4/U). The optimization is performed until a relatively less stringent convergence criterion, namely the type updating convergence criterion, is satisfied. The iMTOP element type is determined to be used for each finite element based on element densities. An alternative approach consists of determining the element type based on the gradient of the material density. For example, iMTOP elements are used where the material density gradient is high and conventional elements are used where the material is relatively more uniform. However, in current implementation, an element *e* is changed from conventional to iMTOP when it is sufficiently "gray", i.e. $\rho_L < \rho_e < \rho_U$, where ρ_L and ρ_U are predefined thresholds, e.g. ρ_L =0.015 and ρ_U =0.99. On the other hand, an iMTOP element is changed to conventional when all of their densities are sufficiently "black" or "white", i.e. $\rho_i>\rho_U$ or $\rho_i < \rho_L$. The "element index" *ei* is then updated whenever the element is changed either from iMTOP to conventional or from conventional to iMTOP. The criteria for the above element type updating scheme to perform is based on the convergence of the objective function. For example, the element type is updated if

the relative change of the objective function is less than a threshold (e.g. 1%) after a certain number of optimization iterations (e.g. 20), The process of element type updating and optimization iterations are repeated until the convergence criteria on maximum number of iterations (e.g. 100 iterations) or the relative change in the objective function (e.g. 0.1%). The flow chart of the adaptive procedure is explained in Figure 3.6.

In summary, an adaptive procedure is proposed to utilize the iMTOP elements only in the selected regions in the domain during the optimization process. The procedure is demonstrated via numerical examples in the subsequent sections.

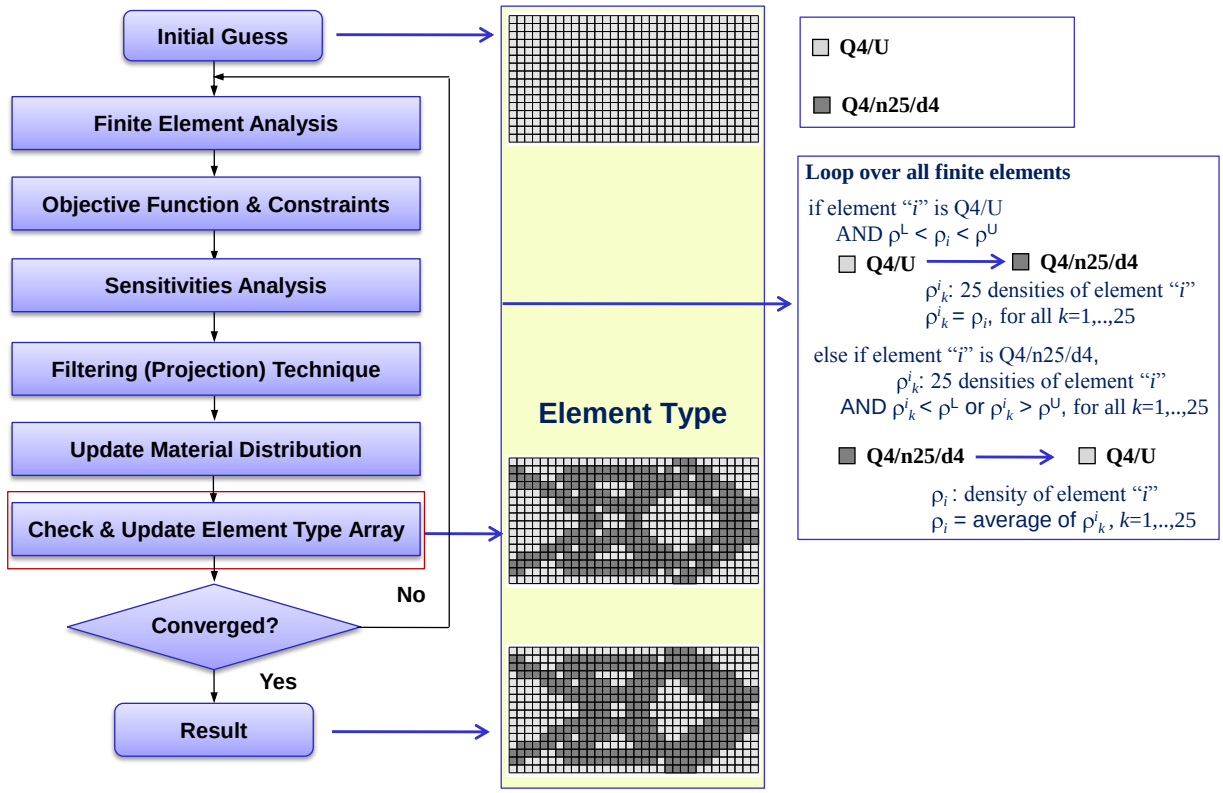

Figure 3.6: Flow chart of the adaptive MTOP scheme (Q4/n25/d4 and Q4/U).

3.4 TWO-DIMENSIONAL NUMERICAL EXAMPLES

In this section, the approaches proposed in this chapter are demonstrated with various two-dimensional applications. First, the minimum compliance problem of a beam under a concentrated load is considered (Figure 3.7a). Second, the compliant mechanism design of a displacement inverter is investigated (Figure 3.7b). Third, a cantilever beam is investigated to demonstrate the adaptive procedure. In these examples, the SIMP model is employed to interpolate the stiffness tensor of the intermediate material density. The method of moving asymptotes (MMA) (Svanberg, 1987) is used as the optimizer. For simplicity, all the quantities are given dimensionless: Young's modulus is chosen as 1 and Poisson's ratio as 0.3 for all examples. Instead of using prescribed volume constraint V_s, volume fraction *volfrac*, which is defined as the ratio of the prescribed volume V_s to the total volume of the domain, is used.

3.4.1 Minimum compliance of an MBB beam

This example presents the solution for minimum compliance problem of a beam subjected to a concentrated vertical load, so-called Messerschmitt-Bolkow-Blohm (MBB beam). Because of the symmetry, only half of the beam is taken into consideration with a length of 60, a height of 20, and unit width, as shown in Figure 3.7a. The volume fraction constraint *volfrac* is taken as 60%, the penalization parameter p is set equal to 3, and the projection radius $r_{\min}$ is set equal to 1/10 of the height of the beam.

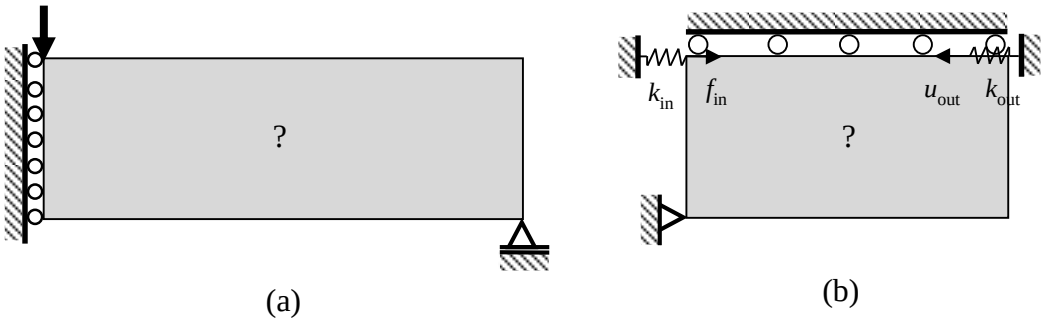

Figure 3.7: Configurations: (a) MBB beam; and (b) displacement inverter.

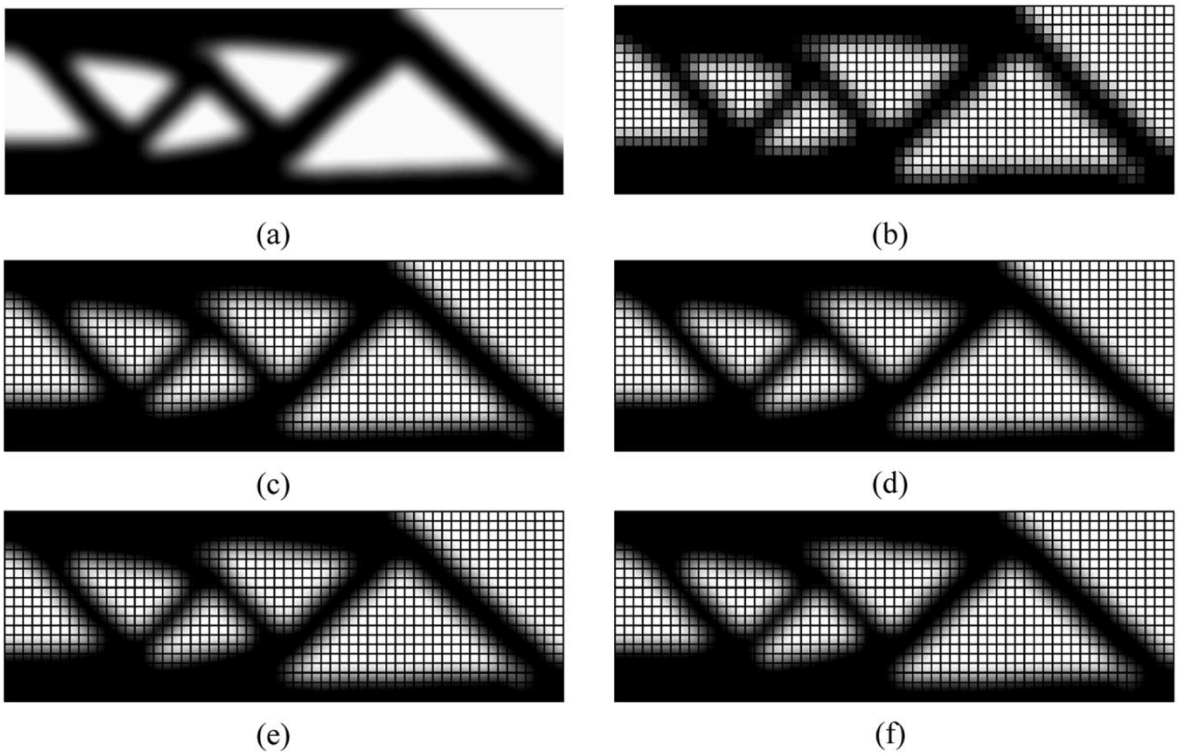

Figure 3.8: Topologies of MBB beam: (a) element-based Q4 FE mesh 300×100 (C=187.71); (b) element-based Q4 FE mesh 60×20 (C=181.04); (c) MTOP Q4/n25 (C=181.90); (d) iMTOP Q4/n25/d16 (C=181.95); (e) iMTOP Q4/n25/d9 (C=181.99); and (f) iMTOP Q4/n25/d4 (C=181.96) (b–f: FE mesh 60×20).

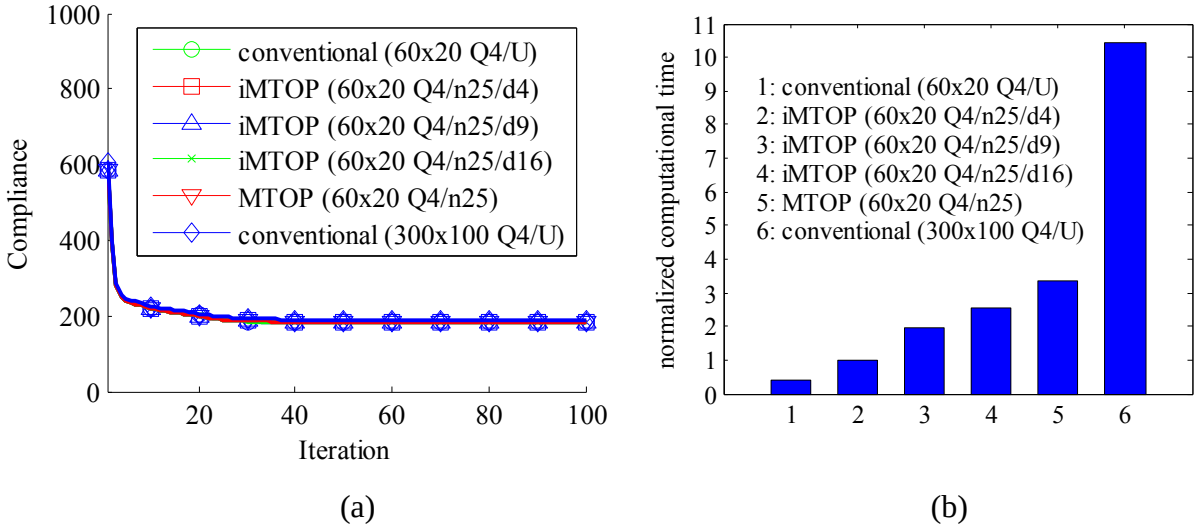

Figure 3.9: Comparison of topology optimization approaches after 100 iterations: (a) convergence history; and (b) computational times.

First, the element-based topology optimization is performed on a fine FE mesh of 300×100 and a coarse FE mesh of 60×20 Q4/U elements – the optimal topologies are shown in Figure 3.8a and Figure 3.8b, respectively. The topology obtained from the fine FE mesh has a higher resolution than that from the coarse mesh. Next, the MTOP approach in Chapter 2 using 60×20 Q4/n25 elements is employed and the topology is obtained as shown in Figure 3.8c. It is noted that the topologies in Figure 3.8a and Figure 3.8c have higher resolution than the topology in Figure 3.8b obtained from a coarse FE mesh.

Second, using the iMTOP approach, the number of design variables is varied for the same resolution (or the same number of density elements). Instead of using MTOP Q4/n25 elements where the number of design variables is equal to the number of density elements, the number of design variables per Q4 finite element is reduced to 16, 9 and 4. This leads to a coarse FE mesh of 60×20, a fine density element mesh of 300×100, and the design variable meshes of 240×80, 180×60, and 120×40, respectively. The optimal topologies are shown in Figures 3.8d, e and f corresponding to iMTOP Q4/n25/d16, Q4/n25/d9, and Q4/n25/d4 elements, respectively. These topologies are similar to the optimal topology obtained with MTOP Q4/n25 elements in Figure 3.8c. Moreover, fairly close values for the compliances of the optimal topologies are observed for the same number of density elements and different number of design variables.

The convergence history of the iMTOP and the element-based approaches are compared in Figure 3.9a. During the optimization process, the compliance convergence history from the iMTOP and element-based approaches are fairly similar. The computational costs are compared in Figure 3.9b. As expected, the element-based approach on a fine mesh has the highest computational cost. The lower computational cost for the iMTOP approach is attributed to a lower number of finite elements, in comparison to element-based approach on a fine FE mesh, and to a lower number of design variables, in comparison to MTOP approach on the same FE mesh. Figure 3.9b shows that MTOP Q4/n25 is about three times less expensive than the element-based approach on a fine mesh. Moreover, the computational cost is further reduced for iMTOP Q4/n25/d16, Q4/n25/d9, and Q4/n25/d4. In this example, the computational cost of iMTOP Q4/n25/d4 is about 3.5 times less than that of MTOP Q4/n25 and about 10 times less than that of the element-based approach on a fine mesh. The computational cost saving in

iMTOP Q4/n25/d4 is attributed to a much lower number of design variables in comparison to that of MTOP Q4/n25. Therefore, the cost in the MMA optimization, the sensitivity analysis, and the projection is reduced.

The MBB example is further investigated using a minimum length scale equal to 1/20 of the height of the beam. First, for the same coarse FE mesh, the element-based approach provides checkerboard result (Figure 3.10b) which is undesirable while the MTOP and iMTOP approaches (Figure 3.10b and Figure 3.10c) provide results comparable to the element-based approach on fine mesh (Figure 3.10a). This is because the element-based approach cannot utilize a length scale smaller than or equal to the element size. Whereas, the results in Figure 3.10 show that MTOP and iMTOP can utilize a length scale equal to the size of the finite element. Second, the optimal topology by iMTOP Q4/n25/d4 in Figure 3.10d is slightly different from the topology by MTOP Q4/n25. However, these two designs have close optimal objective function values. The difference of these two optimal objective functions is only 0.3%. These results indicate the advantages of the iMTOP and MTOP approaches over the element-based approach when the same coarse FE mesh is employed.

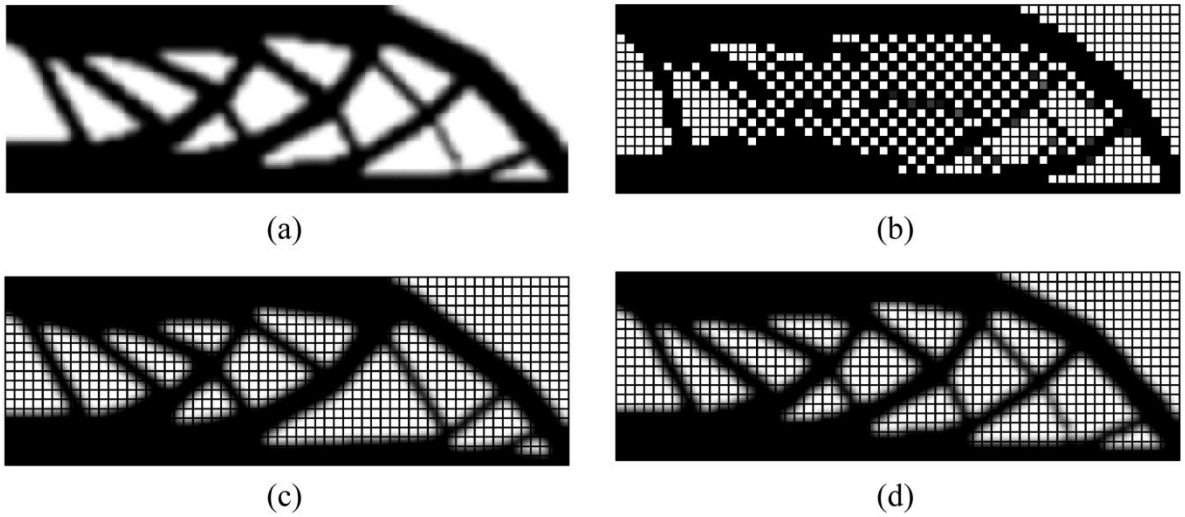

Figure 3.10: Topologies of MBB beam with r_{min}= 5% of height of the beam: (a) element-based Q4 FE mesh 300×100 (C=177.30); (b) element-based Q4 FE mesh 60×20 (C=163.58); (c) MTOP Q4/n25 (C=170.48); and (d) iMTOP Q4/n25/d4 (C=171.07) (b–d: FE mesh 60×20).

In summary, by using iMTOP elements, e.g. Q4/n25/d4, high-resolution topology comparable to MTOP Q4/n25 and element-based approach on a fine mesh can be obtained. However, the computational cost of iMTOP is much lower.

3.4.2 Compliant mechanism of a displacement inverter

The second example presents a 2D compliant mechanism problem, a displacement inverter as shown in Figure 3.7b. The goal is to design a structure to convert the input displacement on the left edge to a displacement on the right edge. The topology optimization seeks for the solution of maximum output displacement with a certain volume fraction of the domain. In this example, a domain of the size 40×20, a volume fraction of 0.3, and a length scale of 1.2 are employed.

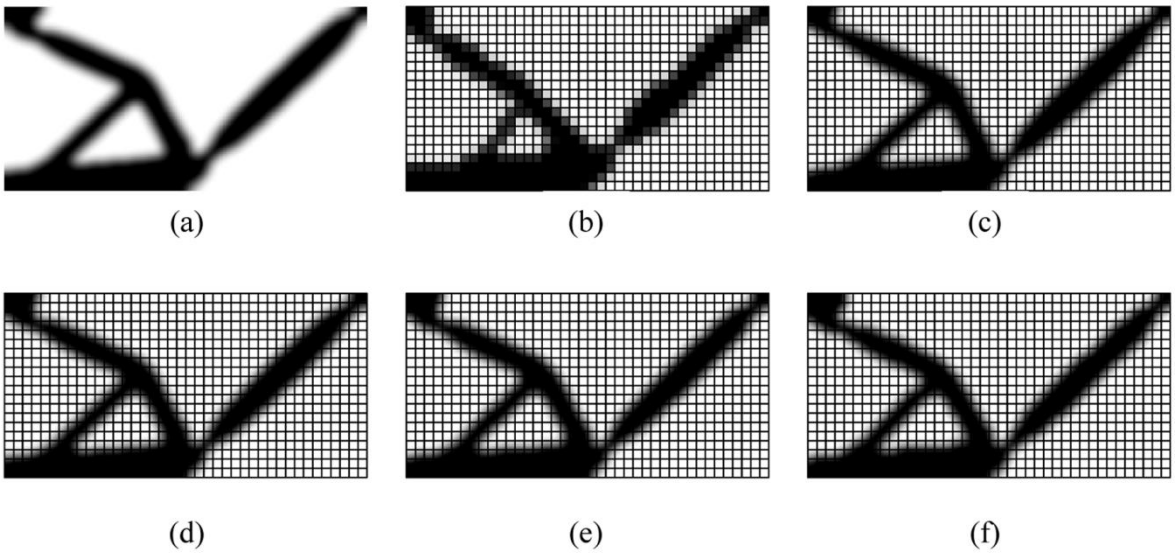

Figure 3.11: Topologies of the displacement inverter: (a) element-based Q4 FE mesh 200×100; (b) element-based Q4 FE mesh 40×20; (c) MTOP Q4/n25; (d) iMTOP Q4/n25/d16; (e) iMTOP Q4/n25/d9; and (f) iMTOP Q4/n25/d4 (b–f: FE mesh 60×20).

In a manner similar to the previous example, the element-based approach is performed on a fine mesh of 200×100 Q4 elements and on a coarse mesh of 40×20 Q4 elements. The optimal topologies from a fine mesh and a coarse mesh are shown in Figure 3.11a and Figure 3.11b, respectively. Next, the MTOP approach is performed using Q4/n25 elements, and the iMTOP

approach is performed using Q4/n25/d16, Q4/n25/d9 and Q4/n25/d4 elements – the optimal topologies are shown in Figures 3.11c, d, e and f, respectively. It can be seen that the topologies from the MTOP and the iMTOP approaches(Figures 3.11 c-f) using a coarse FE mesh are similar to the topology from the element-based approach using a fine FE mesh (Figure 3.11a), whereas the topology obtained from the element-based on coarse FE mesh (Figure 3.11b) is slightly different. This example illustrates that the proposed iMTOP approach can be applied to not only minimum compliance problems but also compliant mechanism problems.

3.4.3 Minimum compliance of a cantilever beam

This example demonstrates the adaptive multiresolution topology optimization procedure proposed in Section 3.3. A domain with a length of 32, a height of 16, and unit width is taken into consideration, as shown in Figure 3.12a. The beam is fixed at the left edge and a unit point load is applied downward at the midpoint of the right end. A volume fraction constraint *volfrac* is taken as 45%, the penalization parameter p is set equal to 4, and projection radius r_{min} is set equal to 1.2.

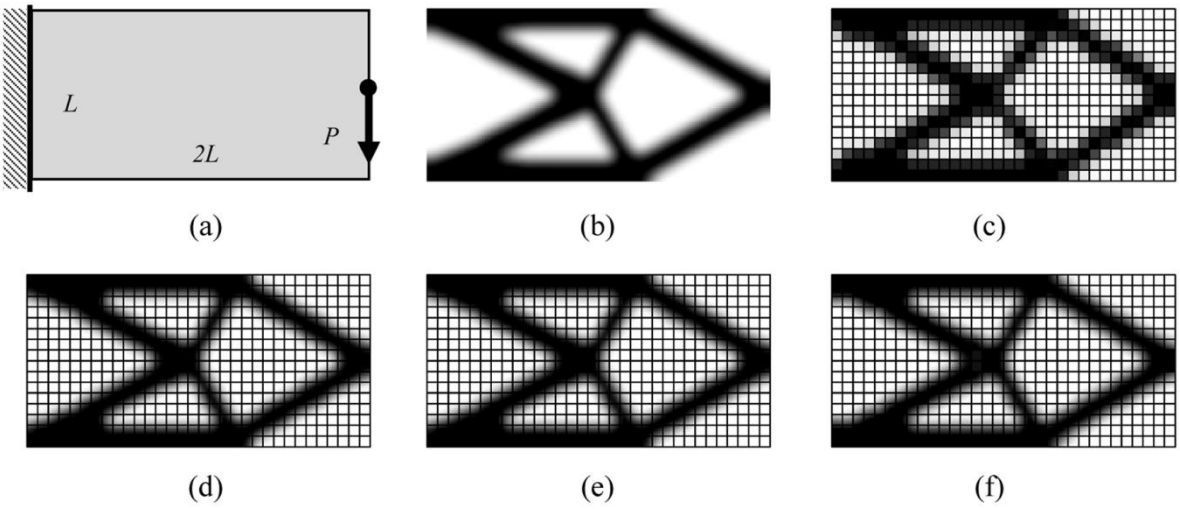

Figure 3.12: Cantilever example considering adaptive topology optimization: (a) geometry; (b) element-based Q4/U FE mesh 160×80 (C=90.11); (c) element-based Q4/U FE mesh 32×16 (C=87.41); (d) MTOP Q4/n25 (C=88.01); (e) iMTOP Q4/n25/d4 (C=88.03); (f) adaptive Q4/U and Q4/n25/d4 (C=88.71); and (c–f: FE mesh 32×16).

First, the topology optimization of the beam is performed by the element-based approach (Q4/U) on a fine FE mesh and also on a coarse FE mesh with the obtained topologies shown in Figure 3.12b and Figure 3.12c, respectively. The MTOP Q4/n25 and the iMTOP Q4/n25/d4 approaches provide the topologies shown in Figure 3.12c and Figure 3.12d, respectively. Finally, the adaptive procedure is performed using Q4/U and Q4/n25/d4 elements and the results are shown in Figure 3.12f. It is noted that the topology obtained by the adaptive scheme is similar to the topologies obtained by MTOP, iMTOP and the element-based approach on a fine mesh.

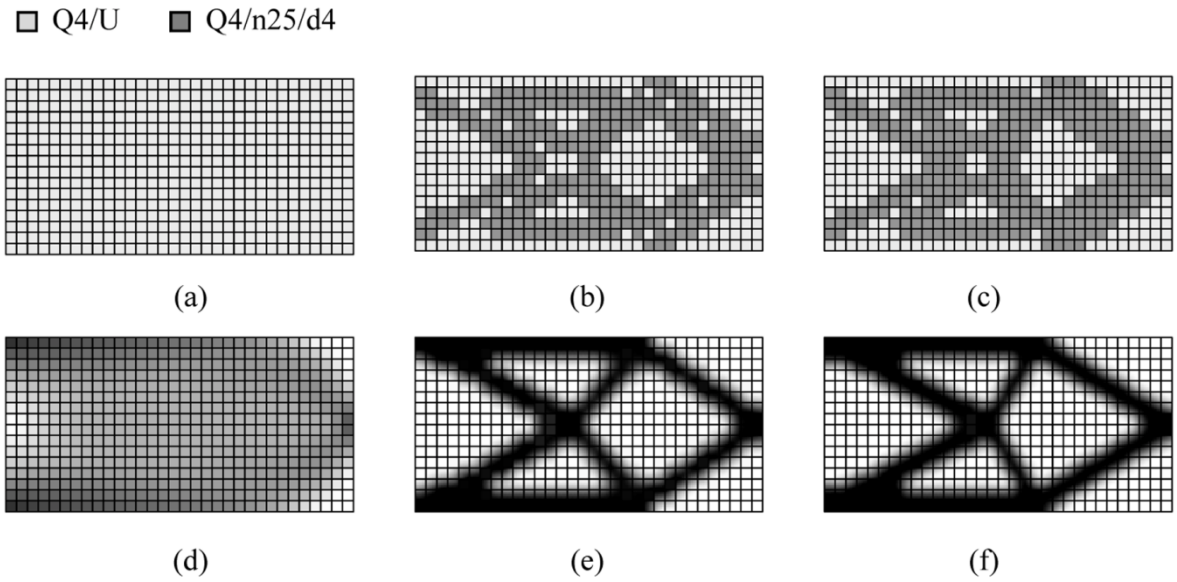

Figure 3.13: Adaptive topology optimization: (a) initial mesh (512 Q4/U); (b) intermediate mesh (244 Q4/U and 268 Q4/n25/d4); (c) final mesh (222 Q4/U and 290 Q4/n25/d4); and (d-e-f) initial, intermediate and final adaptive topologies, respectively.

Figure 3.13 explains the adaptive optimization process. At the initial stage, the optimization problem begins with a uniform distribution of the density over the domain. Therefore, only Q4/U elements are employed (a total of 512 elements), as shown in Figure 3.13a. The corresponding topology is shown in Figure 3.13d. As the optimization progresses, Q4/U elements are used for regions with uniform density (void or solid). In the “gray” regions, i.e. where structural boundaries are forming and thus more information is thus required, the iMTOP Q4/n25/d4 elements are used to increase the resolution. Figure 3.13b shows the mesh of an intermediate

iteration with 244 Q4/U and 268 Q4/n25/d4 elements while the corresponding topology is shown in Figure 3.13e. At the final iteration, the mesh is shown in Figure 3.13c with 222 Q4/U elements and 290 Q4/n25/d4 elements, and the corresponding topology is shown in Figure 3.13f. The adaptive procedure deciding *where* and *when* to use Q4/U or Q4/n25/d4 element is simple via the "*element index*" array described in Section 3.3.

The iMTOP approach reduces the numbers of density elements and design variables in comparison to the element-based approach on a fine mesh. Employing the adaptive approach further reduces the numbers of density/design variables to improve efficiency. In this specific example, the computational time for adaptive approach using Q4/U and Q4/n25/d4 elements (Figure 3.12f) is about 70% of that using iMTOP with Q4/n25/d4 elements (Figure 3.12e).

In summary, this example demonstrates that the adaptive procedure can further improve the efficiency of the iMTOP approach while maintaining the design resolution. In this example, Q4/U and Q4/n25/d4 elements are used in the adaptive procedure; however, it is noted that multiple iMTOP element types can be employed in the proposed approach (Nguyen et al., 2010d).

3.5 THREE-DIMENSIONAL NUMERICAL EXAMPLES

This section demonstrates the capability of the proposed schemes for handling relatively large-scale three-dimensional applications. First, a cube with a concentrated load at the bottom and a building subjected to a torsion load are presented to demonstrate the iMTOP scheme. Second, a three-dimensional cantilever beam is considered to demonstrate the adaptive procedure. Similarly to Section 3.4, all the quantities are dimensionless: Young's modulus is chosen as 1, and Poisson's ratio as 0.3.

3.5.1 A cube with a concentrated load at the bottom center

This example investigates a cube which is constrained at the four bottom corners in the vertical directions and subjected to a vertical load at the center of the bottom face as shown in Figure 3.14a. The cube domain has an edge length of L=48. The domain is divided into 24×24×24 B8 elements which results in a total of 13,824 brick elements. Because of the symmetry condition, only one fourth of the cube is taken into consideration. A volume fraction

constraint of 10%, a minimum length scale of $L/20$, and penalization parameter p=4 are employed.

First, the problem is solved using MTOP B8/n125 elements, which use 125 density elements and 125 design variables per a brick element. The optimal topology is shown in Figure 3.14b. Next, the iMTOP approach reduces the number of design variables by using B8/n125/d64, B8/n125/d27 and B8/n125/d8 elements. The corresponding topologies are shown in Figure 3.14c, Figure 3.14d, and Figure 3.14e, respectively. The resolutions of these designs are comparable to the design shown in Figure 3.14b using MTOP B8/n125 elements. Additionally, the values of the compliances of the optimal topologies obtained from MTOP and iMTOP, using the same number of density elements and a different number of design variables, are fairly close, as shown in the caption of Figure 3.14.

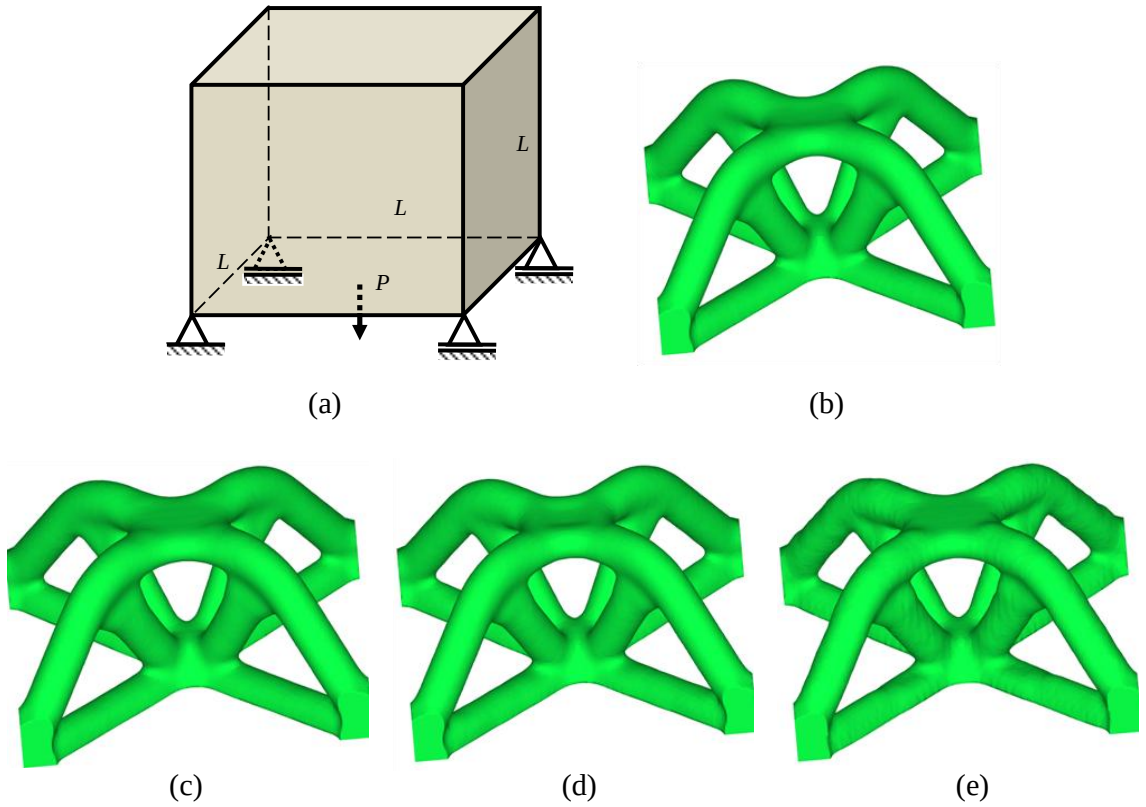

Figure 3.14: Topology optimization of a cube (FE mesh 24×24×24): (a) geometry; (b) MTOP B8/n125 (C=29.04); (c) iMTOP B8/n125/d64 (C=29.06); (d) iMTOP B8/n125/d27 (C=29.08); and (e) iMTOP B8/n125/d8 (C=29.33).

The convergence histories of the optimization process are shown in Figure 3.15a. Similarly to the 2D example in Section 3.4.1, Figure 3.15a shows fairly close convergence history for different iMTOP element types. The computational cost comparison is shown in Figure 3.15b. It is seen that the computational times of B8/n125/d64, B8/n125/d27, and B8/n125/d8 elements are much less than that of the MTOP B8/n125 element. For example, the computational time of B8/n125/d8 element is only one tenth of the B8/n125 element. This is because the iMTOP B8/n125/d8 element utilizes about 15 times fewer design variables than the MTOP B8/n125 element.

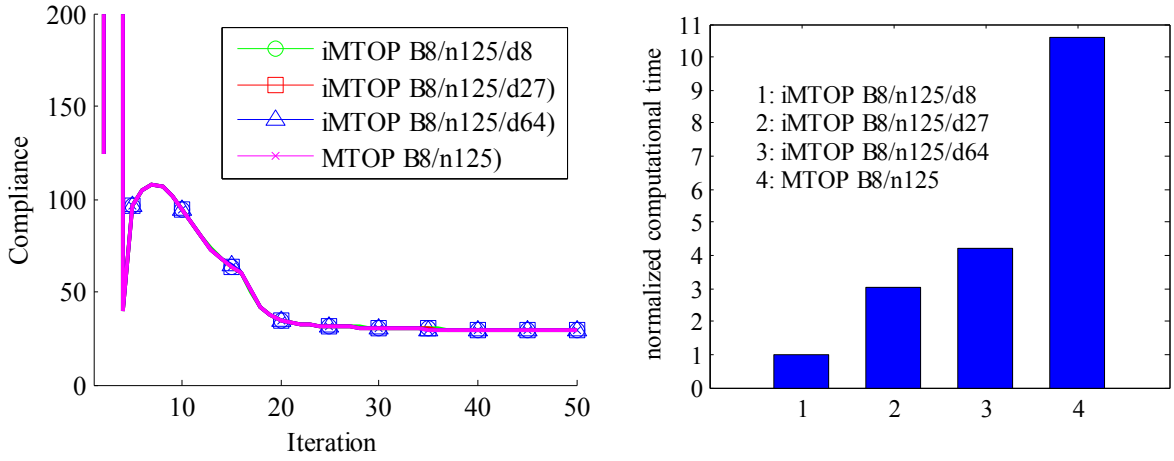

(a) (b)

Figure 3.15: Comparison of the results of cube optimization after 50 iterations: (a) convergence history; and (b) computational times.

3.5.2 A building with torsion loading

This example demonstrates the iMTOP scheme for the structure system of a building under torsion load. The domain is shown in Figure 3.16a with the dimension of $L\times L\times 4L$. Four unit loads are applied at the middle of the four top edges to create a torsion load. The domain is divided into 10×10×40 B8 elements which results in a total of 4,000 brick elements. The volume fraction constraint of 10%, the minimum length scale $r_{\min}=0.12L$, and penalization parameter $p=3$ are employed. Topologies based on different MTOP and iMTOP elements are shown in Figure 3.16. Similarly to the previous example, iMTOP elements using a fewer number of design

variables than density elements can provide topology comparable to the MTOP element. Moreover, the structural member arrangement shown in Figure 3.16 indicates that such a solution is somewhat similar to the Michell type optimal solution for a space-truss subjected to torsion loading (Rozvany, 1996).

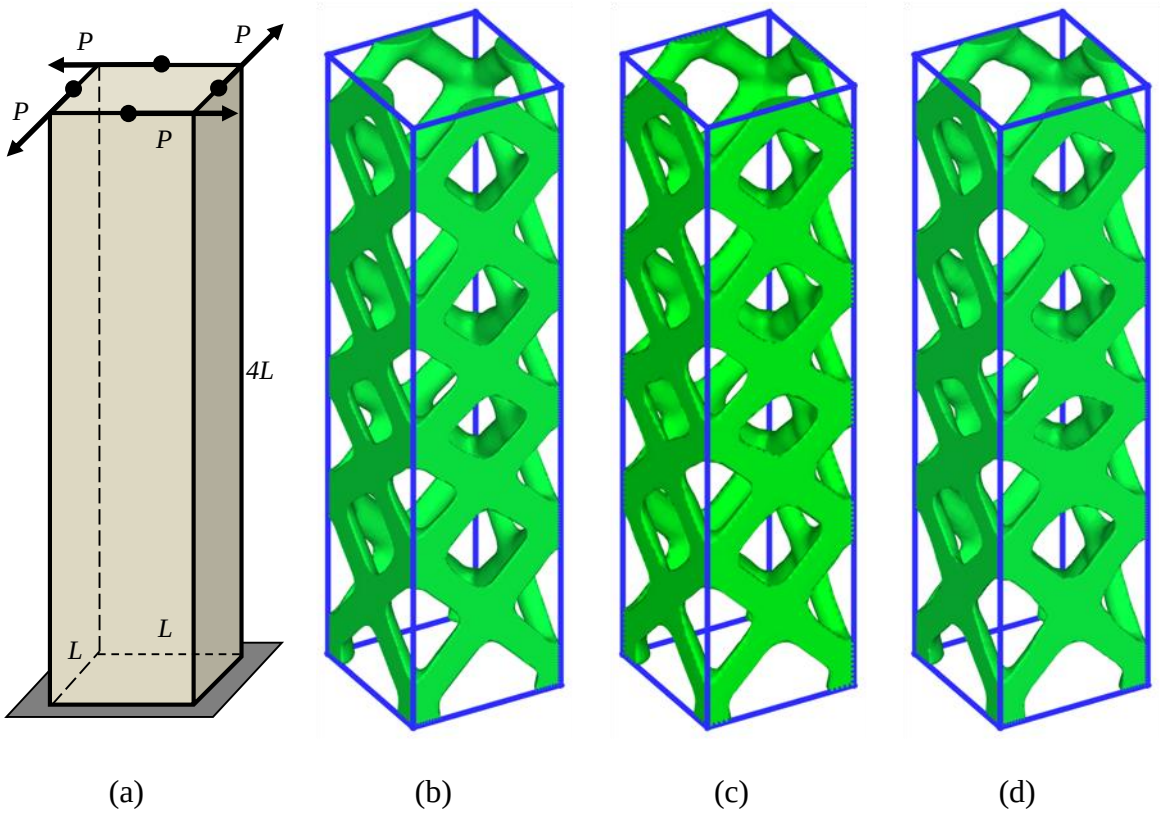

(a) (b) (c) (d)

Figure 3.16: Geometry and topologies of the building under torsion load: (a) geometry; (b) MTOP B8/n125; (c) iMTOP B8/n125/d27; and (d) iMTOP B8/n125/d8.

3.5.3 Cantilever beam with concentrated load

This example demonstrates the capability of the adaptive procedure for three-dimensional applications. A three-dimensional cantilever with the domain $2L\times L\times L$ shown in Figure 3.17a is considered. The domain is divided into 24×12×12 B8 elements which results in a total of 3,456 brick elements. A volume fraction constraint of 30%, a minimum length scale of one tenth of the beam height $r_{min}= L /10$, and penalization parameter p=3 are employed. First, the problem is solved using B8/U elements, which provides the results shown in Figure 3.17b. Second, the

iMTOP approach using B8/n125/d8 leads to the topology shown in Figure 3.17c. Finally, the adaptive approach using B8/U and B8/n125/d8 provides the optimal design shown in Figure 3.17d.

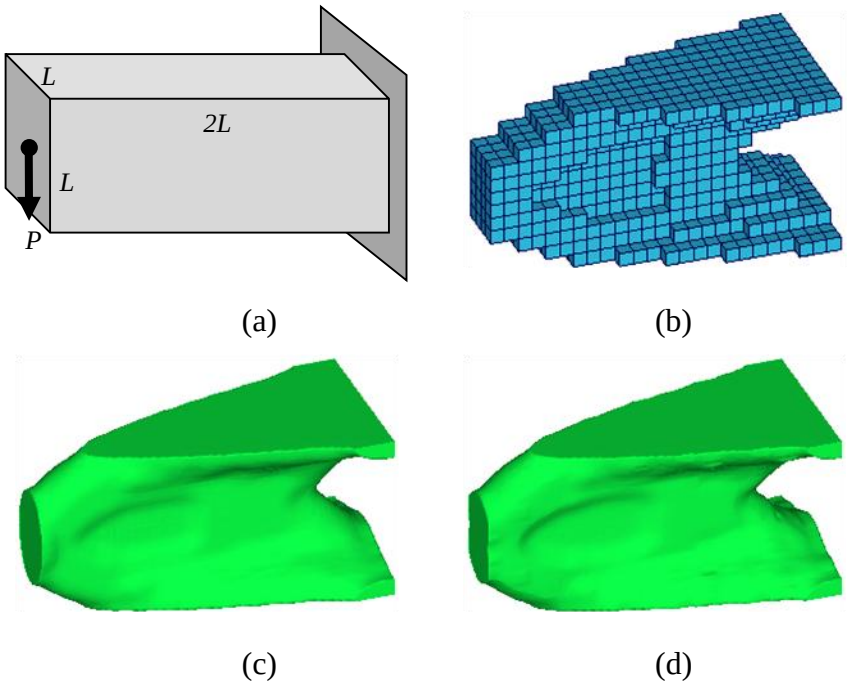

Figure 3.17: Topologies from element-based, iMTOP, and adaptivity on FE mesh 24×12×12: (a) geometry of a cantilever beam 3D (2:1:1); (b) element-based B8/U (*C*=5.088); (c) iMTOP B8/n125/d8 (*C*=5.182); and (d) adaptivity B8/U and B8/n125/d8 (*C*=5.283).

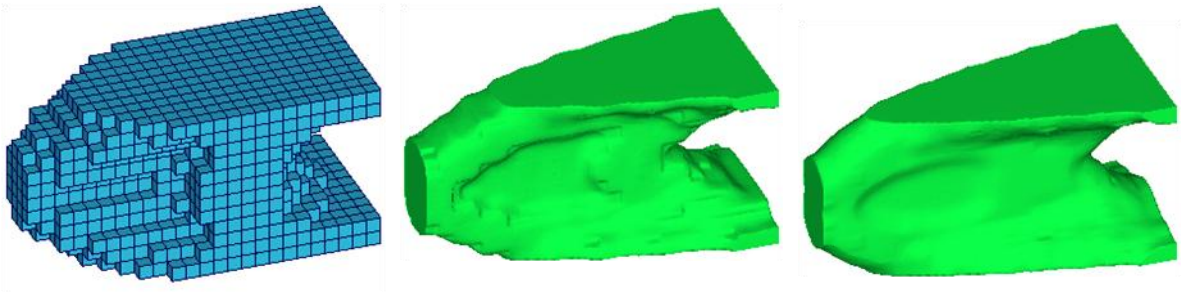

Figure 3.18: Adaptivity topology on FE mesh 24×12×12: (a) initial iteration 3,456 B8/U; (b) an intermediate iteration 2,288 B8/U and 1,168 B8/n125/d8; and (c) final iteration 2,072 B8/U and 1,384 B8/n125/d8.

Similar to the 2D cantilever beam in Section 3.4.3, the adaptive optimization process is shown in Figure 3.18. At the initial iteration, 3,456 B8/U elements are employed and the corresponding topology is shown in Figure 3.18a. An intermediate iteration is shown in Figure 3.18b with 2,288 B8/U and 1,168 B8/n125/d8 elements whereas the final iteration is shown in Figure 3.18c with 2,072 B8/U and 1,384 B8/n125/d8 elements. The adaptive procedure is successfully applied to this 3D example and the optimal topology is shown in Figure 3.17d. The result is comparable to the design using iMTOP B8/n125/d8 elements (Figure 3.17c).

3.6 EFFICIENCY AND RESOLUTION LEVEL

In this section, the computational cost and the achieved resolution for different iMTOP element types are discussed. Moreover, the computational costs in the above examples are compared.

3.6.1 iMTOP ratio – efficiency and resolution measurement

The efficiency and resolution of a topology optimization model can be measured in terms of the total numbers of finite elements, density elements, and design variables. Table 3.1 compares the iMTOP elements with the conventional element-based case, i.e. uniform density element and super-element (Paulino et al., 2008) as shown in Figure 3.19. First, the total number of finite elements is related to the total degrees of freedom in the linear equation of equilibrium. Second, the number of density elements determines the resolution of the design. In the element-based approach, each finite element contains one density element whereas in the super-element approach, each density element represents the densities of several neighboring finite elements. On the other hand, in the iMTOP approach, each finite element consists of a number of density elements. When the number of density elements increases, the resolution of the design increases. However, the computational cost related to stiffness matrix calculation, sensitivity analysis, and projection increases as well. Finally, the number of design variables determines the computational cost in optimization, sensitivity analysis and projection. A ratio is introduced to measure the efficiency and resolution of an iMTOP element type, termed as the “iMTOP ratio,” which is defined as follows

$$\text{iMTOP ratio} = k:n:d = (\text{the number of finite elements}):(\text{the number of density elements}):(\text{the number of design variables}) \tag{3.1}$$

For models with the same number of finite elements (k), the larger the number of density elements (n) is, the higher resolution is obtained. On the other hand, a smaller number of density elements and design variables indicate higher efficiency. Therefore, when models are considered with the same number of finite elements (k), it is desirable to have a larger number of density elements (k) and a smaller number of design variables (d).

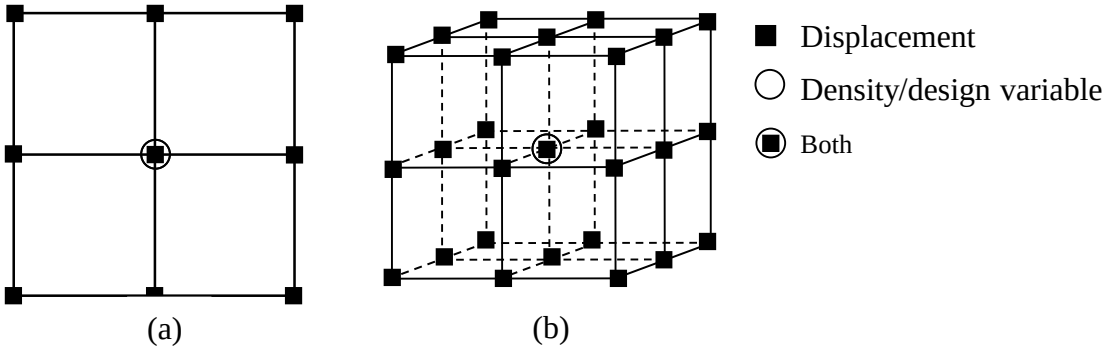

Figure 3.19: Super-element approach: (a) Q4/SE (one density/design variable for 4 Q4 elements); and (b) B8/SE (one density/design variable for 8 B8 elements).

It can be seen from Table 3.1 that the element-based approach has the ratio of k:n:d=1:1:1. The super-element approach, as shown in Figure 3.19, has the ratio k:n:d=4:1:1 for Q4 element or 8:1:1 for 3D brick element. The MTOP approach in Chapter 2 can provide higher resolution design, for example, the Q4/n25 element has the iMTOP ratio k:n:d=1:25:25. The proposed iMTOP approach in this study reduces the computational cost of the MTOP approach in Chapter 2 by reducing the number of design variables. For example, the Q4/n25/d4 element has the iMTOP ratio k:n:d=1:25:4. In addition, for the three-dimensional case, the iMTOP B8/n125/d8 element can improve the ratio significantly (k:n:d=1:125:8) in comparison to the MTOP B8/n125 element (k:n:d=1:125:125).

Table 3.1: Summary of iMTOP ratios for Q4 and B8 elements.

	Approaches	Element types	Number of			iMTOP ratio k:n:d
			finite elements	density elements	design variables	
2D: Q4	Super-element	Q4/SE	4	1	1	4:1:1
	Element-based	Q4/U	1	1	1	1:1:1
	MTOP	Q4/n25	1	25	25	1:25:25
	iMTOP	Q4/n25/d9	1	25	9	1:25:9
		Q4/n25/d4	1	25	4	1:25:4
3D: B8	Super-element	B8/SE	8	1	1	8:1:1
	Element-based	B8/U	1	1	1	1:1:1
	MTOP	B8/n125	1	125	125	1:125:125
	iMTOP	B8/n125/d15	1	125	15	1:125:15
		B8/n125/d8	1	125	8	1:125:8

3.6.2 Comparison of the computational time costs

In the numerical examples in Sections 3.4 and 3.5, the computational times in topology optimization using element-based approach, iMTOP approach, and adaptive approach are compared. For example, the normalized computational time is compared in Figure 3.9b and Figure 3.15b for 2D and 3D examples, respectively. The comparison has shown that the iMTOP approach is more efficient than the element-base approach to obtain a similar resolution design. However, the efficiency comparison shown in Figure 3.9b and Figure 3.15b may not reflect the same efficiency improvement in all cases. For example, one may employ a very fast solver, and then the computational cost of the element-based approach on fine mesh will get closer to the computational cost of the MTOP approach. Also, implementation of the code in different program languages may provide different efficiency improvement from the comparison in Figure 3.9b and 3.15b. Thus, the computational efficiency is described and compared in terms of the number of finite elements, density elements and design variables, and the iMTOP ratio.

Table 3.2: Computational data for the MBB beam and cube examples.

Examples	Approaches	Element types	Figures	Number of			iMTOP ratio k:n:d
				Finite elements	Density elements	Design variables	
MBB	Conv. fine mesh	Q4/U	3.8a	30,000	30,000	30,000	25:25:25
	MTOP	Q4/n25	3.8c	1,200	30,000	30,000	1:25:25
	iMTOP	Q4/n25/d16	3.8d	1,200	30,000	19,200	1:25:16
		Q4/n25/d9	3.8e	1,200	30,000	10,800	1:25:9
		Q4/n25/d4	3.8f	1,200	30,000	4,800	1:25:4
	Conv. coarse mesh	Q4/U	3.8b	1,200	1,200	1,200	1:1:1
Cube	Conv. fine mesh	B8/U	N/A	1,728,000	1,728,000	1,728,000	125:125:125
	MTOP	B8/n125	3.14b	13,824	1,728,000	1,728,000	1:125:125
	iMTOP	B8/n125/d64	3.14c	13,824	1,728,000	884,736	1:125:64
		B8/n125/d27	3.14d	13,824	1,728,000	373,248	1:125:27
		B8/n125/d8	3.14e	13,824	1,728,000	110,592	1:125:8

N/A: Not available, Conv.: Conventional

Table 3.2 shows the computational data for the 2D MBB beam example and the 3D cube example. It shows that the MTOP and iMTOP approaches require a smaller number of finite elements and design variables to achieve the same resolution designs as the conventional approach. For instance, in the cube example, in order to have the same resolution with the MTOP and iMTOP approaches using n=125 density elements per B8, the element-based approach has to utilize 1,728,000 finite elements. By contrast, the MTOP and iMTOP approaches employ only 13,824 finite elements. Moreover, the iMTOP approach can reduce the number of design variables from 1,728,000 in the MTOP approach (for B8/n125) to only 110,592 (for B8/n125/d8) while maintaining the same resolution. The "iMTOP ratio" of the computational data in Table 3.2 can serve as an indicator of the efficiency and resolution of a topology optimization model.

Table 3.3: Computational data of the cantilever examples.

Examples	Approaches	Element types	Figures	Number of			iMTOP ratio k:n:d
				Finite elements	Density elements	Design variables	
2D cantilever	Conventional fine mesh	Q4/U	3.12b	12,800	12,800	12,800	25:25:25
	MTOP	Q4/n25	3.12d	512	12,800	12,800	1:25:25
	iMTOP	Q4/n25/d4	3.12e	512	12,800	2,048	1:25:4
	Adaptive (initial iter.)	Q4/U	3.13a,d	512	512	512	1:1:1
	Adaptive (intermediate iter.)	Q4/U & Q4/n25/d4	3.13b,e	512	6,944	1,316	1:13.6:2.6
	Adaptive (final iter.)	Q4/U & Q4/n25/d4	3.13c,f	512	7,472	1,382	1:14.6:2.7
	Conventional coarse mesh	Q4/U	3.12c	512	512	512	1:1:1
3D cantilever	Conventional fine mesh	B8/U	N/A	432,000	432,000	432,000	125:125:125
	iMTOP	B8/n125/d8	3.17c	3,456	432,000	27,648	1:125:8
	Adaptive (initial iter.)	B8/U	3.18a	3,456	3,456	3,456	1:1:1
	Adaptive (intermediate iter.)	B8/U & B8/n125/d8	3.18b	3,456	148,288	11,632	1:42.9:3.4
	Adaptive (final iter.)	B8/U & B8/n125/d8	3.17d,18c	3,456	175,072	13,144	1:50.7:3.8
	Conventional coarse mesh	B8/U	3.17b	3,456	3,456	3,456	1:1:1

N/A: Not available, iter.: iteration

Additionally, Table 3.3 shows the computational data for the adaptive approach of the cantilever beam for 2D and 3D. It can be seen that the use of the adaptive approach can further

reduce the number of density elements and the number of design variables while maintaining the resolution. In the adaptive approach, the same number of finite elements is considered in the optimization process and the final design has the similar resolution with the iMTOP approach. Therefore, the iMTOP ratio in the adaptive approach with a lower number of density elements (n) and design variables (d) means more efficient model in comparison to the iMTOP approach. For example in the 2D cantilever, the "iMTOP ratio" is 1:1:1 for element-based approach on a coarse mesh. This ratio can be improved to 1:25:25 for MTOP Q4/n25 elements and 1:25:4 for iMTOP Q4/n25/d4 elements. The adaptive approach can further improve the iMTOP ratio to 1:14.5:2.5 at the final adaptive iteration. In the 3D case, the iMTOP ratio is improved since the iMTOP ratio changes from 1:125:8 in B8/n125/d8 elements to 1:50.7:3.8 at the final adaptive iteration. This means that a large number of density elements and design variables are reduced by the adaptive approach in comparison to the iMTOP and element-based approaches while a design with similar resolution is achieved.

3.7 CONCLUDING REMARKS

In this chapter, the MTOP approach in Chapter 2 is further improved by allowing different level of resolution between the design variable and density fields. A computational paradigm for improving multiresolution topology optimization (iMTOP) is developed using three distinct meshes: the finite element mesh, the density mesh, and the design variable mesh. Using a *relatively coarse* mesh for analysis, a *moderately fine* mesh for design variables, and a *relatively fine* mesh for density elements, high fidelity designs are obtained with a relatively low computational cost. Furthermore, an adaptive multiresolution topology optimization procedure is proposed to further reduce the computational cost in the iMTOP approach above by using the iMTOP elements only *where* needed and *when* needed. Therefore, the total numbers of density elements and design variables are potentially less than in the original iMTOP approach. The techniques are verified by various two- and three-dimensional numerical examples.

CHAPTER 4 – SINGLE-LOOP SYSTEM RELIABILITY-BASED DESIGN OPTIMIZATION USING MATRIX-BASED SYSTEM RELIABILITY METHOD

This chapter proposes a single-loop system reliability-based design optimization (SRBDO) approach using a matrix-based system reliability (MSR) method. A single-loop method is employed to eliminate the inner loop of SRBDO that evaluates probabilistic constraints. The MSR method enables us to compute the system failure probability and its parameter sensitivities efficiently and accurately through convenient matrix calculations. The SRBDO/MSR approach proposed in this thesis is applicable to general systems including series, parallel, cut-set and link-set system events. After a brief overview on SRBDO algorithms and the MSR method, the SRBDO/MSR approach is introduced. Three numerical examples demonstrate the proposed approach. The results based on different optimization approaches are compared for further investigation. Monte Carlo simulation is performed on each example to confirm the accuracy of the system failure probability computed by the MSR method.

4.1 INTRODUCTION

The main objective of design optimization is to obtain the values of design variables that minimize or maximize the objective function(s) of interest while satisfying given design constraints. If design optimization is performed in a deterministic manner, that is, uncertainties are not taken into account during the optimization; the resultant optimal design may have unquantified risk of violating the given constraints. Various reliability-based design optimization (RBDO) methods have been developed to achieve optimal designs with acceptable failure probabilities (see Refs. (Frangopol and Maute, 2005) and (Tsompanakis et al., 2008) for a state-of-the-art review of RBDO methods and recent applications to civil and aerospace structural systems). During RBDO, the probability of violating given constraint(s), namely, the failure

probability, is often computed by reliability analysis methods such as first-order reliability method (FORM), second-order reliability method (SORM) (see Ref. (Der Kiureghian, 2005) for a comprehensive review of FORM and SORM methods) or response surface methods.

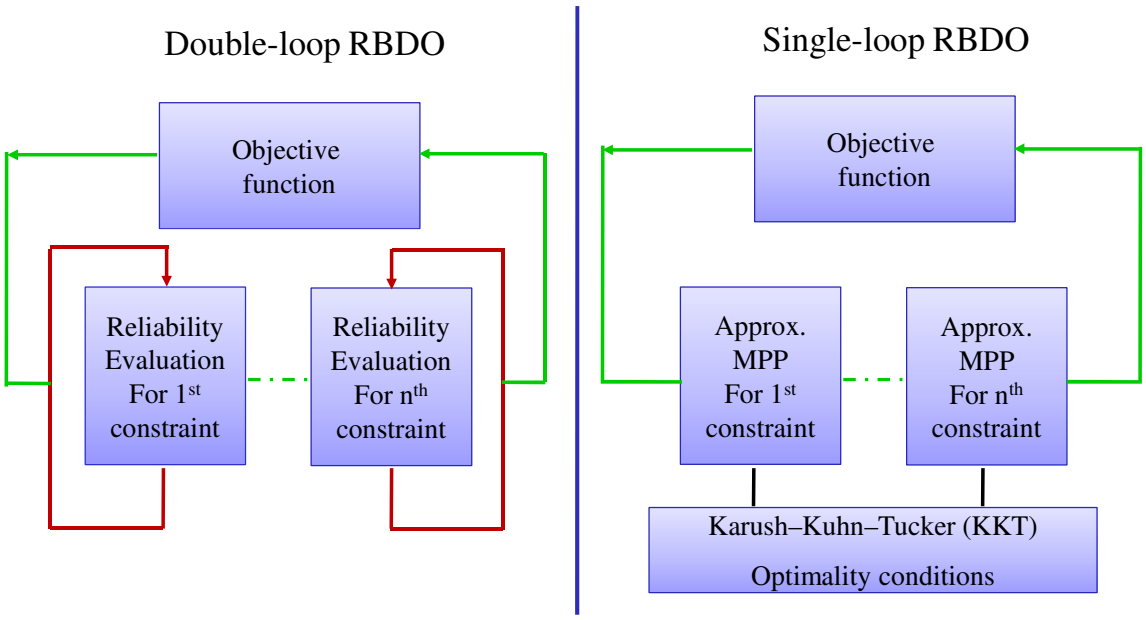

Figure 4.1: Double-loop and single-loop RBDOs.

Traditionally, RBDO has been performed by use of a nested or "double loop" approach, in which each step of the iterations for design optimization involves another loop of iteration for reliability analysis as shown in Figure 4.1. For example, the reliability index approach (RIA: Enevoldsen and Sørensen, 1994) and performance measure approach (PMA; Tu et al., 1999) employ FORM to perform the reliability analysis, which requires nonlinear constrained optimization. If the constraints are active, the two approaches yield the same results. However, it is known that PMA is generally more efficient and stable than RIA (Tu et al., 1999; Youn et al., 2003). These double loop computations can be prohibitive if the function evaluation cost is expensive because the inner-loop often involves iterative reliability analysis to search for the most probable point (MPP) (Yang et al., 2005; Youn et al., 2005; Shan and Wang, 2008). As an effort to overcome the computational burden of RBDO, many approximate RBDO approaches have been developed to decouple the double-loop (Thanedar and Kodiyalam, 1992; Wu and

Wang, 1998; Du and Chen, 2000; Kuschel and Rackwitz, 2000; Royset et al., 2001; Du and Chen, 2004; Streicher and Rackwitz, 2004; Chan et al., 2007; Liang et al., 2008; Shan and Wang, 2008). For example, a single-loop approach (Liang et al., 2008) was proposed by using the Karush-Kuhn-Tucker (KKT) optimality condition to approximate the solution of the inner-loop optimization as shown in Figure 4.1. As a result, the inner-loop is replaced by a deterministic procedure, which transforms a double-loop RBDO problem into an equivalent single-loop optimization problem.

When multiple failure modes need to be considered as the constraints of a design optimization, RBDO is often formulated such that the optimal structure satisfies each failure mode with predetermined probabilities. This approach is termed as "component reliability-based design optimization (CRBDO)" in this study. In some cases, however, the failure event needs to be described by a system event, i.e. a logical (or Boolean) function of multiple failure modes. In this case, the probabilistic constraint should be given for the system event, not on individual component failure modes. This approach is called "system reliability-based design optimization (SRBDO)." The SRBDO requires system reliability analysis, which is not trivial especially for systems with statistically dependent component events, or for events that are not series or parallel systems. Theoretical bounding formulas are applicable to parallel and series systems only (see Ref. (Song and Der Kiureghian, 2003) for a review), and it is difficult to deal with probability bounds during RBDO. Various sampling methods are available, but they may render SRBDO inefficient in practice. Song and Kang (2009) recently developed a matrix-based system reliability (MSR) method that computes the system reliability by convenient matrix-based framework. The MSR method is applicable to general system events including series, parallel, cut-set and link-set systems while statistical dependence between component events are considered. It also provides parameter sensitivities of the failure probability for general system events, which are useful during RBDO.

In this chapter, the single-loop SRBDO approach is integrated with the MSR method (SRBDO/MSR) to overcome aforementioned challenges in SRBDO. The remainder of this chapter is structured as follows: Section 4.2 describes an overview of existing RBDO formulations; Section 4.3 presents the MSR method and proposes the single-loop SRBDO/MSR

procedure; Section 4.4 demonstrates the proposed SRBDO/MSR approach by three numerical examples; and finally Section 4.5 provides concluding remarks of this chapter.

4.2 SYSTEM RELIABILITY-BASED DESIGN OPTIMIZATION

4.2.1 Component reliability-based design optimization

In general, RBDO problems are formulated as follows:

$$\begin{aligned} \min_{\mathbf{d},\boldsymbol{\mu}_\mathbf{X}} \quad & f(\mathbf{d},\boldsymbol{\mu}_\mathbf{X}) \\ s.t. \quad & P\left[g_i(\mathbf{d},\mathbf{X}) \le 0\right] \le P_i^t, \quad i=1,...,n \\ & \mathbf{d}^L \le \mathbf{d} \le \mathbf{d}^U, \qquad \boldsymbol{\mu}_\mathbf{X}^L \le \boldsymbol{\mu}_\mathbf{X} \le \boldsymbol{\mu}_\mathbf{X}^U \end{aligned} \tag{4.1}$$

where $\mathbf{d} \in \Re^k$ is the vector of deterministic design variables; $\mathbf{X} \in \Re^m$ is the vector of random variables; $\boldsymbol{\mu}_\mathbf{X}$ is the vector of the means of $\mathbf{X}$; $f(.)$ is the objective function; $g_i(.),\ i=1,\ldots,n$ is the *i*-th limit-state function indicating the occurrence of the failure by $g_i(.) \le 0$; P_i^t is the constraint on the probability of the *i*-th limit-state; $\mathbf{d}^L$ and $\mathbf{d}^U$ are the lower/upper bounds on $\mathbf{d}$; $\boldsymbol{\mu}_\mathbf{X}^L$ and $\boldsymbol{\mu}_\mathbf{X}^U$ are the lower/upper bounds on $\boldsymbol{\mu}_\mathbf{X}$ (for simplicity, these boundary values will be omitted in the following RBDO formulations); and *n*, *k*, *m* are the number of constraints, deterministic design variables, and random variables, respectively. The probabilistic constraint in Equation (4.1) can be given alternatively by use of the cumulative distribution function (CDF) of the limit state function, that is,

$$P[g_i(\mathbf{d},\mathbf{X}) \le 0] = F_{g_i}(0) \le \Phi(-\beta_i^t) \tag{4.2}$$

where $F_{g_i}(\cdot)$ denotes the CDF of $g_i(\cdot)$; $\Phi(\cdot)$ is the CDF of the standard normal distribution; and β_i^t is the target reliability index. First-order reliability method (FORM) (Der Kiureghian, 2005) is widely employed to compute failure probability in Equation (4.2) (Nguyen et al., 2006; Song et al., 2006). In all the numerical examples of this chapter, FORM is used for component-level reliability analysis.

This RBDO problem has two nested optimization loops: the outer-loop for design optimization and the inner-loop for reliability analysis. One of the common double-loop

approaches available for RBDO is the reliability index approach (RIA; Enevoldsen and Sørensen, 1994) which uses the formulation:

$$\begin{aligned} &\min_{\mathbf{d},\boldsymbol{\mu}_\mathbf{X}} \quad f(\mathbf{d},\boldsymbol{\mu}_\mathbf{X}) \\ &s.t. \quad \beta_i = -\Phi^{-1}\left[F_{g_i}(0)\right] \geq \beta_i^t \quad i=1,...,n \end{aligned} \tag{4.3}$$

where β_i is the distance from the origin of the space of standard normal random variables $\mathbf{U} = \mathbf{U}(\mathbf{X})$ to the nearest point on the limit state surface $G_i(\mathbf{d},\mathbf{U}) = 0$ in which $G_i(\cdot)$ is the limit-state function $g_i(\cdot)$ determined in terms of $\mathbf{U}$, that is, $g_i(\mathbf{d},\mathbf{X}) = G_i(\mathbf{d},\mathbf{U}(\mathbf{X}))$. This distance β_i is termed as "reliability index." The nearest point on the limit state surface, often termed as "design point" or "most probable failure point" (MPP) is identified by solving a nonlinear constrained optimization (Der Kiureghian, 2005):

$$\begin{aligned} &\mathbf{U}_i^* = \arg\min_{\mathbf{U}} \ \|\mathbf{U}\| \\ &s.t. \quad G_i(\mathbf{d},\mathbf{U}) = 0 \end{aligned} \tag{4.4}$$

where $\mathbf{U}_i^*$ is the MPP of the *i*-th limit state function, and "arg min" denotes the argument of the minimum of a function.

The RIA formulation in Equation (4.3) can be inefficient if the constraints are inactive. Moreover, the algorithm may not provide an optimal design solution if the failure events $G_i(\mathbf{d},\mathbf{U}) \leq 0$ never occur in the given feasible domain. To overcome these issues, Tu et al. (1999) proposed the performance measure approach (PMA) in which the probabilistic constraint is described in terms of "performance function," which is defined as the quantile of the limit-state function $g_i(\cdot)$ at the target failure probability $\Phi(-\beta_i^t)$. It is thus formulated as

$$\begin{aligned} &\min_{\mathbf{d},\boldsymbol{\mu}_\mathbf{X}} \quad f(\mathbf{d},\boldsymbol{\mu}_\mathbf{X}) \\ &s.t. \quad g_{p_i} = F_{g_i}^{-1}\left[\Phi(-\beta_i^t)\right] \geq 0 \quad i=1,...,n \end{aligned} \tag{4.5}$$

where g_{p_i} is the performance function. The constraint in Equation (4.5) implies that $F_{g_i}(g_{p_i}) = \Phi(-\beta_i^t)$ is greater than $F_{g_i}(0) = \Phi(-\beta_i)$, so it is equivalent to the constraint in Equation

(4.3), $\beta_i \geq \beta_i^t$. The performance function can be obtained by solving a constrained optimization problem (Tu et al., 1999; Du et al., 2004; Youn et al., 2005).

$$\begin{aligned} g_{p_i} &= \min_{\mathbf{U}} \; G_i(\mathbf{d}, \mathbf{U}) \\ s.t. \quad & \|\mathbf{U}\| = \beta_i^t \end{aligned} \tag{4.6}$$

To improve the efficiency of these double-loop RBDOs, several single-loop RBDO approaches have been developed. For example, a sequential optimization and reliability assessment (SORA) method was recently proposed (Du and Chen, 2004). The idea is to decouple the outer-loop optimization from reliability analysis. Using the information from the previous design iteration, the boundaries of the constraints are shifted to the feasible direction and the design point is updated accordingly. Additionally, the safety-factor approach (Wu and Wang, 1998), one of the single-loop approaches, was developed by using the approximate equivalent deterministic constraint to convert the double-loop into single-loop problem. The efficiency of the double-loop approach can be enhanced by some efficiency strategies such as the enriched performance measure approach (PMA+) (Youn et al., 2005). It was reported that with such efficiency strategies, the double-loop approach can be significantly improved (Yang et al., 2005; Youn et al., 2005).

Recently, Liang et al. (2008) proposed a single-loop RBDO by approximating the result of the nonlinear constrained optimization in Equation (4.6) by solving the system equation that describes the Karush-Kuhn-Tucker (KKT) condition:

$$\begin{aligned} &\nabla_{\mathbf{U}} G_i(\mathbf{d}, \mathbf{U}) + \lambda \cdot \nabla_{\mathbf{U}} \left(\|\mathbf{U}\| - \beta_i^t \right) = 0 \\ &\|\mathbf{U}\| - \beta_i^t = 0 \end{aligned} \tag{4.7}$$

in which λ denotes a Lagrange multiplier. Next, the "negative normalized gradient vector" (Der Kiureghian, 2005) of the limit-state function at the solution of Equation (4.6) is approximately obtained by evaluating it at the solution of Equation (4.7), $\mathbf{U} = \tilde{\mathbf{U}}_i$, that is

$$\hat{\boldsymbol{\alpha}}_i^t \cong \left(-\frac{\nabla_{\mathbf{X}} g_i(\mathbf{d}, \mathbf{X}(\mathbf{U}))}{\left\| \nabla_{\mathbf{X}} g_i(\mathbf{d}, \mathbf{X}(\mathbf{U})) \right\|} \mathbf{J}_{\mathbf{X},\mathbf{U}} \right)_{\mathbf{U}=\tilde{\mathbf{U}}_i} \tag{4.8}$$

where $\mathbf{J}_{\mathbf{X},\mathbf{U}}$ is the Jacobian of the $\mathbf{X}=\mathbf{X}(\mathbf{U})$ transformation. The solution of Equation (4.6) is then approximated by scaling this unit vector by the target reliability index, i.e.

$$\mathbf{U}_i^t \cong \beta_i^t \hat{\boldsymbol{\alpha}}_i^t \tag{4.9}$$

The performance function is approximated by evaluating the limit-state function at $\mathbf{U}_i^t$. As a result, the RBDO is formulated as

$$\begin{aligned} &\min_{\mathbf{d},\boldsymbol{\mu}_\mathbf{X}} \quad f(\mathbf{d},\boldsymbol{\mu}_\mathbf{X}) \\ &s.t. \quad g_{p_i} \cong g_i\left(\mathbf{d},\mathbf{X}(\mathbf{U}_i^t)\right) \geq 0 \quad i=1,...,n \end{aligned} \tag{4.10}$$

In summary, the inner-loop of the PMA RBDO is replaced by the approximate, non-iterative procedures shown in Equations (4.7)–(4.9). Figure 4.2 illustrates the approximation scheme of the single-loop RBDO algorithm. This single-loop approach was reported to have the accuracy comparable with the double-loop approach and the efficiency almost equivalent to deterministic optimization (Liang et al., 2008). This study aims to improve this single-loop RBDO approach when *system* reliability analysis is needed for failure probability calculations.

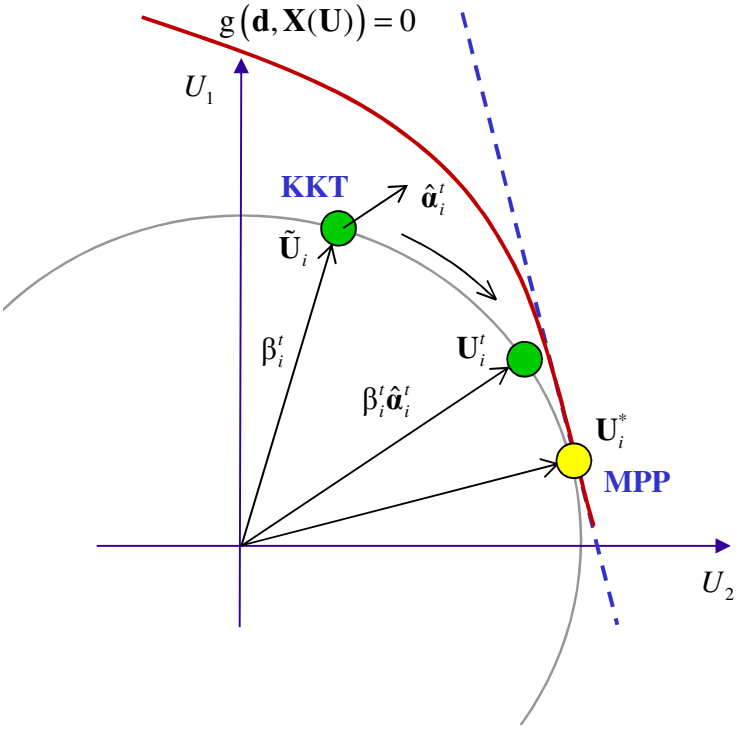

Figure 4.2: Approximation scheme in the single-loop RBDO algorithm.

4.2.2 System reliability-based design optimization

In the case when the failure event in the design constraint needs to be described by a system event, i.e. a logical (Boolean) function of multiple component events, the RBDO requires a system reliability analysis. This system reliability-based design optimization (SRBDO) can be formulated as

$$\begin{aligned} &\min_{\mathbf{d},\boldsymbol{\mu}_\mathbf{X}} \quad f(\mathbf{d},\boldsymbol{\mu}_\mathbf{X}) \\ &s.t. \qquad P_{\text{sys}}=P(E_{\text{sys}})=P\left[\bigcup_{k}\bigcap_{i\in C_k} \text{g}_i(\mathbf{d},\mathbf{X})\le 0\right]\le P_{sys}^t \end{aligned} \tag{4.11}$$

where P_{sys} is the system failure probability; E_{sys} is the system failure event; C_k is the index set of the components in the *k*-th cut-set; and P_{sys}^t is the target system failure probability. Any type of system event may be used during SRBDO but, for illustration purpose, Equation (4.11) shows a cut-set system formulation that can represent series, parallel, and cut-set systems. Royset et al. (2001) proposed a decouple procedure for reliability and optimization calculations of the SRBDO problem (4.11) for series system. The target system reliability is satisfied by adjusting the target component reliabilities heuristically.

An SRBDO approach was proposed for series system problems in (Ba-Abbad et al., 2006). In this approach, the failure probability of a series system is approximated as the sum of the component failure probabilities, i.e.,

$$P_{sys}=\text{P}\left[\bigcup_{i=1}^{n} g_i(\mathbf{d},\mathbf{X})\le 0\right]\cong \min\left(1,\sum_{i=1}^{n} P_i\right) \tag{4.12}$$

Then, SRBDO problems are formulated as

$$\begin{aligned} &\min_{\mathbf{d},\boldsymbol{\mu}_\mathbf{X},P_1^t,\ldots,P_n^t} \quad f(\mathbf{d},\boldsymbol{\mu}_\mathbf{X}) \\ &s.t. \qquad \text{P}\left[g_i(\mathbf{d},\mathbf{X})\le 0\right]\le P_i^t \quad i=1,\ldots,n \\ &\qquad\qquad P_{sys}\cong \min\left(1,\sum_{i=1}^{n} P_i^t\right)\le P_{sys}^t \end{aligned} \tag{4.13}$$

Note that the constraints on the component probabilities, P_i^t's, are used as design variables. This approach can significantly overestimate the system risk because the approximation in Equation (4.12) provides a fairly conservative upper bound, see Ref. (Song and Der Kiureghian, 2003) for a review on system reliability bounding formulas. Moreover, this approach cannot account for the effect of the statistical dependence between component events, which is caused by common random variables or statistical correlation between random variables.

A single-loop SRBDO approach was recently proposed for series systems by Liang et al. (2007). This approach also uses P_i^t's as design variables. The inner loop is eliminated by approximating the design points by KKT conditions as explained above. The system failure probability is approximated by the upper bound in the bi-component theoretical bounding formula (Ditlevsen, 1979). As a result, the single-loop SRBDO is formulated as

$$\begin{aligned} \min_{\mathbf{d},\boldsymbol{\mu}_\mathbf{X},P_1^t,\ldots,P_n^t} \quad & f(\mathbf{d},\boldsymbol{\mu}_\mathbf{X}) \\ s.t. \quad & g_i(\mathbf{d},\mathbf{X}(\mathbf{U}_i^t)) \geq 0 \quad i=1,\ldots,n \\ & P_{sys} \cong \sum_{i=1}^{n} P_i^t - \sum_{i=2}^{n} \max_{j<i} P_{ij}^t \leq P_{sys}^t \end{aligned} \tag{4.14}$$

in which $\mathbf{U}_i^t$ is obtained by Equations (4.7)–(4.9); and P_{ij}^t is the joint failure probability of the i-th and j-th constraints, computed by a numerical integration based on P_i^t, P_j^t and the inner product of approximated negative normalized gradient vectors (Liang et al., 2007). Despite its improved accuracy in estimating the system failure probability by using a higher-order bounding formula, it still overestimates the system failure probability and is not applicable to non-series system events for which general theoretical bounding formulas are not available.

The matrix-based system reliability (MSR) method is employed to compute P_{sys} in the single-loop SRBDO shown in Equation (4.14). The method enables us to compute P_{sys} of general system events including series, parallel, cut-set and link-set systems efficiently and accurately during SRBDO. The sensitivity of P_{sys} with respect to design variables further facilitates the use of gradient-based optimization algorithms.

4.3 SYSTEM RELIABILITY-BASED DESIGN OPTIMIZATION USING MSR METHOD

4.3.1 Matrix-based system reliability (MSR) method

Although system reliability analysis is a well established research area, it is still challenging to compute the probability of a general system event and its parameter sensitivity, especially when component events are statistically dependent. Song and Der Kiureghian (2003) introduced a method to compute the bounds on the probability of a general system event by linear programming (LP). This "LP bounds" method subdivides the sample space of component events into the mutually exclusive and collectively exhaustive events (termed as basic MECE events), and the probability of any event is described by use of vectors representing the probabilities of basic MECE events. Then, its upper and lower bounds are obtained by solving the LP problems subjected to the constraints derived from given information such as component probabilities and statistical dependence. This matrix-based framework of system reliability analysis enables obtaining the narrowest possible bounds on the probability of any general system, and the parameter sensitivities of the bounds (Song and Der Kiureghian, 2005) as well.

Song and Kang (2009) recently proposed the matrix-based system reliability (MSR) method to compute the probability of general system events in a uniform manner by use of simple matrix calculation instead of solving LP. Consider a system event with n components each of which has two distinct states, e.g., "failure" and "safe." Then, the sample space can be subdivided into $N = 2^n$ basic MECE events, denoted by e_j, $j = 1,...,N$. Then any system event can be presented by an "event" vector $\mathbf{c}$ whose j-th element is 1 if e_j belongs to the system event and 0 otherwise. Let $p_i = P(e_j),\ j = 1,...,N,$ denote the probability of e_j. Because e_j's are mutually exclusive to each other, the probability of system event, P_{sys} is simply the sum of the probability of e_j's that belong to the system event E_{sys}. Therefore, the system probability is computed by the inner-product of the two vectors.

$$P_{\text{sys}} = \sum_{j:e_j \subseteq E_{sys}} p_j = \mathbf{c}^{\mathrm{T}}\mathbf{p} \tag{4.15}$$

where $\mathbf{p}$ is the "probability" vector that contains p_j's, $j = 1,...,N$. Both $\mathbf{c}$ and $\mathbf{p}$ are column vectors in this study, and can be constructed efficiently using matrix-based procedures proposed

in (Song and Kang, 2009). The method has been further developed and successfully applied to various system reliability problems (Kang et al., 2008; Kang et al., 2010; Song and Ok, 2010; Lee et al., 2010b).

When component events are statistically dependent, the construction of **p** requires numerous system reliability analyses for each element. This challenge can be overcome by achieving conditional independence between component events given outcomes of a few random variables representing the sources of "environment dependence" or "common source effects." For example, during a risk analysis of a transportation network based on bridge failure probabilities, the uncertain magnitude of earthquake was considered as a random variable representing the common source effect (Kang et al., 2008). Let **S** denote the vector of such random variables, named "common source random variables" (CSRV). By the total probability theorem, the system failure probability can be then computed as

$$\begin{aligned} P_{\text{sys}} &= \int_{\mathbf{s}} P\left(E_{sys} \mid \mathbf{s}\right) f_{\mathbf{S}}\left(\mathbf{s}\right) d\mathbf{s} \\ &= \int_{\mathbf{s}} \mathbf{c}^{\mathrm{T}} \mathbf{p}(\mathbf{s}) f_{\mathbf{S}}\left(\mathbf{s}\right) d\mathbf{s} \end{aligned} \tag{4.16}$$

where $P(E_{\text{sys}} \mid \mathbf{s})$ is the conditional probability of the system event given an outcome of CSRV, $\mathbf{S}=\mathbf{s}$; $f_{\mathbf{S}}(\mathbf{s})$ is the joint probability density function (PDF) of $\mathbf{S}$; and $\mathbf{p}(\mathbf{s})$ is the conditional probability vector given $\mathbf{S}=\mathbf{s}$, which can be constructed efficiently by the proposed matrix-based procedure employing conditional probabilities of component events given $\mathbf{S}=\mathbf{s}$, i.e. $P_i(\mathbf{s}) = P(E_i \mid \mathbf{S}=\mathbf{s})$ instead of the marginal probabilities $P_i = P(E_i)$.

The approach in Equation (4.16) can be used even in the case when the CSRVs are not explicitly identified. One way to identify such implicit common source effect as CSRVs is to fit the correlation coefficient matrix of random variables representing component events such as safety margin (or factor) with a special correlation matrix model that allows such identification. For example, Song and Kang (2009) generalized Dunnett-Sobel (DS) class correlation matrix (Dunnett and Sobel, 1955) to identify CSRVs. Consider correlated standard normal random variables Z_i, $i=1,...,n$. Their correlation matrix can be fit with the following generalized DS model through an optimization:

$$Z_i = \left(1 - \sum_{k=1}^{m} r_{ik}^2\right)^{0.5} Y_i + \sum_{k=1}^{m} r_{ik} S_k, \text{ for } i = 1, \ldots, n \tag{4.17}$$

in which Y_i, $i = 1,...,n$ and S_k, $k = 1,...,m$ are uncorrelated standard normal random variables; and r_{ik}'s are the coefficients of the generalized DS model that determine the correlation coefficient between Z_i and Z_j as $\rho_{ij} = \sum_{k=1}^{m} (r_{ik}.r_{jk})$ for $i \neq j$. Note Z_i and Z_j are conditionally independent of each other given the outcome of CSRVs S_k, $k = 1,...,m$. The MSR method is demonstrated in an illustrative example in the Appendix B.

4.3.2 Parameter sensitivity of system failure probability

The MSR method enables us to compute the parameter sensitivity of the probability of a general system event. First, when the component events are statistically independent, the sensitivity of the system failure probability with respect to a parameter θ is computed as

$$\frac{\partial P_{\text{sys}}}{\partial \theta} = \mathbf{c}^{\text{T}} \frac{\partial \mathbf{p}}{\partial \theta} \tag{4.18}$$

The separation of the system event description (**c**) and the probabilities (**p**) in the MSR framework allows us to compute the parameter sensitivity for general system events in a uniform manner. The sensitivity of $\mathbf{p}$ in Equation (4.18) can be computed by the following matrix-based procedure (Song and Kang, 2009):

$$\frac{\partial \mathbf{p}}{\partial \theta} = \left[\mathbf{p}^{\langle 1 \rangle} \ \mathbf{p}^{\langle 2 \rangle} \ldots \mathbf{p}^{\langle n \rangle}\right] \frac{\partial \mathbf{P}}{\partial \theta} = \hat{\mathbf{P}} \frac{\partial \mathbf{P}}{\partial \theta} \tag{4.19}$$

where $\mathbf{P} = [P_1 \ P_2 \ \cdots P_n]^{\text{T}}$ in which P_i is the probability of the *i*-th component event; and $\mathbf{p}^{\langle j \rangle}$, $j = 1,...,n$ is the probability vector constructed by the matrix-based procedure developed for $\mathbf{p}$ except that the probabilities of the *j*-th component event and its complementary event are replaced by 1 and -1, respectively during the construction. In summary, the MSR framework allows us to compute the system-level parameter sensitivities by use of component probabilities and their parameter sensitivities.

When the components are statistically dependent, the parameter sensitivity is computed as

$$\frac{\partial P_{\text{sys}}}{\partial \theta} = \int_{\mathbf{s}} \mathbf{c}^{\mathrm{T}} \frac{\partial \mathbf{p}(\mathbf{s})}{\partial \theta} f_{\mathbf{S}}(\mathbf{s}) d\mathbf{s} \tag{4.20}$$

in which the sensitivity in the integral is constructed by the procedure in Equation (4.19) except that the conditional probability of the component events given $\mathbf{S} = \mathbf{s}$, i.e.

$$P_i(\mathbf{s}) = P\left(\beta_i - Z_i \le 0 | \mathbf{S} = \mathbf{s}\right), \; i = 1, \ldots, n \tag{4.21}$$

is used instead of P_i. Substituting (4.17) into (4.21), the conditional probability is computed as

$$P_i(\mathbf{s}) = \Phi\left[-\frac{\beta_i - \sum_{k=1}^{m} r_{ik} s_k}{\left(1 - \sum_{k=1}^{m} r_{ik}^2\right)^{0.5}} \right] \tag{4.22}$$

4.3.3 Single-loop SRBDO/MSR procedure

The proposed SRBDO/MSR as shown in Figure 4.3 adopts the same single-loop SRBDO approach in Equation (4.14) except that P_{sys} is computed by the MSR method. It is thus formulated as

$$\begin{aligned} &\min_{\mathbf{d}, \boldsymbol{\mu}_{\mathbf{X}}, P_1^t, \ldots, P_n^t} \quad f(\mathbf{d}, \boldsymbol{\mu}_{\mathbf{X}}) \\ &s.t. \quad g_i(\mathbf{d}, \mathbf{X}(\mathbf{U}_i^t)) \ge 0 \quad i=1,\ldots,n \\ &\qquad P_{sys} = \begin{cases} \int_{\mathbf{s}} \mathbf{c}^{\mathrm{T}} \mathbf{p}(\mathbf{s}) f_{\mathbf{S}}(\mathbf{s}) d\mathbf{s} \le P_{sys}^t & \text{dependent} \\ \mathbf{c}^{\mathrm{T}} \mathbf{p} \le P_{sys}^t & \text{indepdendent} \end{cases} \end{aligned} \tag{4.23}$$

Figure 4.3 shows the flowchart of the proposed SRBDO/MSR algorithm.

If the sensitivities of P_{sys} with respect to $\mathbf{d}$ and P_i^t's, $i = 1,\ldots,n$ are available, one can use a gradient-based optimization algorithm for the SRBDO. As shown in Section 4.3.2, the MSR method provides the sensitivity of P_{sys} with respect to general parameters if the parameter sensitivities of component probabilities are available. For example, one can obtain such sensitivities using FORM (Bjerager and Krenk, 1989). Herein it is explained how the sensitivity

with respect to P_i's can be computed by the MSR method. First, the sensitivity of $P_i(\mathbf{s})$ with respect to the reliability index β_i is derived as

$$\frac{\partial P_i(\mathbf{s})}{\partial \beta_i} = -\frac{\varphi\left[-\left(\beta_i - \sum_{k=1}^{m} r_{ik} s_k\right) \Big/ \left(1 - \sum_{k=1}^{m} r_{ik}^2\right)^{0.5}\right]}{\left(1 - \sum_{k=1}^{m} r_{ik}^2\right)^{0.5}} \tag{4.24}$$

in which $\varphi(\cdot)$ denotes the PDF of the standard normal distribution. Then, the sensitivity with respect to the *i*-th component probability is derived as

$$\frac{\partial P_i(\mathbf{s})}{\partial P_i} = \frac{\partial P_i(\mathbf{s})}{\partial \beta_i} \cdot \frac{\partial \beta_i}{\partial P_i} = -\frac{\partial P_i(\mathbf{s})}{\partial \beta_i} \cdot \frac{1}{\varphi(-\beta_i)} \tag{4.25}$$

This sensitivity is used for computing the sensitivity vector in Equation (4.18) or (4.20).

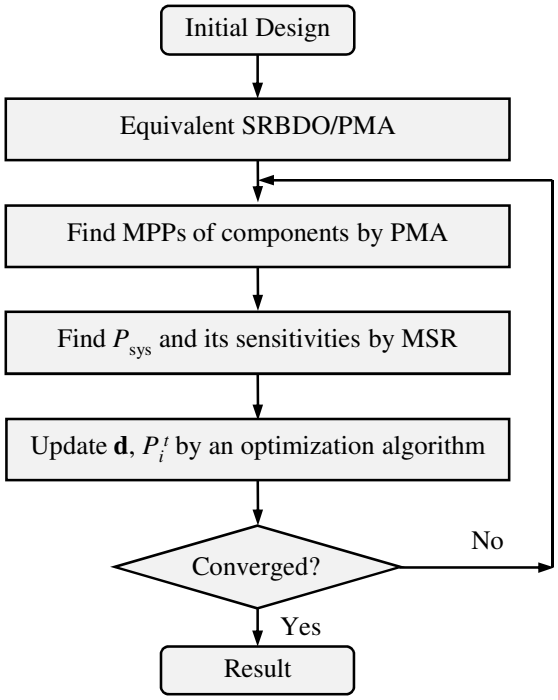

Figure 4.3: Flowchart of the proposed SRBDO/MSR algorithm.

4.4 NUMERICAL EXAMPLES

In this section, three numerical examples are presented to demonstrate the capability and accuracy of the proposed SRBDO/MSR approach. In the first example, the optimal design of a combustion engine is obtained in which the failure is described as a series system event. In the second example, the cross-sectional areas of the members of a statically indeterminate truss structure are determined for minimum total weight. A constraint is given on the probability of the system failure described by a cut-set system event. In the third example, the redistribution of the member forces caused by member failures is considered for the truss system in the second example. The results based on different RBDO approaches are compared for further investigations. Monte Carlo simulations are also performed to confirm the accuracy of the system failure probability computed by the MSR method.

4.4.1 Design of an internal combustion engine

This example adopted from Liang et al. (2007) deals with the optimal design of the flat head of an internal combustion engine (McAllister and Simpson, 2003). The objective is to find the mean values of the random design variables that maximize the "specific power" (or minimize the negative specific power). A constraint is given on the probability that the design will violate at least one of the requirements – a series system event. This SRBDO problem is formulated using the negative specific power as follows.

$$\min_{\boldsymbol{\mu}_{\mathbf{X}}} f(\boldsymbol{\mu}_{\mathbf{X}}) = -\frac{\mu_\omega}{120}\left[3688\cdot\eta_t\left(\mu_{c_r},\mu_b,\mu_\omega\right)\cdot\eta_v\left(\mu_\omega,\mu_{d_1}\right)-\mathrm{FMEP}\left(\mu_{c_r},\mu_b,\mu_\omega\right)\right]$$

where

$$\begin{aligned}
&\mathrm{FMEP}=4.826\cdot\left(\mu_{c_r}-9.2\right)+7.97+0.253\cdot[8V/(\pi N_c)]\mu_\omega(\mu_b)^{-2}+\\
&\qquad(9.7\times10^{-6})\cdot\{[8V/(\pi N_c)]\mu_\omega(\mu_b)^{-2}\}^2\\
&\eta_t = 0.8595\cdot[1-(\mu_{c_r})^{-0.33}]-S_v\cdot(1.5/\mu_\omega)^{0.5}\\
&S_v = 0.83\cdot[8+4\mu_{c_r}+1.5\cdot(\mu_{c_r}-1)\mu_b^3\pi N_c/V]/[(2+\mu_{c_r})\mu_b]\\
&\eta_v = \eta_{vb}\cdot(1+5.96\times10^{-3}\mu_\omega^2)/\{1+[(9.428\times10^{-5})4V/(\pi N_c C_s)\times(\mu_\omega/\mu_{d_1}^2)]^2\}\\
&\eta_{vb} = \begin{cases}1.067-0.038e^{(\mu_\omega-5.25)} & \mu_\omega\geq5.25\\ 0.637+0.13\mu_\omega-0.014\mu_\omega^2+0.00066\mu_\omega^3 & \mu_\omega\leq5.25\end{cases}
\end{aligned} \tag{4.26}$$

$$s.t. \quad P_{\text{sys}} = P\left[\bigcup_{i=1}^{9} g_i(\mathbf{X}) \le 0\right] \le P_{sys}^t$$

$g_1 = 400 - 1.2N_c b$ (min. bore wall thickness)

$g_2 = b - [8V/(200\pi N_c)]^{0.5}$ (max. engine height)

$g_3 = 0.82b - d_I - d_E$ (valve geometry and structure)

$g_4 = d_E - 0.83d_I$ (min. valve diameter ratio)

$g_5 = 0.89d_I - d_E$ (max. valve diameter ratio)

$g_6 = 0.6C_s - (9.428\times10^{-5})(4V/\pi N_c)(\omega/d_I^2)$ (max. Mech/Index)

$g_7 = -0.045b - c_r + 13.2$ (knock-limit compression ratio)

$g_8 = 6.5 - \omega$ (max. torque converter rpm)

$g_9 = 230.5Q\{0.8595\cdot(1-c_r^{-0.33}) - 0.83\cdot[8+4c_r+1.5\cdot(c_r-1)b^3\pi N_c/V]/[(2+c_r)b]\} - 3.6\times10^6$ (max. fuel economy)

where $V = 1.859\times10^6$ mm^3, $Q = 43{,}958$ kJ/kg, $C_s = 0.44$, $N_c = 4$, and $\mu_{(\cdot)}$ denotes the mean of the corresponding random variable in the subscript. The following five random variables are considered: the cylinder bore b, compression ratio c_r, exhaust valve diameter d_E, intake valve diameter d_I and the revolution per minute (rpm) at peak power (divided by 1,000), denoted by ω. These are assumed to follow normal distributions. Table 4.1 shows the standard deviations of the random variables and the lower and upper bound values for their means, i.e., $\boldsymbol{\mu}_{\mathbf{X}}^L$ and $\boldsymbol{\mu}_{\mathbf{X}}^U$.

Table 4.1: Standard deviations of the random variables and bounds given on their means.

Random variables	Std dev	Lower bounds	Upper bounds
Cylinder bore, b (mm)	0.40	70	90
Intake valve diameter, d_I (mm)	0.15	25	50
Exhaust valve diameter, d_E (mm)	0.15	25	50
Compression ratio, c_r	0.05	6	12
(rpm at peak power)/1000, ω	0.25	5	12

Liang et al. (2007) first performed a PMA-based CRBDO, shown in Equation (4.10), for the given problem. For each of the 9 requirements, the constraint on the component failure probability $P_i^t = 0.00135$ (equivalent to target reliability index $\beta_i^t = 3.0$) was assigned. The

second column of Table 4.2 shows the optimal mean values and the corresponding maximum specific power 50.9713. The system failure probability was estimated as 0.006539 by Monte Carlo simulation (MCS) (Liang et al., 2007). For the purpose of comparison, this MCS estimate was used as the constraint on P_{sys} during the single-loop SRBDO in (Liang et al., 2007) and SRBDO/MSR in this study. During SRBDO in (Liang et al., 2007), the "active set" strategy was introduced to deal with a convergence issue caused by small failure probabilities. They assigned "1" to active components whose failure probabilities P_i^t are greater than 10^{-7}, and "0" to the inactive components with smaller probabilities. The "inactive" components (those with "N/A" in Table 4.2) were excluded from the system failure probability calculations. The SRBDO/MSR in this study used a different optimizer (Svanberg, 1987) and did not experience the convergence issue, so the active set strategy was not used, but the lower bounds 10^{-7} were assigned on component probabilities P_i^t, $i = 1,...,9$ to facilitate the convergence. The component events whose probabilities are lower than the lower bound were not considered during the MSR analysis.

For the given problem, the optimal mean values and the maximum specific power by CRBDO are similar to those by SRBDOs. However, it should be noted that for a given SRBDO problem, the CRBDO approach may require repeated optimizations to find the level of constraints on the component failure probabilities that lead to the desired system level reliability. It is also noted that the maximum specific power by CRBDO is smaller than those by SRBDOs even if the system failure probability is the same. This is because the CRBDO approach (assigning fixed constraints on individual components) is generally more constrained than SRBDOs (assigning a constraint on system event, not on the individual components) at the same level of system reliability.

Table 4.2. Results of CRBDO (Liang et al., 2007), single-loop SRBDO (Liang et al., 2007), and SRBDO/MSR for combustion engine.

	CRBDO by (Liang et al., 2007)	SRBDO		
		SRBDO by (Liang et al., 2007)	SRBDO/MSR	MCS for design by SBRDO/MSR
μ_b	82.1333	82.1419	82.1434	82.1434
μ_{d_I}	35.8430	35.8456	35.8394	35.8394
μ_{d_E}	30.3345	30.3641	30.3639	30.3639
μ_{c_r}	9.3446	9.3174	9.3194	9.3194
μ_ω	5.3141	5.3598	5.3621	5.3621
P_1^t	0.00135[a]	0.001448	0.001467	0.0014686
P_2^t	0.00135[a]	N/A	10^{-7}	0
P_3^t	0.00135[a]	0.001665	0.001558	0.0015627
P_4^t	0.00135[a]	0.000811	0.000778	0.0007713
P_5^t	0.00135[a]	N/A	10^{-7}	0
P_6^t	0.00135[a]	0.002370	0.002502	0.002503
P_7^t	0.00135[a]	0.000232	0.000266	0.0002573
P_8^t	0.00135[a]	N/A	0.000003	0.0000023
P_9^t	0.00135[a]	N/A	10^{-7}	0
P_{sys}^t	N/A	0.006539[a]	0.006539[a]	
P_{sys}	0.006539 (MCS)			0.006546
Max. Power: $-f(\boldsymbol{\mu}_{\mathbf{X}})$	50.9713	51.1023	51.1014	51.1014

[a] Pre-determined constraints.

The comparison in Table 4.2 confirms that the two SRBDO approaches provide fairly close results for the series system problem. The small difference is caused by the upper bound approximation in SRBDO in (Liang et al., 2007). According to the component failure probabilities of the optimal designs, the contribution of components 2, 5, 8 and 9 to system reliability are insignificant. The importance ranking of the other significant components is as

follows: 6→3→1→4→7. This ranking of component contributions is an important by-product of the SRBDO approaches. The fifth column of Table 4.2 shows the results of MCS (10^7 times; coefficient of variation c.o.v = 0.004) performed using the optimal design variables from SRBDO/MSR. The results confirm that the optimal design by SRBDO/MSR leads to the component/system failure probabilities that are compatible with the component failure probabilities found during optimization and with the assigned constraint on the system failure probability.

4.4.2 SRBDO of an intermediate truss structure

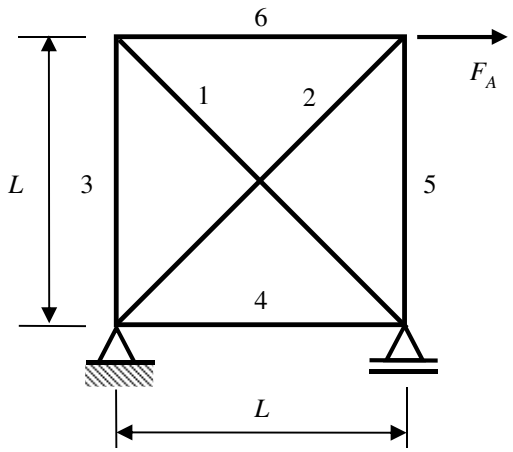

Figure 4.4: A six-member indeterminate truss example.

The uniform applicability of SRBDO/MSR to general system problems is demonstrated by an SRBDO example of a statically indeterminate truss system by McDonald and Mahadevan (2008). Figure 4.4 shows the geometry and the applied load of the truss system. The yielding failures of the six members are modeled as component failure events. When the buckling failure modes, the dynamic effect of member damages, and the influence of the load redistribution during progressive failures (Song and Kang, 2008) are neglected, the system fails when at least two members fail. The system failure event is described by the union of 15 minimal cut-sets: $\{C_k\}$ = { (1,2), (1,3), (1,4), (1,5), (1,6), (2,3), (2,4), (2,5), (2,6), (3,4), (3,5), (3,6), (4,5), (4,6), (5,6)}, each of which represents the joint failure of the corresponding members (see Figure 4.4 for the member numbering choice).

In order to minimize the total weight of the structure, the objective function is defined such that it is proportional to the total weight of the members. The design variables are the cross sectional areas of the members, A_i, $i = 1,...,6$ which are considered deterministic in this problem. The applied load F_A is assumed to follow a normal distribution with the mean of 4,450 kN and a standard deviation of 445 kN while the yield strengths of the members (in stress), F_i, $i = 1,...,6$ are assumed to be a normal distribution with the mean 745 MPa and the standard deviation 62 MPa. All random variables, $F_1,...,F_6$ and F_A, are assumed to be statistically independent of each other. The member forces are derived in terms of the applied load assuming that the two diagonal bars carry equal forces. The target system failure probability P_{sys}^t is given as 0.001. As a result, the SRBDO problem is formulated as

$$\begin{aligned} &\min_{\mathbf{d}=\{A_1,...,A_6\}} f(\mathbf{d}) = \sqrt{2}(A_1 + A_2) + A_3 + A_4 + A_5 + A_6 \\ &s.t. \quad P_{\text{sys}} = P\left[\bigcup_{k=1}^{15} \bigcap_{i \in C_k} \text{g}_i(\mathbf{d}, \mathbf{X}) \le 0\right] \le P_{sys}^t = 0.001 \\ &\quad g_i(\mathbf{d},\mathbf{X}) = \begin{cases} A_i F_i - 0.707 F_A & i = 1, 2 \\ A_i F_i - 0.500 F_A & i = 3,...,6 \end{cases} \\ &\quad A_1, A_2, A_3, A_4, A_5, A_6 \ge 0 \end{aligned} \tag{4.27}$$

In the study by McDonald and Mahadevan (2008), a single-loop SRBDO approach shown in Equation (4.14) was used except that the system failure probability was computed as follows. First, the probability of each cut-set was calculated as a parallel system using the product of conditional marginals method (Pandey, 1998). Considering the entire system event as a series system whose components are the cut-sets, the system failure probability was approximated by the first-order bounding formula in Equation (4.12) with P_i's replaced by the probabilities of the cut-sets.

Table 4.3. Results of SRBDO (McDonald and Mahadevan, 2008) and SRBDO/MSR for the indeterminate truss system.

Members	Area: A_i ($\times 10^{-3}$ mm^2)		Reliability index: β_i	
	SRBDO by (McDonald and Mahadevan, 2008)	SRBDO/MSR	SRBDO by (McDonald and Mahadevan, 2008)	SRBDO/MSR
1	18.43	17.89	2.89	2.67
2	18.27	17.89	2.83	2.67
3	13.51	13.20	3.16	2.99
4	13.44	13.20	3.12	2.99
5	13.33	13.20	3.06	2.99
6	13.09	13.20	2.92	2.99

The proposed SRBDO/MSR approach in Equation (4.23) is applied to this example. The system failure probability and its sensitivities with respect to P_i^t are computed by MSR method as explained in Section 4.3. The system failure probability is accurately estimated without using a bounding formula. The computed sensitivities facilitate the use of a gradient-based optimization algorithm. Table 4.3 compares the results by the two approaches. Except a slightly more conservative design in member 6, SRBDO/MSR approach finds less conservative designs in all members while the same requirement on the system-level reliability is achieved. The minimum objective function value (i.e. minimum total weight) of the proposed approach is 103.36×10^3, which is less than that by the approximation method (McDonald and Mahadevan, 2008), 105.24×10^3. This is due to the overestimation of the system failure probability by the first-order bounding method, which results in a more conservative design than required. This is also evidenced by the lower reliability indexes of the component events by the proposed approach shown in Table 4.3. It is also noteworthy that, due to the accurate system reliability estimates during the SRBDO/MSR, the symmetric conditions between diagonal members (1 and 2) and between non-diagonal members (3-6) give rise to symmetric results in the optimal design (i.e. cross-sectional areas) and the component failure probabilities (i.e. reliability indexes) as well. The system failure probability P_{sys} of the optimal cross sectional areas found by SRBDO/MSR is

evaluated as 0.001 by the MSR analysis and as 0.00107 by MCS (10^6 times, c.o.v = 0.03). Both estimates are fairly close to the given constraint 0.001.

According to the magnitude of component failure probabilities of the optimal design, the importance ranking of the components is identified as (1,2)→(3,4,5,6). In order to quantify the relative importance of components based on their actual contributions to the system failure probability (not on the magnitude of individual component events), the conditional probability importance measure (CIM; Kang and Song) of the *i*-th component event,

$$\text{CIM}_i = P(E_i|E_{sys}) = \frac{P(E_i E_{sys})}{P(E_{sys})} \tag{4.28}$$

can be used. This importance measure can be computed by the MSR method without significant additional computational cost. The system failure probability in the denominator is already available. Because the probability vector can be used once again, the only additional task required is to find the event vector for the new system event $E'_{sys} = E_i E_{sys}$. Figure 4.5 shows the CIMs of the truss members. The importance ranking is the same as that based on the individual component failure probabilities for this particular problem, but it should be noted that these rankings can be different in some cases. For example, if a constraint having high likelihood of violation does not contribute much to violating the system-level constraint, its CIM can be negligible despite its high failure probability.

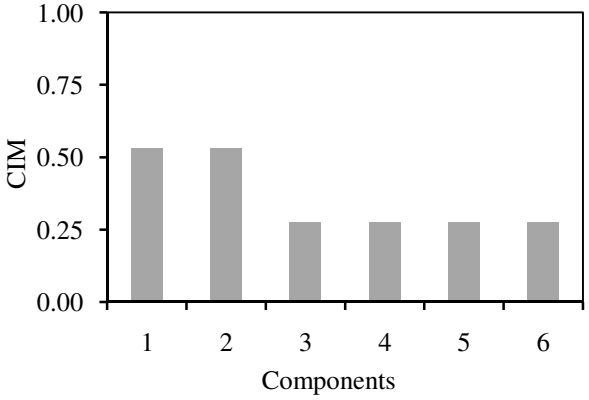

Figure 4.5: Conditional probability importance measures of the truss member.

Table 4.4. Results of SRBDO/MSR for normal and lognormal distribution cases.

Members	Area: A_i ($\times 10^{-3}$ mm^2)		Reliability Index: β_i	
	Normal	Lognormal	Normal	Lognormal
1	17.89	18.18	2.67	2.79
2	17.89	18.18	2.67	2.79
3	13.20	13.51	2.99	3.17
4	13.20	13.51	2.99	3.17
5	13.20	13.51	2.99	3.17
6	13.20	13.51	2.99	3.17

Next, all the random variables in the above example are assumed to follow the lognormal distributions with the same means and standard deviations. This is to investigate the effect of the types of the probabilistic distributions on the optimal design and to demonstrate the general applicability of the proposed method. The minimum objective function value is obtained as 105.46×10^3, which is slightly larger than that of the normal distribution case. Table 4.4 shows that the reliability indexes of the component events and the optimal cross sectional areas of the lognormal distribution case are slightly larger than that of the normal distribution case. The system failure probability P_{sys} of the optimal design from the SRBDO/MSR analysis is evaluated as 0.000998 by MCS (10^6 times, c.o.v = 0.032), which is close to the given constraint $P_{sys}^t = 0.001$.

4.4.3 SRBDO of an intermediate truss structure considering progressive failure

In this example, the SRBDO problem in Section 4.4.2 is re-investigated with consideration of load redistribution in the truss system caused by member failures. This load redistribution can cause a progressive failure of the system. All the parameters are the same as the previous example. The complexity of estimating the likelihood of this system event arises from the fact that the failures of the remaining members should be described as new component events due to the load re-distribution. Figure 4.6 shows the numbering choice of the component failure events defined for the members in the original structure and the structures with one failed member.

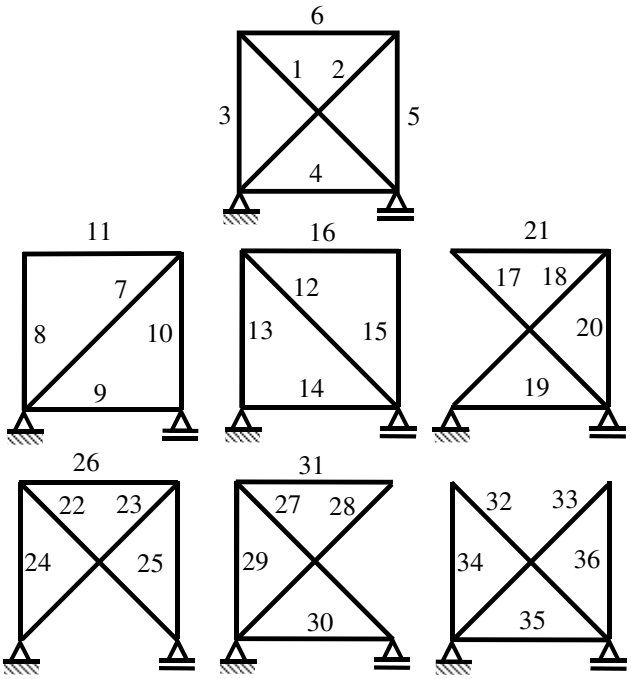

Figure 4.6: Component failure events defined for the original system and system with failed members.

The structure survives if (1) no member fails in the original configuration or (2) one member fails but no further member failures take place. Using the component numbering choice shown in Figure 4.6, the probability of system survival $\overline{E}_{sys}$ is described as

$$\begin{aligned} P\left(\overline{E}_{sys}\right) = P\Big[& \overline{E}_1\overline{E}_2\overline{E}_3\overline{E}_4\overline{E}_5\overline{E}_6 \cup \\ & \left(E_1\overline{E}_2\overline{E}_3\overline{E}_4\overline{E}_5\overline{E}_6\right)\left(\overline{E}_7\overline{E}_8\overline{E}_9\overline{E}_{10}\overline{E}_{11}\right) \cup \left(\overline{E}_1E_2\overline{E}_3\overline{E}_4\overline{E}_5\overline{E}_6\right)\left(\overline{E}_{12}\overline{E}_{13}\overline{E}_{14}\overline{E}_{15}\overline{E}_{16}\right) \cup \\ & \left(\overline{E}_1\overline{E}_2E_3\overline{E}_4\overline{E}_5\overline{E}_6\right)\left(\overline{E}_{17}\overline{E}_{18}\overline{E}_{19}\overline{E}_{20}\overline{E}_{21}\right) \cup \left(\overline{E}_1\overline{E}_2\overline{E}_3E_4\overline{E}_5\overline{E}_6\right)\left(\overline{E}_{22}\overline{E}_{23}\overline{E}_{24}\overline{E}_{25}\overline{E}_{26}\right) \cup \\ & \left(\overline{E}_1\overline{E}_2\overline{E}_3\overline{E}_4E_5\overline{E}_6\right)\left(\overline{E}_{27}\overline{E}_{28}\overline{E}_{29}\overline{E}_{30}\overline{E}_{31}\right) \cup \left(\overline{E}_1\overline{E}_2\overline{E}_3\overline{E}_4\overline{E}_5E_6\right)\left(\overline{E}_{32}\overline{E}_{33}\overline{E}_{34}\overline{E}_{35}\overline{E}_{36}\right)\Big] \end{aligned} \tag{4.29}$$

in which E_i and $\overline{E}_i$ respectively denote the failure and survival event of the *i*-th component. This is a link-set system event consisting of 36 components. The size of **c** and **p** is $2^{36} \cong 6.87\times10^{10}$. However, the size of the vectors used in MSR analysis can be further reduced as follows. Due to the mutual exclusiveness of the seven link-sets, the probability can be computed as the sum of the probabilities of the individual link-sets, which reduces the maximum number of components

appearing in an MSR analysis from 36 to 11. It can be further reduced by considering the fact that some link-sets include component events defined for the same member. For example, the component events $\overline{E}_1$ and $\overline{E}_{12}$ are defined for the same member as shown in Figure 4.6. Since their limit state functions indicate $\overline{E}_1 \supset \overline{E}_{12}$ for positive values of F_1 and F_A, $\overline{E}_1\overline{E}_{12}$ is simplified to $\overline{E}_{12}$. As a result, the system reliability can be computed as

$$\begin{aligned} P\left(\overline{E}_{sys}\right) &= P\left(\overline{E}_1\overline{E}_2\overline{E}_3\overline{E}_4\overline{E}_5\overline{E}_6\right) + P\left(E_1\overline{E}_3\overline{E}_4\overline{E}_6\overline{E}_7\overline{E}_{10}\right) + P\left(E_2\overline{E}_5\overline{E}_{12}\overline{E}_{13}\overline{E}_{14}\overline{E}_{16}\right) + \\ &P\left(\overline{E}_1E_3\overline{E}_4\overline{E}_6\overline{E}_{18}\overline{E}_{20}\right) + P\left(\overline{E}_1\overline{E}_3E_4\overline{E}_6\overline{E}_{23}\overline{E}_{25}\right) + P\left(\overline{E}_2E_5\overline{E}_{27}\overline{E}_{29}\overline{E}_{30}\overline{E}_{31}\right) + P\left(\overline{E}_1\overline{E}_3\overline{E}_4E_6\overline{E}_{33}\overline{E}_{36}\right) \end{aligned} \tag{4.30}$$

This system decomposition reduces the maximum number of components appearing an MSR analysis to 6. The size of the vectors is only $2^6 = 64.$ Noting some component events having the same limit-state functions, Equation (4.30) is rewritten using twelve distinct component events as follows.

$$\begin{aligned} P\left(\overline{E}_{sys}\right) &= P\left(\overline{E}_1\overline{E}_2\overline{E}_3\overline{E}_4\overline{E}_5\overline{E}_6\right) + P\left(E_1\overline{E}_3\overline{E}_4\overline{E}_6\overline{E}_7\overline{E}_{10}\right) + P\left(E_2\overline{E}_5\overline{E}_{12}\overline{E}_{13}\overline{E}_{14}\overline{E}_{16}\right) \\ &+P\left(\overline{E}_1E_3\overline{E}_4\overline{E}_6\overline{E}_7\overline{E}_{10}\right) + P\left(\overline{E}_1\overline{E}_3E_4\overline{E}_6\overline{E}_7\overline{E}_{10}\right) + P\left(\overline{E}_2E_5\overline{E}_{12}\overline{E}_{13}\overline{E}_{14}\overline{E}_{16}\right) + P\left(\overline{E}_1\overline{E}_3\overline{E}_4E_6\overline{E}_7\overline{E}_{10}\right) \end{aligned} \tag{4.31}$$

Thus, the SRBDO problem is formulated as

$$\begin{aligned} &\min_{\mathbf{d}=\{A_1,\ldots,A_6\}} f(\mathbf{d}) = \sqrt{2}(A_1 + A_2) + A_3 + A_4 + A_5 + A_6 \\ &s.t. \qquad P_{\text{sys}} = 1 - P(\overline{E}_{sys}) = 1 - \sum_{k=1}^{7} P\left(\bigcap_{i\in L_k} \text{g}_i(\mathbf{d},\mathbf{X}) > 0\right) \le 0.001 \\ &\qquad g_i(\mathbf{d},\mathbf{X}) = \begin{cases} A_iF_i - 0.707F_A & i = 1,2 \\ A_iF_i - 0.500F_A & i = 3,\ldots,6 \\ A_2F_2 - 1.414F_A & i = 7 \\ A_5F_5 - 1.000F_A & i = 10 \\ A_1F_1 - 1.414F_A & i = 12 \\ A_3F_3 - 1.000F_A & i = 13 \\ A_4F_4 - 1.000F_A & i = 14 \\ A_6F_6 - 1.000F_A & i = 16 \end{cases} \\ &\qquad A_1, A_2, A_3, A_4, A_5, A_6 \ge 0 \end{aligned} \tag{4.32}$$

where L_k, $k = 1,...,7$ is the component index set from Equation (4.31), that is, $\{L_k\}$ = {(1,2,3,4,5,6), (1,3,4,6,7,10), (2,5,12,13,14,16), (1,3,4,6,7,10), (1,3,4,6,7,10), (2,5,12,13,14,16), (1,3,4,6,7,10)}.

Table 4.5 compares the results of the SRBDO in Equation (4.32) (denoted by "Ex. 3" in the following tables) with those given in the previous example ("Ex. 2"). It is seen that the optimal cross sectional areas increase significantly as the effect of load re-distribution is considered. The objective function value also increases from 103.36×10^3 to 114.13×10^3. This implies that neglecting the load redistribution during an SRBDO may result in a design that does not satisfy the system-level safety criteria. As expected, when the load redistribution is considered, the system failure probability of the optimal design from the previous example ("Ex. 2") is estimated as 0.01208 by MSR analysis and 0.01205 by MCS (10^6 times; c.o.v = 0.009), which clearly exceed the given constraint 0.001. By contrast, the system failure probability of the optimal design in this example is estimated as 0.001 by MSR and 0.000986 by MCS (10^6 times, c.o.v = 0.0318), which are close to the given constraint.

Table 4.5. Results of SRBDO/MSR of the truss system with/without consideration of load redistribution.

Member (Figure 4.4)	Component events (Equation 4.31)	Area: A_i ($\times10^{-3}$ mm^2)		Reliability index: β_i	
		Ex. 2	Ex. 3	Ex. 2	Ex. 3[a]
1	1, 12	17.89	19.94	2.668	3.48, −2.07
2	2, 7	17.89	19.94	2.668	3.48, −1.78
3	3, 13	13.20	14.44	2.987	3.65, −1.95
4	4, 14	13.20	14.44	2.987	3.65, −1.95
5	5, 10	13.20	14.44	2.987	3.65, −1.62
6	6, 16	13.20	14.44	2.987	3.65, −1.95

[a] two reliability indexes correspond to the component events in the second column (in the same order)

The impact of statistical correlation between random yielding strengths F_i's on the optimal design is investigated by varying their correlation coefficients $\rho_{i,j}$. For simplicity, the correlation coefficients are assumed to be uniform, i.e. $\rho_{i,j} = \rho$. The SRBDO problems in Equation (4.27) and Equation (4.32) are solved again with correlation coefficient ρ varying from 0.00 to

0.75.The optimal cross-sectional areas and the objective function values are shown in Table 4.6. It is seen that considering the effect of load redistribution results in more conservative designs for all levels of correlation considered. It is also observed that the higher correlation among member yield strengths increase the cross-sectional areas when redistribution is not considered, but decreases if redistribution considered. Figure 4.7 presents this trend more clearly by showing the objective function values of the SRBDOs.

Table 4.6. Optimal design and correlation between member yield strengths.

		Area: A_i ($\times 10^{-3}$ mm^2)							
		ρ =0.00*		ρ =0.25		ρ =0.50		ρ =0.75	
		Ex. 2	Ex. 3	Ex. 2	Ex. 3	Ex. 2	Ex. 3	Ex. 2	Ex. 3
Members (Figure 4.4)	1	17.89	19.94	18.03	19.90	18.14	19.83	18.31	19.68
	2	17.89	19.94	18.03	19.90	18.14	19.83	18.31	19.68
	3	13.20	14.44	13.53	14.40	13.91	14.33	14.28	14.16
	4	13.20	14.44	13.53	14.40	13.91	14.33	14.28	14.16
	5	13.20	14.44	13.53	14.40	13.91	14.33	14.28	14.16
	6	13.20	14.44	13.53	14.40	13.91	14.33	14.28	14.16
Objective Function		103.36	114.13	105.12	113.93	106.93	113.42	108.90	112.34

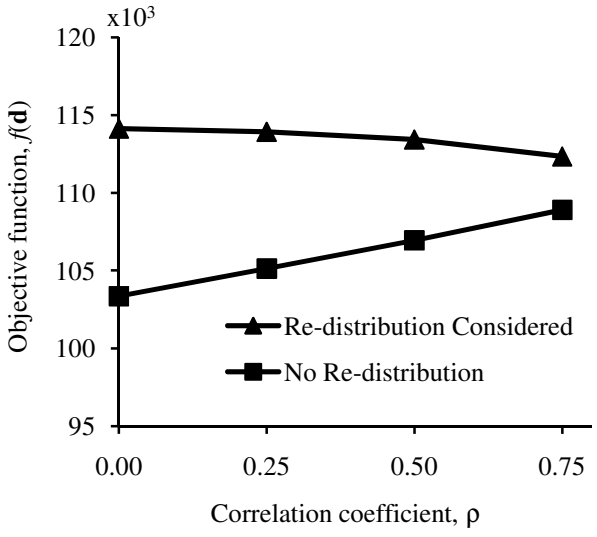

Figure 4.7: Objective functions versus correlation between member yield strengths.

4.5 CONCLUDING REMARKS

In this chapter, an efficient and accurate system reliability-based design optimization (SRBDO) approach is developed by integrating a single-loop RBDO algorithm with the recently developed matrix-based system reliability (MSR) method. The use of MSR improves the efficiency and accuracy of the computation of the system probability and its sensitivities in the existing single-loop SRBDO approach (Liang et al., 2007). The MSR method enables us to compute the probabilities of general system events including series, parallel, cut-set and link-set systems in a uniform manner without using approximate bounds or random samplings. It can account for statistical dependence between component events and can compute the sensitivities of the system failure probability to various parameters as well, which facilitates the use of gradient-based optimization algorithms. Three numerical examples demonstrate the uniform applicability of the proposed SRBDO/MSR approach to series, cut-set and link-set systems. It is seen that the accuracy of system reliability analysis by the MSR method enables us to obtain less conservative optimal design than SRBDO algorithms using upper bounds. The effect of load redistribution by member failures on the optimal designs is investigated as well. In each example, the accuracy of the MSR method is verified by Monte Carlo simulations. It is noteworthy that the SRBDO/MSR in this study employs FORM for component reliability analysis and MSR accurately estimates system probability based on the provided component probabilities. Therefore, if the component reliability analysis FORM provides inaccurate component probabilities due to the nonlinearity of the limit-state functions, this inaccuracy will affect the accuracy of any FORM-based SRBDO algorithm including SRBDO/MSR.

CHAPTER 5 – SYSTEM RELIABILITY-BASED TOPOLOGY OPTIMIZATION CONSIDERING STATISTICAL DEPENDENCE BETWEEN LIMIT-STATES

This chapter presents a single-loop algorithm for system reliability-based *topology* optimization (SRBTO) that can account for statistical dependence between multiple limit-states, and its applications to computationally demanding topology optimization problems. The proposed single-loop SRBTO algorithm accounts for the statistical dependence between the limit-states by using the matrix-based system reliability (MSR) method in computing the system failure probability and its parameter sensitivities. In order to improve the accuracy of the reliability calculations for RBDO or RBTO problems with high nonlinearity, new single-loop RBDO schemes utilizing the second-order reliability method are proposed. Numerical examples of two- and three-dimensional topology optimization problems demonstrate the proposed SRBTO algorithm and its applications

5.1 INTRODUCTION

Topology optimization aims to find optimal structural layout under given constraints through iterative computational simulations. In the past decades, a large number of studies have been devoted to this important research area of structural optimization (Bendsøe and Sigmund, 2003). Topology optimization methods have been successfully applied to a wide range of practical engineering problems (Rozvany, 2001; Bendsøe and Sigmund, 2003). However, most of the efforts have been conducted in a deterministic manner although uncertainties in loads or material properties may result in significant probability of violating design constraints. In this study, this approach is referred to as deterministic topology optimization (DTO). Recently, active research has been performed to achieve reliable topologies under probabilistic constraints. This approach is often termed as reliability-based topology optimization (RBTO), and has been successfully

applied to a variety of topology optimization problems (Bae et al., 2002; Maute and Frangopol, 2003; Allen et al., 2004; Jung and Cho, 2004; Kang et al., 2004; Kharmanda et al., 2004; Kim et al., 2006; Guest and Igusa, 2008; Rozvany, 2008; Lógó et al., 2009; Luo et al., 2009; Chen et al., 2010). For example, Maute and Frangopol (2003) employed RBTO in the design of compliant micro-electromechanical system mechanism (MEMS). Jung and Cho (2004) applied RBTO to geometrically nonlinear structures with uncertain loads and material properties. Additionally, Rozvany (2008) derived the analytical solution for benchmark problems in probabilistic topology optimization. It is noted that most research efforts on RBTO have been focused on satisfying the probabilistic constraint given for each failure mode. In the current study, this approach is referred to as component reliability-based topology optimization (CRBTO). A generic formulation for CRBTO problems is given as follows

$$\begin{aligned} &\min_{\mathbf{d}} f(\rho(\boldsymbol{\psi};\mathbf{d})) \\ &s.t.\ \ P[g_i(\rho(\boldsymbol{\psi};\mathbf{d}),\mathbf{X}) \le 0] \le P_i^t,\ \ i=1,...,n \\ &\quad \mathbf{K}(\rho(\boldsymbol{\psi};\mathbf{d}))\cdot\mathbf{u}_d = \mathbf{f} \\ &\quad \mathbf{d}^L \le \mathbf{d} \le \mathbf{d}^U \end{aligned} \tag{5.1}$$

where $\mathbf{d} \in \Re^k$ is the vector of deterministic design variables; $\rho(\boldsymbol{\psi};\mathbf{d})$ is the material density at the position $\boldsymbol{\psi} \in \Re^2$ or $\Re^3$ that is generally determined by a projection function $f_p(\cdot)$ and the design variables, i.e. $\rho(\boldsymbol{\psi};\mathbf{d}) = f_p(\mathbf{d})$; $f(\cdot)$ is the objective function that gives volume, compliance, or displacement; $\mathbf{X} \in \Re^m$ is the vector of random variables representing the uncertainties in the problem; $g_i(\cdot),\ i=1,...,n$ is the *i*-th "limit-state function" that indicates violating a design constraint given in terms of volume, displacement, or compliance by its negative sign, i.e. $g_i(\cdot) \le 0$; P_i^t is the constraint on the probability of the *i*-th limit state; $\mathbf{K}$, $\mathbf{u}_d$ and $\mathbf{f}$ respectively denote the stiffness matrix, displacement vector and load vector in the equilibrium constraint; and $\mathbf{d}^L$ and $\mathbf{d}^U$ are the lower and upper bounds on $\mathbf{d}$, respectively. For simplicity, the equilibrium constraint and bounds on the design variables will be omitted in the following RBTO formulations of this chapter. The probability constraint in Equation (5.1) is described in terms of either the reliability index (RIA: Enevoldsen and Sørensen, 1994) or the performance function, i.e. the P_i^t - quantile of the limit-state function (PMA: Tu et al., 1999), which is

obtained by use of structural reliability analysis methods such as the first-order reliability method (FORM).

While most research efforts in the literature have been focused on CRBTO, in certain circumstances, the probabilistic constraint should be given on a *system* failure event, i.e. a logical (or Boolean) function of multiple failure modes. For example, the failure of a topology design can be defined as an event in which at least one of the potential failure modes occurs. This is termed as *system* reliability-based topology optimization (SRBTO). SRBTO introduces additional complexity to reliability calculations especially when component events are statistically dependent, or when the system event is not a series (i.e. union of events) or parallel system (i.e. intersection of events). A generic formulation for SRBTO is as follows.

$$\begin{aligned} &\min_{\mathbf{d}} f(\rho(\boldsymbol{\psi};\mathbf{d})) \\ &s.t.\ \ P(E_{sys}) = P\left[\bigcup_{k}\bigcap_{i\in C_k} g_i(\rho(\boldsymbol{\psi};\mathbf{d}),\mathbf{X}) \le 0\right] \le P_{sys}^{t},\ \ i=1,...,n \end{aligned} \tag{5.2}$$

where $P(E_{sys})$ is the probability of the system failure event; C_k is the index set of the components (limit-states) in the *k*-th cut-set; and P_{sys}^{t} is the constraint on the system failure probability. Any type of system event may be considered in SRBTO but, for illustration purpose, Equation (5.2) shows a cut-set system formulation that can represent series, parallel, and cut-set systems. A limited number of studies have been performed on SRBTO because calculation of system probability and its parameter sensitivities introduces additional complexity to the topology optimization that already requires high computational cost. For example, SRBTO has been considered for cases in which all component events are statistically independent of each other (Silva et al., 2010). In this case, the system failure probability and its parameter sensitivities can be obtained by algebraic calculations of the component probabilities and sensitivities. However, the limit-states of SRBTO problems often show strong statistical dependence because of shared or correlated random variables. SRBTO has been also applied to discrete structures that require less computational cost than continuum topology optimization (Mogami et al., 2006). However, the discrete approach (or so-called size approach) cannot change the structural topology during the solution process, so the solution will have the same

topology as the initial design (Eschenauer and Olhoff, 2001) whereas continuum topology optimization can control size, shape and connectivity of the structure.

As an effort to overcome impediments to adopting SRBTO techniques in current design practice, this study focuses on developing new SRBTO algorithms for continuum linear elastic structures that can consider statistical dependence between component events (limit-states). First, an SRBTO procedure using a matrix-based system reliability (MSR) method (Song and Kang, 2009) is introduced to handle the statistical dependence between limit-states. The MSR method enables accurate and efficient calculation of system failure probability and its parameter sensitivities for general system problems including series, parallel, cut-set and link-set systems. Second, a new single-loop algorithm to improve the accuracy of FORM-based RBTO (Mogami et al., 2006; Nguyen et al., 2009; Silva et al., 2010) by use of the second-order reliability method (SORM) is introduced. Finally, the multiresolution topology optimization (MTOP) in Chapter 2 is integrated with the SRBTO algorithm to enhance efficiency in computationally demanding topology optimization problems. This approach uses three distinct meshes with different resolutions for finite element, density and design variables in order to achieve high-resolution optimal designs with significantly reduced computational costs.

The remainder of this chapter is structured as follows: Section 5.2 describes the single-loop system reliability-based topology optimization using the matrix-based system reliability method; Section 5.3 provides a single-loop algorithm to enhance component and system reliability-based topology optimization by use of the second-order reliability method; Section 5.4 presents the multiresolution topology optimization approach; Section 5.5 provides numerical examples of SRBTO; and Section 5.6 provides concluding remarks of this chapter.

5.2 SYSTEM RELIABILITY-BASED TOPOLOGY OPTIMIZATION USING MSR METHOD

In this section, a single-loop formulation for system reliability-based topology optimization, that can account for statistical dependence between limit-states for general system failure events, is introduced. After a brief review on single-loop approaches for component and system RBTO

and methods to account for statistical dependence, the new SRBTO formulation using matrix-based system reliability (MSR) method is introduced.

5.2.1 Single-loop component and system reliability-based topology optimization

For CRBTO and SRBTO shown in (5.1) and (5.2), a nested or "double-loop" approach has been often used, in which each step of the iterations for design optimization involves another loop of iterations for reliability analysis. However, this double-loop computation can be prohibitive if the computational cost for evaluating limit-state function(s) during the inner-loop search for the "most probable point" (MPP) or "design point" (Yang et al., 2005) is expensive. There have been active research efforts to overcome this computational challenge by decoupling the reliability analysis and the design optimization loops (Wu and Wang, 1998; Royset et al., 2001; Du and Chen, 2004; Liang et al., 2007; Liang et al., 2008; Shan and Wang, 2008). For example, a single-loop approach (Liang et al., 2007; Liang et al., 2008) replaces the inner-loop calculations by an approximate solution obtained by the Karush-Kuhn-Tucker (KKT) optimality condition. As a result, the double-loop optimization problem is converted into an equivalent single-loop problem. This single-loop approach was reported to have the accuracy comparable with the double-loop approach and the efficiency almost equivalent to deterministic optimization (Liang et al., 2008). In this study, this single-loop approach (Liang et al., 2007; Liang et al., 2008) is utilized for the SRBTO formulations.

The single-loop formulation for the CRBTO problem in Equation (5.1) is given as follows.

$$
\begin{aligned}
&\min_{\mathbf{d}} \quad f(\rho(\boldsymbol{\psi};\mathbf{d})) \\
&s.t. \quad \mathrm{g}_{P_i^t} \cong \mathrm{g}_i\left(\rho(\boldsymbol{\psi};\mathbf{d}), \mathbf{x}(\mathbf{u}_i^t)\right) \geq 0, \quad i=1,...,n \\
&\text{where} \ \ \mathbf{u}_i^t \cong \beta_i^t \cdot (\hat{\boldsymbol{\alpha}}_i^t)^{\mathrm{T}} \\
&\qquad \hat{\boldsymbol{\alpha}}_i^t \cong \left(-\frac{\nabla_{\mathbf{x}} g_i(\rho(\boldsymbol{\psi};\mathbf{d}), \mathbf{x}(\mathbf{u}))}{\left\| \nabla_{\mathbf{x}} g_i(\rho(\boldsymbol{\psi};\mathbf{d}), \mathbf{x}(\mathbf{u})) \right\|} \mathbf{J}_{\mathbf{x},\mathbf{u}} \right)_{\mathbf{u}=\tilde{\mathbf{u}}_i}
\end{aligned}
\tag{5.3}
$$

where $g_{P_i^t}$ is the P_i^t-quantile of the i-th limit-state function $g_i(\cdot)$; $\beta_i^t = -\Phi^{-1}(P_i^t)$ is the target (generalized) reliability index where $\Phi^{-1}(\cdot)$ denotes the inverse cumulative distribution function (CDF) of the standard normal distribution; $\mathbf{J}_{\mathbf{x},\mathbf{u}}$ is the Jacobian matrix of the transformation from

the standard normal space to the original random variable space, i.e. $\mathbf{x}=\mathbf{x}(\mathbf{u})$; $\hat{\boldsymbol{\alpha}}_i^t$ is the negative normalized gradient (row) vector of the *i*-th limit-state function evaluated at the approximate MPP $\tilde{\mathbf{u}}_i$. Instead of searching for the exact MPP at each step of the design iterations, the single-loop approach obtains an approximate MPP $\tilde{\mathbf{u}}_i$ by solving the following system equation given by the KKT condition (Liang et al., 2008):

$$\begin{aligned}&\nabla_{\mathbf{x}} g_i(\rho(\boldsymbol{\psi};\mathbf{d}),\mathbf{x}(\tilde{\mathbf{u}}_i))\mathbf{J}_{\mathbf{x},\mathbf{u}}+\lambda\cdot\nabla_{\mathbf{u}}\left(\|\tilde{\mathbf{u}}_i\|-\beta_i^t\right)=\mathbf{0}\\&\|\tilde{\mathbf{u}}_i\|-\beta_i^t=0\end{aligned} \tag{5.4}$$

Then, the negative normalized gradient is scaled by the target reliability index β_i^t to determine the location where $g_{P_i^t}$ is approximately evaluated, i.e. $\mathbf{u}_i^t$. Figure 5.1 shows the flowchart of the single-loop CRBTO algorithm.

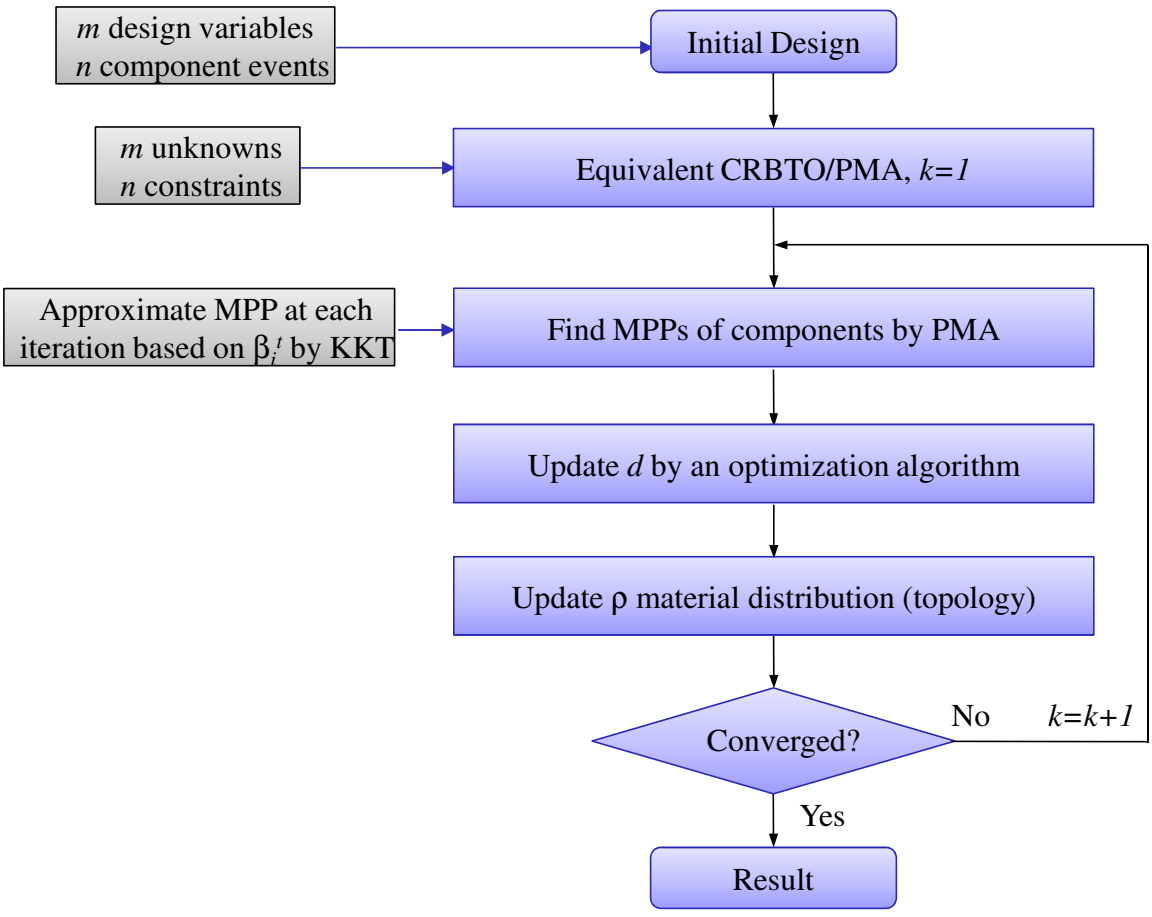

Figure 5.1: Flow chart of the single-loop CRBTO algorithm.

Similarly, the SRBTO problem in Equation (5.2) can be solved by a single-loop approach as follows.

$$\begin{aligned}
&\min_{\mathbf{d},\mathbf{P}^t} \quad f(\rho(\boldsymbol{\psi};\mathbf{d})) \\
&s.t. \quad \mathrm{g}_{P_i^t} \cong \mathrm{g}_i\left(\rho(\boldsymbol{\psi};\mathbf{d}), \mathbf{x}(\mathbf{u}_i^t)\right) \geq 0 \quad i=1,...,n \\
&\qquad P(E_{sys};\mathbf{P}^t) = P\left[\bigcup_k \bigcap_{i\in C_k} g_i(\rho(\boldsymbol{\psi};\mathbf{d}), \mathbf{X}) \leq 0\right] \leq P_{sys}^t \qquad (5.5) \\
&\text{where} \quad \mathbf{u}_i^t \cong \beta_i^t \cdot (\hat{\boldsymbol{\alpha}}_i^t)^{\mathrm{T}} \\
&\qquad \hat{\boldsymbol{\alpha}}_i^t \cong \left(-\frac{\nabla_{\mathbf{x}} g_i(\rho(\boldsymbol{\psi};\mathbf{d}), \mathbf{x}(\mathbf{u}))}{\left\|\nabla_{\mathbf{x}} g_i(\rho(\boldsymbol{\psi};\mathbf{d}), \mathbf{x}(\mathbf{u}))\right\|} \mathbf{J}_{\mathbf{x},\mathbf{u}} \right)_{\mathbf{u}=\tilde{\mathbf{u}}_i}
\end{aligned}$$

where $\mathbf{P}^t$ is the vector of the target failure probabilities, P_i^t, i=1,…,n. Note that in Equation (5.5), the target failure probabilities are treated as design variables rather than pre-defined constraint values as in Equation (5.3). This is to control the system failure probability $P(E_{sys})$ indirectly in the single-loop approach by controlling the radii $\beta_i^t = -\Phi^{-1}(P_i^t)$, i=1,…,n of the spheres on which the approximate MPPs are found.

5.2.2 System reliability-based topology optimization under statistical dependence

When the limit-states in an SRBTO problem are assumed to be statistically independent (Silva et al., 2010), the system probability can be computed by algebraic calculations of the probabilities of the individual limit-states. For example, the failure probability of a series system event is computed by use of the inclusion-exclusion formula

$$P\left(\bigcup_{i=1}^{n} E_i\right) = \sum_{i=1}^{n} P(E_i) - \sum_{i=1}^{n-1} \sum_{j=i+1}^{n} P(E_i E_j) + \cdots + (-1)^{n-1} P(E_1 E_2 \cdots E_n) \qquad (5.6)$$

where E_i denotes the failure event of the i-th limit-state. When these events are statistically independent of each other, each joint probability in (5.6) can be computed by the product of the component probabilities, e.g., $P(E_1E_2E_3) = P(E_1)P(E_2)P(E_3)$. If there exists significant statistical dependence between limit-states due to shared or correlated random variables, one needs to use other system reliability analysis methods to compute the system failure probability.

The parameter sensitivities of the system failure probability would facilitate the use of gradient-based optimization algorithm. However, computation of the parameter sensitivities of a system failure probability is challenging when component events are statistically dependent or the system event is not a series or parallel system.

The matrix-based system reliability (MSR) method has been applied to general reliability-based design optimization problems in Chapter 4. This chapter aims to use the MSR method for SRBTO problem. The MSR method (Song and Kang, 2009) computes the probability of a general system including series, parallel, cut-set and link-set system and its parameter sensitivities by systematic matrix calculations. Consider a system event whose *i*-th component, $i = 1,...,n$ has two distinct states, e.g., failure or survival. Then, the sample space can be subdivided into $N = 2^n$ mutually exclusive and collectively exhaustive (MECE) events, denoted by e_j, $j = 1,..,N$. Then, any system event can be represented by an "event" vector **c** whose *j*-th element is 1 if e_j belongs to the system event and 0 otherwise. Let $p_j = P(e_j),\ \ j = 1,..,N$ denote the probability of e_j. Due to the e_j's mutual exclusiveness, the probability of the system event E_{sys}, i.e. $P(E_{sys})$ is the sum of the probabilities of e_j's that belong to the system event. Therefore, the system probability is computed by the inner product of the two vectors, that is

$$P(E_{sys}) = \begin{cases} \mathbf{c}^{\mathrm{T}}\mathbf{p} & \text{(independent components)} \\ \int_{\mathbf{s}} \mathbf{c}^{\mathrm{T}}\mathbf{p}(\mathbf{s}) f_{\mathbf{S}}(\mathbf{s}) d\mathbf{s} & \text{(dependent components)} \end{cases} \tag{5.7}$$

where **p** is the "probability" vector that contains p_j's $j = 1,..,N$; **S** denotes the random variables identified as the sources of statistical dependence between components, termed as common source random variables (CSRVs). For a given outcome of CSRVs, the component events are conditionally independent of each other, which allows us to use the efficient procedure to construct the probability vector that is applicable to independent components (Song and Kang 2009); $\mathbf{p}(\mathbf{s})$ denotes the probability vector constructed by use of the conditional failure probabilities of the limit-states given $\mathbf{S} = \mathbf{s}$, i.e. $P_i(\mathbf{s}) \equiv P(E_i \mid \mathbf{S} = \mathbf{s})$ instead of $P_i \equiv P(E_i)$; and $f_{\mathbf{S}}(\mathbf{s})$ is joint probability density function (PDF) of **S**. Song and Kang (2009) developed matrix-based procedures to construct the vectors **c** and **p** efficiently; to compute conditional

probabilities and component importance measures; and to evaluate parameter sensitivities of the system failure probability. The details of these procedures and merits of the method are summarized in (Song and Kang, 2009). The method has been further developed and successfully applied to various system reliability problems (Kang et al., 2008; Kang et al., 2010; Song and Ok, 2010; Lee et al., 2010b).

When CSRVs are not clearly shown as in Kang et al. (2008), one can identify the source of statistical dependence between limit-states by using the results of the component reliability analyses. For example, when the first-order reliability method (FORM) is used for the component reliability analyses, the component events are described as $Z_i \le -\beta_i,\ i = 1,...,n,$ where Z_i and β_i respectively denote the standard normal random variable and the reliability index obtained by FORM. If $Z_i,\ i = 1,...,n,$ follow the generalized Dunnett-Sobel (DS) class correlation model (Dunnett and Sobel, 1955; Song and Kang, 2009), they are represented in the form:

$$Z_i = \left(1 - \sum_{k=1}^{m} r_{ik}^2\right)^{0.5} Y_i + \sum_{k=1}^{m} r_{ik} S_k, \quad \text{for } i = 1,\ldots,n \tag{5.8}$$

in which $Y_i,\ i = 1,...,n$ and $S_k,\ i = 1,...,m$ are uncorrelated standard normal random variables; and r_{ik}'s are the coefficients of the generalized DS model that determine the correlation coefficient between Z_i and Z_j as $\rho_{ij} = \sum_{k=1}^{m} (r_{ik}.r_{jk})$ for $i \neq j$. Note Z_i and Z_j are conditionally independent of each other given the outcome of CSRVs $S_k,\ i = 1,...,m$. The conditional probability of the *i*-th component event given $\mathbf{S} = \mathbf{s}$ is then derived as

$$P_i(\mathbf{s}) = P(Z_i \le -\beta_i \mid \mathbf{s}) = \Phi\left(\frac{-\beta_i - \Sigma_{k=1}^{m}(r_{ik} s_k)}{\sqrt{1 - \Sigma_{k=1}^{m} r_{ik}^2}}\right) \tag{5.9}$$

If a given correlation matrix cannot be described exactly by a generalized DS class, one can approximate it by obtaining a generalized DS model with the minimum fitting error (Kang et al., 2010).

5.2.3 Single-loop SRBTO algorithm using MSR method

The single-loop SRBTO using the MSR method is formulated as follows

$$
\begin{aligned}
&\min_{\mathbf{d},\mathbf{P}^t} f(\rho(\boldsymbol{\psi};\mathbf{d})) \\
&s.t. \quad g_{P_i^t} \cong g_i(\rho(\boldsymbol{\psi};\mathbf{d}),\mathbf{x}(\mathbf{u}_i^t)) \geq 0 \quad i=1,...,n \\
&\qquad P(E_{sys};\mathbf{P}^t) = \begin{cases} \int_{\mathbf{s}} \mathbf{c}^{\mathrm{T}}\mathbf{p}^t(\mathbf{s}) f_{\mathbf{S}}(\mathbf{s}) d\mathbf{s} \leq P_{sys}^t & \text{dependent} \\ \mathbf{c}^{\mathrm{T}}\mathbf{p}^t \leq P_{sys}^t & \text{independent} \end{cases} \\
&\text{where} \quad \mathbf{u}_i^t \cong \beta_i^t \cdot (\hat{\boldsymbol{\alpha}}_i^t)^{\mathrm{T}} \\
&\qquad \hat{\boldsymbol{\alpha}}_i^t \cong \left(-\frac{\nabla_{\mathbf{x}} g_i(\rho(\boldsymbol{\psi};\mathbf{d}),\mathbf{x}(\mathbf{u}))}{\left\| \nabla_{\mathbf{x}} g_i(\rho(\boldsymbol{\psi};\mathbf{d}),\mathbf{x}(\mathbf{u})) \right\|} \mathbf{J}_{\mathbf{x},\mathbf{u}} \right)_{\mathbf{u}=\tilde{\mathbf{u}}_i}
\end{aligned}
\tag{5.10}
$$

When limit-states are statistically dependent, the system failure probability is defined as a function of design variables in $\mathbf{P}_i^t$ by constructing $\mathbf{p}(\mathbf{s})$ using $P_i(\mathbf{s})$ in Equation (5.9) with β_i replaced by $\beta_i^t = -\Phi^{-1}(P_i^t)$. For a case with statistically independent limit-states, the probability vector $\mathbf{p}$ is constructed by use of $P_i = \Phi(-\beta_i^t)$. In Equation (5.10), the probability vectors are denoted as $\mathbf{p}^t$ and $\mathbf{p}^t(\mathbf{s})$ to indicate that the probability vectors are constructed by use of β_i^t instead of β_i. Inheriting the merits of the MSR method, the proposed SRBTO/MSR approach can evaluate the probability of a general system event efficiently and accurately with statistical dependence considered. This helps reduce the risk of having under- or over-conservative optimal designs caused by inaccurate system reliability calculations (Nguyen et al., 2010a). Figure 5.2 shows the flowchart of the single-loop SRBTO/MSR algorithm.

The MSR method provides the parameter sensitivities of $P(E_{sys})$ with respect to design variables so as to facilitate the use of gradient-based optimization algorithms. From Equation (5.7), the sensitivity of the system failure probability with respect to a parameter θ can be computed as follows

$$
\frac{\partial P(E_{sys})}{\partial \theta} = \begin{cases} \int_{\mathbf{s}} \mathbf{c}^{\mathrm{T}} \dfrac{\partial \mathbf{p}(\mathbf{s})}{\partial \theta} f_{\mathbf{S}}(\mathbf{s}) d\mathbf{s} & \text{dependent} \\ \mathbf{c}^{\mathrm{T}} \dfrac{\partial \mathbf{p}}{\partial \theta} & \text{independent} \end{cases}
\tag{5.11}
$$

Song and Kang (2009) developed an efficient matrix procedure to construct $\partial \mathbf{p}/\partial\theta$ and $\partial \mathbf{p}(\mathbf{s})/\partial\theta$ from the parameter sensitivities of component probabilities $\partial P_i/\partial\theta$ and $\partial P_i(\mathbf{s})/\partial\theta$, respectively. For example, one can obtain component-level parameter sensitivities using the FORM (Bjerager and Krenk, 1989).

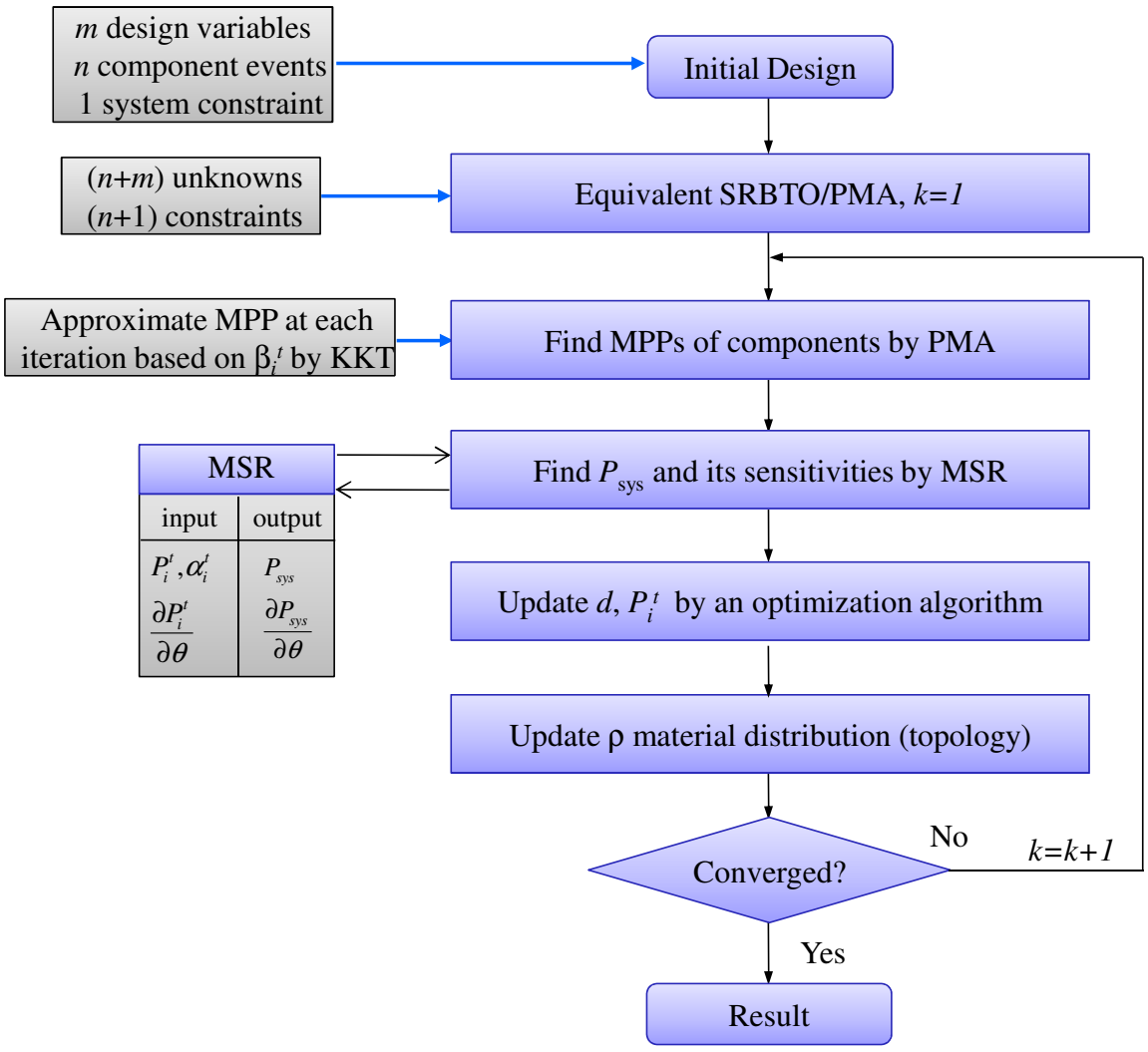

Figure 5.2: Flow chart of the single-loop SRBTO/MSR algorithm.

Herein the sensitivity of $P_i(\mathbf{s})$ with respect to the design variables in the proposed single-loop SRBTO, P_i^t, $i=1,...,n$ is derived so as to construct $\partial \mathbf{p}/\partial\theta$ and $\partial \mathbf{p}(\mathbf{s})/\partial\theta$ in Equation

(5.11) using the aforementioned matrix procedure in Song and Kang (2009). The sensitivity of $P_i(\mathbf{s})$ with respect to P_i^t is derived as

$$\frac{\partial P_i(\mathbf{s})}{\partial P_i^t} = \frac{\partial P_i(\mathbf{s})}{\partial \beta_i^t} \cdot \frac{\partial \beta_i^t}{\partial P_i^t} = -\frac{\partial P_i(\mathbf{s})}{\partial \beta_i^t} \cdot \frac{1}{\varphi(-\beta_i^t)} \tag{5.12}$$

in which $\varphi(\cdot)$ denotes the PDF of the standard normal distribution; and from (5.9), the sensitivity with respect to the target reliability index is derived as

$$\frac{\partial P_i(\mathbf{s})}{\partial \beta_i^t} = -\frac{1}{\sqrt{1-\Sigma_{k=1}^m r_{ik}^2}} \varphi\left(\frac{-\beta_i^t - \Sigma_{k=1}^m (r_{ik} s_k)}{\sqrt{1-\Sigma_{k=1}^m r_{ik}^2}} \right) \tag{5.13}$$

It is noted that the partial derivative of $P_i(\mathbf{s})$ with respect to $\mathbf{d}$ is zero (with P_i^t fixed). Therefore, for the constraint $P(E_{sys}) \le P_{sys}^t$, it is not necessary to evaluate the sensitivity of $P(E_{sys})$ with respect to $\mathbf{d}$.

Next, the sensitivities of $g_{P_i^t} \cong g_i(\rho(\boldsymbol{\psi};\mathbf{d}), \mathbf{x}(\mathbf{u}_i^t))$ with respect to the design variables are derived as follows. First, the sensitivities with respect to design variables $\mathbf{d}$ are evaluated as

$$\frac{\partial g_i(\rho(\boldsymbol{\psi};\mathbf{d}), \mathbf{x}(\mathbf{u}_i^t))}{\partial \mathbf{d}} = \frac{\partial g_i(\rho(\boldsymbol{\psi};\mathbf{d}), \mathbf{x}(\mathbf{u}_i^t))}{\partial \rho} \cdot \frac{\partial \rho(\boldsymbol{\psi};\mathbf{d})}{\partial \mathbf{d}} \tag{5.14}$$

where $\partial g_i(\rho, \mathbf{x}) / \partial \rho$ is computed for the given limit-state definition, e.g., volume, compliance and displacement. For example, the adjoin method (Bendsøe and Sigmund, 2003) may facilitate the sensitivity calculation; and $\partial \rho(\boldsymbol{\psi};\mathbf{d}) / \partial \mathbf{d}$ is obtained from the given projection function presented in (Nguyen et al., 2010b). The sensitivity of $g_{P_i^t}$ with respect to P_i^t is derived as

$$\begin{aligned} \frac{\partial g_{P_i^t}}{\partial P_i^t} &= \left[\nabla_{\mathbf{u}} g_i(\rho(\boldsymbol{\psi};\mathbf{d}), \mathbf{x}(\mathbf{u})) \right]_{\mathbf{u}=\mathbf{u}_i^t} \frac{\partial \mathbf{u}_i^t}{\partial P_i^t} \\ &\cong \left[\nabla_{\mathbf{x}} g_i(\rho(\boldsymbol{\psi};\mathbf{d}), \mathbf{x}(\mathbf{u})) \cdot \mathbf{J}_{\mathbf{x},\mathbf{u}} \right]_{\mathbf{u}=\mathbf{u}_i^t} \frac{\partial \beta_i^t}{\partial P_i^t} (\hat{\boldsymbol{\alpha}}_i^t)^{\mathrm{T}} \\ &= -\frac{1}{\varphi(-\beta_i^t)} \left[\nabla_{\mathbf{x}} g_i(\rho(\boldsymbol{\psi};\mathbf{d}), \mathbf{x}(\mathbf{u})) \cdot \mathbf{J}_{\mathbf{x},\mathbf{u}} \right]_{\mathbf{u}=\mathbf{u}_i^t} (\hat{\boldsymbol{\alpha}}_i^t)^{\mathrm{T}} \end{aligned} \tag{5.15}$$

Note that this partial derivative is approximate because $\hat{\boldsymbol{\alpha}}_i^t$ is assumed to be insensitive to the changes in P_i^t during the design iterations.

5.3 IMPROVING ACCURACY OF COMPONENT AND SYSTEM RBTO

This section introduces single-loop approaches to improve the accuracy of reliability calculations in component and system RBTO problems with highly nonlinear limit-state functions.

5.3.1 Accuracy in FORM-based reliability-based design and topology optimization

As shown in Equations (5.2), (5.5) and (5.10), the system reliability analysis during an SRBTO employs the results from the component reliability analyses on the given limit-states. Therefore, the accuracy of SRBTOs in satisfying the probabilistic constraint on the system event, i.e. $P(E_{sys}) \le P_{sys}^t$, depends on that of the component reliability analyses. The inaccuracy of the FORM-based reliability-based design and topology optimization has been reported in the literature (Mogami et al., 2006; Royset et al., 2006; McDonald and Mahadevan, 2008; Rahman and Wei, 2008; Silva et al., 2010; Lee et al., 2010a). Some studies have been conducted to improve the accuracy. For example, Royset et al. (2006) employed the first-order approximation for failure probability and then used higher-order reliability approximations or Monte Carlo simulations to adjust parameters to improve the accuracy of system reliability-based design optimization. Lee et. al. (2010a) also proposed to use the MPP-based dimension reduction method (Xu and Rahman, 2005) in the SRBDO framework.

Most of the single-loop SRBDO and SRBTO approaches (Liang et al., 2007; McDonald and Mahadevan, 2008; Silva et al., 2010; Nguyen et al., 2010a; Nguyen et al., 2010c) also employ the FORM for component probability analyses, which potentially results in unconservative or non-optimal solutions when the limit-state functions are highly nonlinear. For example, if a limit-state function is defined in term of the compliance under uncertain loads, the function is a quadratic function of the random variables representing the uncertainty in the loads. Therefore, the linear approximation by FORM may cause significant errors in component reliability analyses, and thus also in system reliability calculations. As an effort to apply the single-loop

approach to a wide range of topology optimization problems, a method to enhance the accuracy of the component failure probabilities into the single-loop component and system RBTO formulations is implemented.

5.3.2 Single-loop component reliability design and topology optimization with improved accuracy

First, let us consider the single-loop CRBTO in (5.3). At each step of the design iterations, the approximate MPP $\mathbf{u}_i^t$ is obtained by scaling the negative normalized gradient vector at $\mathbf{u} = \tilde{\mathbf{u}}_i$, i.e. $\hat{\boldsymbol{\alpha}}_i^t$ by the target reliability index β_i^t. The validity of the approximate MPP is checked at the final step of the design iterations. This procedure is modified to improve the accuracy of the single-loop approach. Instead of finding the approximate MPP on the surface of the sphere with the fixed radius β_i^t, the radius is updated at each step of the design iterations by the ratio of β_i^t to the reliability index by a more accurate reliability method such as the second-order reliability method (SORM). The formulation of the proposed scheme is as follows

$$
\begin{aligned}
&\min_{\mathbf{d}} f(\rho(\boldsymbol{\psi};\mathbf{d})) \\
&s.t. \quad g_{P_i^t} \cong g_i(\rho(\boldsymbol{\psi};\mathbf{d}), \mathbf{x}(\mathbf{u}_i^t)) \geq 0 \quad i = 1,...,n \\
&\text{at the } k\text{-th step: } \mathbf{u}_i^t \cong \beta_i^{t(k)} \cdot (\hat{\boldsymbol{\alpha}}_i^t)^{\mathrm{T}} \qquad (5.16) \\
&\beta_i^{t(k)} = \begin{cases} \beta_i^t & k = 1 \\ \dfrac{\beta_i^t}{\beta_i^{t(k-1)(SORM)}} \times \beta_i^{t(k-1)} & \text{otherwise} \end{cases} \\
&\hat{\boldsymbol{\alpha}}_i^t \cong \left(-\frac{\nabla_{\mathbf{x}} g_i(\rho(\boldsymbol{\psi};\mathbf{d}), \mathbf{x}(\mathbf{u}))}{\left\| \nabla_{\mathbf{x}} g_i(\rho(\boldsymbol{\psi};\mathbf{d}), \mathbf{x}(\mathbf{u})) \right\|} \mathbf{J}_{\mathbf{x},\mathbf{u}} \right)_{\mathbf{u}=\tilde{\mathbf{u}}_i}
\end{aligned}
$$

where $\beta_i^{t(k)}$ is the radius used for the scaling at the k-th step of the iterations; $\beta_i^{t(k-1)(SORM)}$ is the reliability index by the SORM, which is obtained based on the principal curvatures around $\mathbf{u} = \mathbf{u}_i^t$ at the (k−1)th step; and $\tilde{\mathbf{u}}_i$ is obtained by use of the KKT condition using β_i^t. The convergence of the radius $\beta_i^{t(k)}$ indicates that the reliability index by the SORM approaches the target reliability index β_i^t. Figure 5.3 shows the flowchart of the improved single-loop SRBTO/MSR algorithm. Compared to similar techniques appear in the literature (Royset et al., 2006; Rahman and Wei, 2008; Lee et al., 2010a), this study focuses on implementation into the

single-loop RBTO based on FORM (Nguyen et al., 2010e). In this study, the improved CRBTO by SORM in (5.16) is termed as SORM-based CRBTO. It should be noted that other reliability analysis methods such as importance sampling method or dimension reduction method can be used for the updating rule in the proposed approach if necessary.

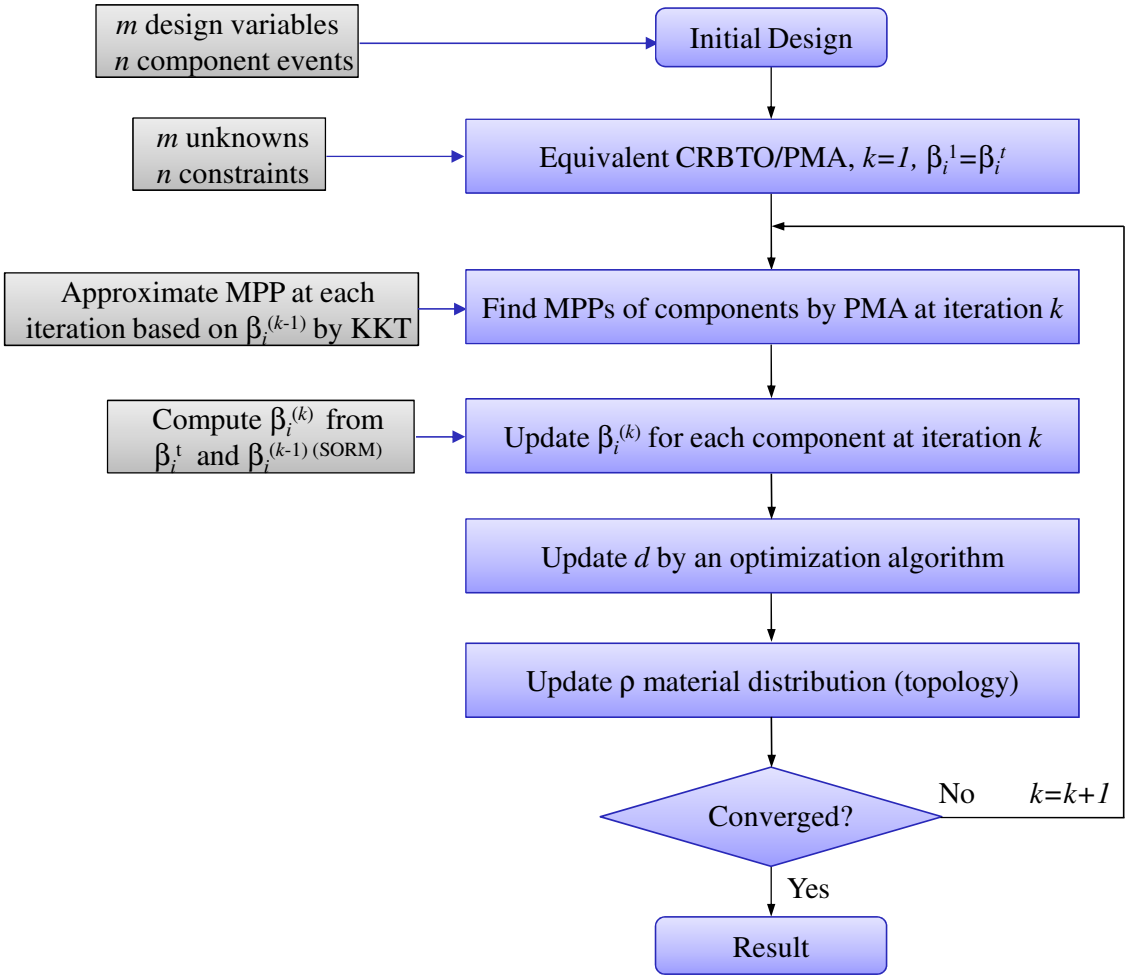

Figure 5.3: Flow chart of the improved single-loop CRBTO algorithm.

5.3.3 Single-loop system reliability-based design and topology optimization with improved accuracy

The single-loop SRBTO/MSR in Equation (5.10) is also improved by enhancing the accuracy of component reliability analysis results that are used for system reliability analyses (Nguyen et al., 2010f). The formulation of the SORM-based SRBTO/MSR is as follows

$$\begin{aligned}
&\min_{\mathbf{d},\mathbf{P}^t} f(\rho(\boldsymbol{\psi};\mathbf{d})) \\
&s.t. \quad g_{P_i^t} \cong g_i(\rho(\boldsymbol{\psi};\mathbf{d}),\mathbf{x}(\mathbf{u}_i^t)) \geq 0 \quad i=1,...,n \\
&\qquad P(E_{sys};\mathbf{P}^{t(SORM)}) = \begin{cases} \int_{\mathbf{S}} \mathbf{c}^{\mathrm{T}}\mathbf{p}^{t(SORM)}(\mathbf{s}) f_{\mathbf{S}}(\mathbf{s}) d\mathbf{s} \leq P_{sys}^t & \text{dependent} \\ \mathbf{c}^{\mathrm{T}}\mathbf{p}^{t(SORM)} \leq P_{sys}^t & \text{independent} \end{cases} \\
&\text{where } \mathbf{u}_i^t \cong \beta_i^t.(\hat{\boldsymbol{\alpha}}_i^t)^{\mathrm{T}} \\
&\qquad \hat{\boldsymbol{\alpha}}_i^t \cong \left(-\frac{\nabla_{\mathbf{x}} g_i(\rho(\boldsymbol{\psi};\mathbf{d}),\mathbf{x}(\mathbf{u}))}{\left\| \nabla_{\mathbf{x}} g_i(\rho(\boldsymbol{\psi};\mathbf{d}),\mathbf{x}(\mathbf{u})) \right\|} \mathbf{J}_{\mathbf{x},\mathbf{u}} \right)_{\mathbf{u}=\tilde{\mathbf{u}}_i}
\end{aligned} \tag{5.17}$$

where $\mathbf{P}^{t(SORM)}$ is the vector of the component failure probabilities by the SORM at the approximate MPPs, $\mathbf{u}_i^t,\ i=1,...,n$; $\mathbf{p}^{t(SORM)}(\mathbf{s})$ and $\mathbf{p}^{t(SORM)}$ denote the probability vector constructed by use of the SORM reliability indexes $\beta_i^{t(SORM)}$ instead of β_i^t; and $\tilde{\mathbf{u}}_i$ is obtained by use of the KKT condition using β_i^t. The only change from Equation (5.10) is that the probability vector is constructed by use of the SORM reliability indexes instead of the FORM reliability indexes at the approximate MPPs. Figure 5.4 shows the flowchart of the improved single-loop SRBTO/MSR algorithm.

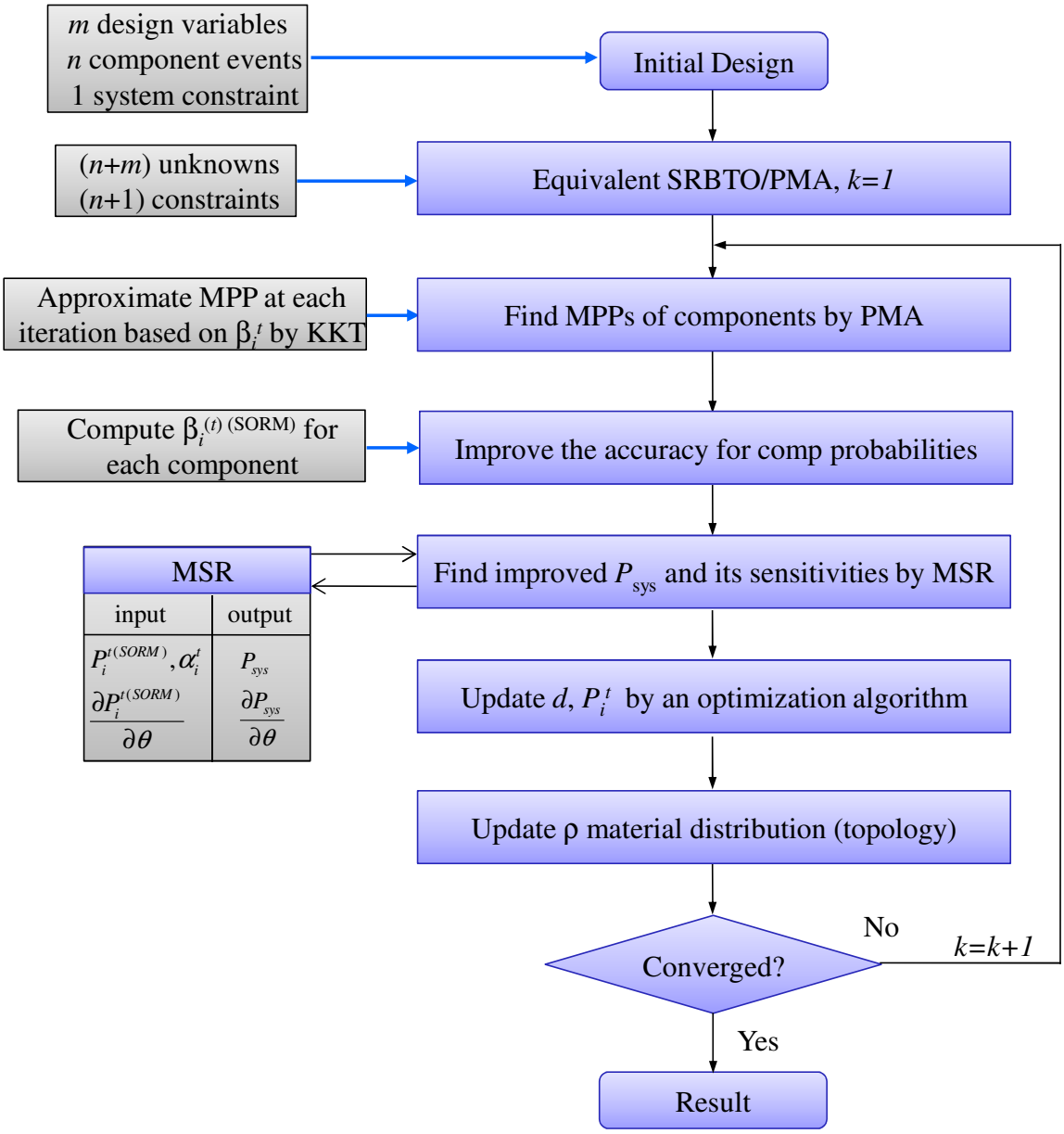

Figure 5.4: Flow chart of the improved single-loop SRBTO/MSR algorithm.

5.4 MULTIRESOLUTION TOPOLOGY OPTIMIZATION AND PATTERN REPETITION

In this section, the MTOP approach is briefly reviewed and further developed to include pattern symmetry and pattern repetition constraints.

5.4.1 MTOP formulations

A main challenge in performing RBTOs for realistic problems is the high computational cost which is inherited from deterministic topology optimization. The material distribution topology optimization method (Bendsøe, 1989) is often used in topology optimization. This method rasterizes the domain via the density of pixels/voxels, and thus often requires a large number of design variables, especially in three-dimensional applications. Most of the research efforts to overcome this challenge focused on finite element analysis that constitutes the dominant computational cost in topology optimization. For example, researchers make use of powerful computing resources such as parallel computing (Borrvall and Petersson, 2001; Evgrafov et al., 2008), approximation procedure (Amir et al., 2009), or fast iterative solvers (Wang et al., 2007; Amir et al., 2010). These studies employ the same level of resolution for finite element mesh and the design mesh during the optimization process. In order to obtain high-resolution topology designs with a relatively low computational cost, the multiresolution topology optimization approach in Chapter 2 is employed for RBTO problems. In this section, the MTOP approach is briefly reviewed and further developed to include pattern symmetry and pattern repetition constraints.

Different from the conventional approaches which use the same mesh for finite element analysis and design, the MTOP approach utilizes three different meshes: a *relatively coarse finite element (FE) mesh* to perform the analysis, a *fine design variable mesh* to perform the optimization, and a *fine density mesh* to represent material distribution. The density mesh is finer than the finite element mesh so that each finite element consists of a number of density elements (sub-elements). The theory and formulation of the MTOP approach can be found in Chapter 2. The basic statement formulation for a "minimum compliance" (i.e. maximum stiffness) topology optimization problem to illustrate the MTOP approach is as follows

$$\begin{aligned} &\min_{\mathbf{d}} \quad f(\rho(\boldsymbol{\psi};\mathbf{d})) = C(\rho(\boldsymbol{\psi};\mathbf{d}),\mathbf{u}_d) = \mathbf{f}^{\mathrm{T}}\mathbf{u}_d \\ &s.t. \quad V(\rho(\boldsymbol{\psi};\mathbf{d})) = \int_{\Omega} \rho(\boldsymbol{\psi};\mathbf{d}) dV \le V_s \end{aligned} \tag{5.18}$$

where $C(\rho,\mathbf{u}) = \mathbf{f}^{\mathrm{T}}\mathbf{u}_d$ is the compliance of the continuum; $V(\rho)$ is the total volume; and V_s is the prescribed volume constraint.

5.4.2 Pattern symmetry and pattern repetition in MTOP

The topology optimization approach is usually applied to concept design of structures. Due to some practical constraints or demands, these structures may require pattern symmetry and/or pattern repetition in the design. For example, pattern symmetry and repetition have been successfully incorporated into the topology optimization of functionally graded material in two-dimensional structures (Almeida et al., 2010). In this chapter, pattern symmetry and repetition conditions are implemented into the framework of the multiresolution topology optimization. Because the design variables are separated from the analysis model in the MTOP framework in (5.18), a basic set of design variables can be chosen and mapped to the whole domain to satisfy the pattern symmetry and/or pattern repetition condition. Figure 5.5 illustrates the mapping schemes to gain pattern symmetry and repetition in the optimal design.

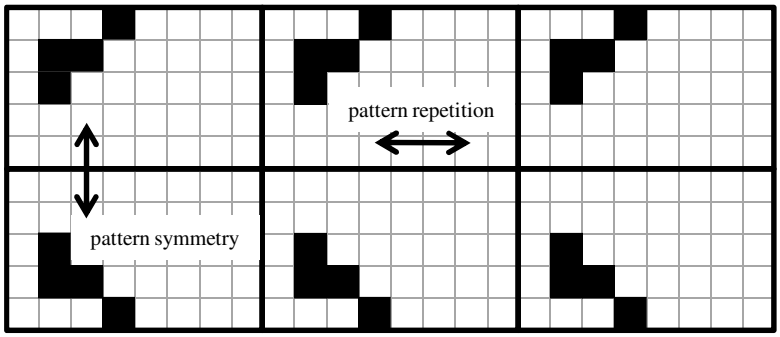

Figure 5.5: Design variables mapping for pattern symmetry and pattern repetition.

5.5 NUMERICAL EXAMPLES

In this section, the proposed SRBTO/MSR procedure and the SORM-based improvement on CRBTO and SRBTO/MSR are demonstrated by numerical examples. In all numerical examples, MTOP is used for computational efficiency. First, a two-dimensional bridge example demonstrates the impact of statistical dependence between the limit-states in SRBTO, which can

be considered appropriately by the SRBTO/MSR approach. Second, a three-dimensional cube example shows the improvement in the accuracy of the SORM-based RBTOs over the FORM-based RBTOs. Third, a three-dimensional building example demonstrates that the SORM-based SRBTO approach can be applied to computationally demanding topology optimization problems with pattern repetition scheme by use of MTOP. For simplicity, all the quantities are given dimensionless.

5.5.1 Two-dimensional bridge

The first example considers a two-dimensional bridge design in a domain of 250×50 and thickness of 0.05 as shown in Figure 5.6. The objective of the optimal design is to minimize the volume of the structure under constraints on the displacements at selected locations. The isotropic material is assumed to have Young's modulus E^0 of 2×10^8 and Poisson's ratio ν of 0.3. The minimum length scale $r_{\min}$=1.25, and penalization parameter p=3 are employed. These material properties are hereby assumed to be deterministic since the uncertainties in material properties usually have minimal impacts on reliability-based optimal topologies for a structure under linear elastic behavior. Stochastic loads are applied at nine locations on a non-designable layer (with thickness of two) at the bottom of the bridge as shown in Figure 5.6. A symmetric loading condition is assumed, so the nine loads are modeled by use of five random variables. Each of the five random variables is assumed to follow a Gaussian distribution with the mean (μ_F) of 100,000 and coefficient of variations (ratios of the standard deviations to the means) of 1/6. All the five random variables are assumed to be uncorrelated. The constraints on the displacements at the locations of the applied forces are described by the limit-state functions

$$g_i(\boldsymbol{\rho},\mathbf{F}) = d_i^0 - d_i(\boldsymbol{\rho},\mathbf{F}),\ \ i=1,..,5 \tag{5.19}$$

where $\boldsymbol{\rho}$ denotes the vector of the element densities; $\mathbf{F}$ is the vector of the random variables representing applied forces; $d_i(\boldsymbol{\rho},\mathbf{F})$ is the vertical displacement at the i-th location predicted by a finite element analysis; and d_i^0 is the limit on the displacement. In this example, the displacement limit is given as $\{d_i^0\} = \{1.25, 1.50, 1.75, 2.00, 2.25\},\ i = 1,..,5.$ Because of the

symmetry conditions, only a half of the domain is taken into the analysis model with 125×50 MTOP elements (Q4/n9/d9).

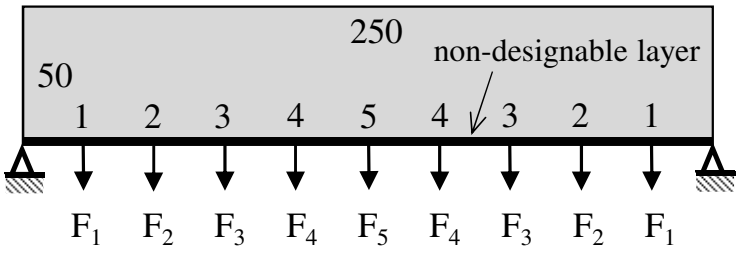

Figure 5.6: Configurations of two-dimensional bridge example.

First, a deterministic topology optimization (DTO) is performed with the loads equal to the given mean values. This is performed by Equation (5.1) except that the probabilistic constraints are replaced by deterministic ones, i.e. $g_i(\boldsymbol{\rho}, \mathbf{F}) \geq 0$. The corresponding optimal design is shown in Figure 5.7a. The volume fraction (*volfrac*) of the optimal design, i.e. the ratio of the optimal volume to that of the original domain is 39.07%. Next, a FORM-based CRBTO is conducted as in (5.3) with all the reliability index targets $\beta_i^t = 2$ (or $P_i^t = 0.02275$). The optimal topology shown in Figure 5.7b has the volume fraction of 48.64%. The optimal volume is higher than that by the DTO since the topology that avoids the failure under the mean loads is expected to have significantly higher probability to violate the constraints than the given target failure probability. After the CRBTO optimization is completed, the probability that at least one of the constraints is violated (i.e. series system) is estimated by the MSR method as $P_{\text{sys}} = 0.066517$. Next, a FORM-based SRBTO/MSR is performed for the series system event with the same target system failure probability $P_{\text{sys}} = 0.066517$. This is to compare the optimal topologies by CRBTO and SRBTO that have the same system failure probability. The SRBTO optimal topology, which is different from those by DTO and CRBTO, is shown in Figure 5.7c (volume fraction of 47.70%). Another SRBTO is performed with the means of loads reduced to 25% (Figure 5.7d) to see the impacts of the load intensity on the optimal topology.

Table 5.1 shows the component and system failure probabilities by Monte Carlo simulations (MCS) for the optimal designs by the CRBTO and SRBTO in order to verify the accuracy of the

FORM-based RBTO procedures in this example. The results confirm that the FORM-based RBTO designs provide failure probabilities that are compatible with the target probabilities on component events (CRBTO) and system event (SRBTO). This is because the limit-state functions in this example are linear function of the uncertain loads and the random variables are assumed to follow Gaussian distributions. Thus, the improvement schemes proposed in Section 5.3 are not required.

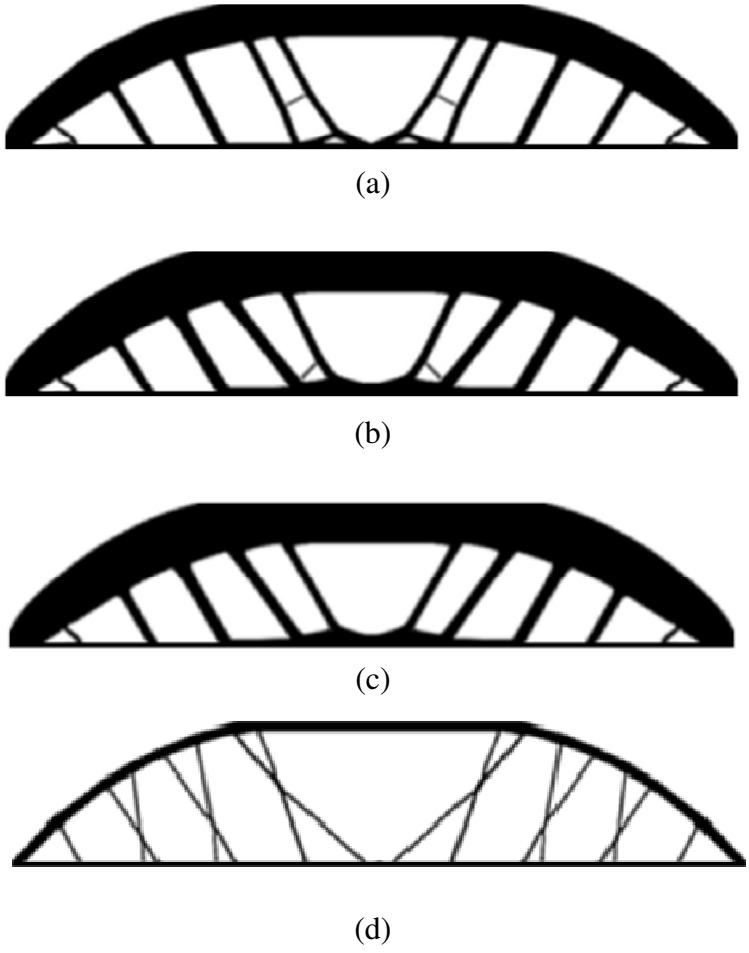

(a)

(b)

(c)

(d)

Figure 5.7: The results of two-dimensional bridge example: (a) DTO ($\mu_F = 10^5$, *volfrac* = 39.07%); (b) FORM-based CRBTO ($\mu_F = 10^5$, *volfrac* = 48.64%); (c) FORM-based SRBTO/MSR ($\mu_F = 10^5$, *volfrac* = 47.70%); and (d) FORM-based SRBTO/MSR ($\mu_F = 2.5\times10^4$, *volfrac* = 16.66%).

The efficiency of MTOP over the conventional element-based approach is investigated using the SRBTO problem above. To obtain a similar level of resolution using the element-based

approach, it is necessary to use 375×150 Q4/U elements. After 50 iterations, the computer run time of the element-based approach is about two times more than the MTOP Q4/n9/d9 approach. The efficiency is further increased as a higher level of resolution is employed. More details on comparison of computational cost are found in Chapter 2.

Table 5.1: Two-dimensional bridge example: verification of failure probabilities of CRBTO and SRBTO designs by MCS (10^6 times, c.o.v = 0.005).

	CRBTO	MCS on CRBTO design	SRBTO/MSR	MCS on SRBTO design
P_1	0.002275	0.002266	0.001214	0.001281
P_2	0.002275	0.022798	0.016284	0.016331
P_3	0.002275	0.023119	0.039239	0.039377
P_4	0.002275	0.023019	0.042740	0.042662
P_5	0.002275	0.023132	0.023450	0.023239
P_{sys}	0.066517	0.066990	0.06652	0.066719

In this example, the volume fraction from SRBTO (47.70%) is fairly close to that of the CRBTO (48.64%) that gives the same system failure probability. This might give an impression that SRBTO is not necessary considering the additional computations for the system failure probability. However, SRBTO is still preferred for RBTO problems under probabilistic constraint on the system failure event for the following reasons. First of all, the probabilistic constraints on individual limit-states that would satisfy the given constraint on the system failure probability are not known a priori. In this numerical example, the constraint on the system failure probability in SRBTO is chosen as the system failure probability of the result of the CRBTO just for comparison purpose. Second, in using CRBTO formulation for solving SRBTO problems, all the component target failure probabilities are often given equal mainly because the actual component failure probabilities of an optimal design that would satisfy the system constraint are not known. Introducing such uniform target component failure probabilities often makes the SRBTO problems more constrained than necessary, which may lead to non-optimal solutions (Nguyen et al., 2010a). Finally, in SRBTO, one can identify the relative contribution of each limit-state to

the system probability based on components probabilities of the optimal design or by use of the component importance measures by the MSR method (Song and Kang, 2009; Nguyen et al., 2010a). According to the component failure probabilities of the optimal designs, the importance ranking of the limit-states is as follows: 4 (most important) →3→5→2→1 (least important).

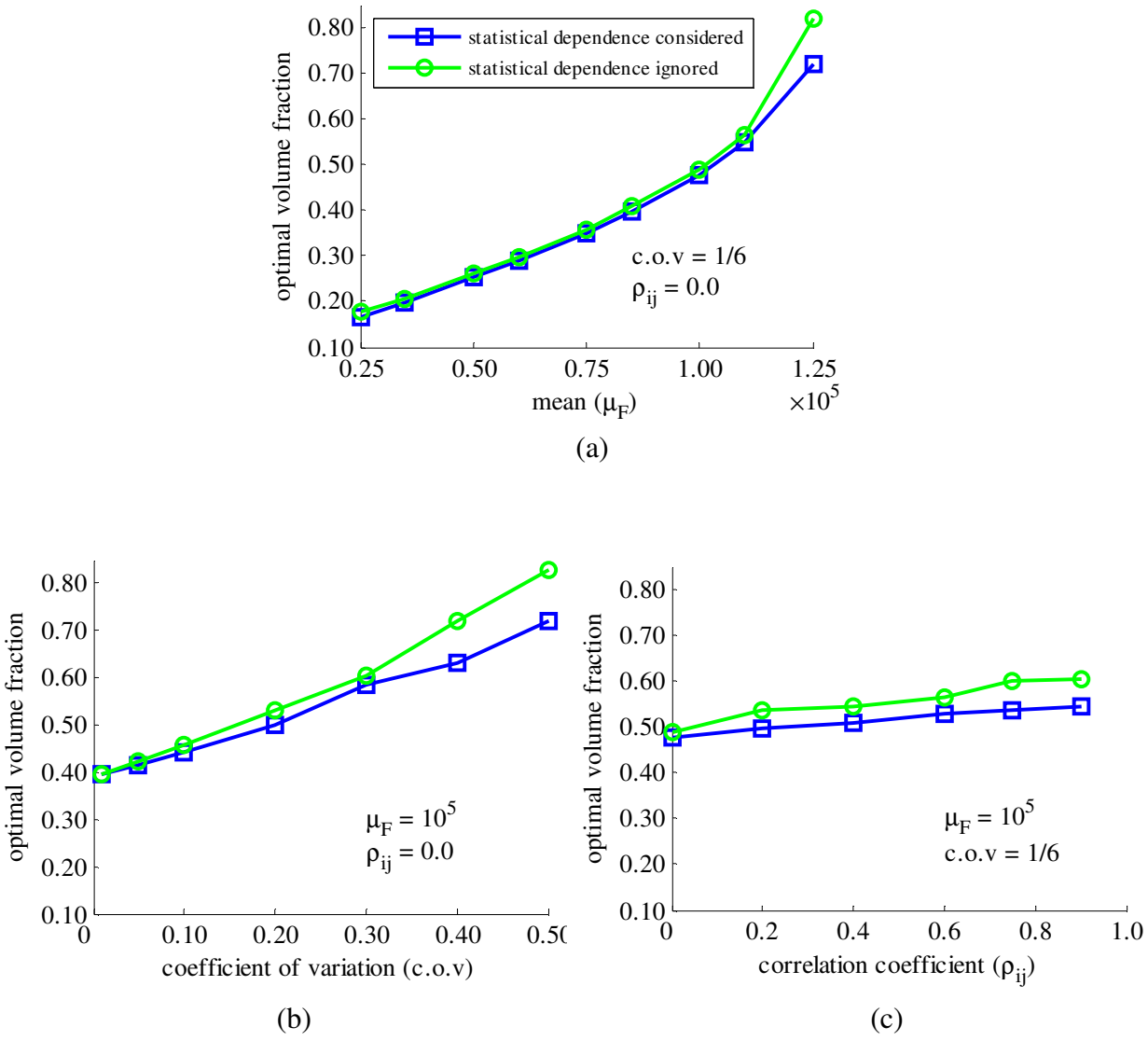

Figure 5.8: Impact on FORM-based SRBTO results (volume fraction) by changes in (a) mean values (c.o.v = 1/6, ρ_{ij} = 0.0); (b) coefficients of variation (μ_F = 100,000, ρ_{ij} = 0.0); and (c) correlation coefficients (μ_F = 100,000, c.o.v = 1/6) of the load random variables.

The effects of the means, coefficient of variations, and the correlations between random variables F_i's on the optimal topologies are also investigated. For simplicity, all the loads are assumed to have the same mean values (μ_F), coefficients of variation (c.o.v), and correlation coefficients (ρ_{ij}). The SRBTO problem is solved again with the same target system probability of 0.066517 while the mean values, coefficient of variations and correlation coefficients are varied. First, Figure 5.8a and Figure 5.8b show how the increase in means (from 0.25×10^5 to 1.25×10^5) and coefficient of variations (from 0.01 to 0.50) results in the increase in volume fractions of the optimal topology. Next, the impacts of changes in the correlation coefficients (from 0.00 to 0.90) of the load random variables are shown in Figure 5.8c. It is seen that positive correlation among the random loads results in higher volume fractions, i.e. more conservative design. This is because positively correlated loads increase the displacements, and thus the failure probabilities. Therefore, in this problem, if the positive correlation is ignored, the RBTO may lead to an unsafe design. Also presented in each plot are the results with the statistical dependence between limit-states ignored, i.e. the system failure probability is approximated by (5.6). As shown in Figure 5.8, designs become more conservative than necessary when statistical dependence is ignored. This is because the failure probability of a series system is overestimated when statistical dependence is ignored. From Figure 5.8b and Figure 5.8c, it is also noted that the effect of statistical dependence on the optimal designs increases as the coefficients of variation or the correlation coefficients of the random loads increase.

5.5.2 Three-dimensional cube

This numerical example is to demonstrate the improved accuracy of the proposed SORM-based RBTO methods. The objective of optimization is to minimize the volume in a cube domain shown in Figure 5.9 while satisfying constraints on the compliances for multiple load cases. One corner is fixed in all three directions while the other corners are restricted in the vertical direction only. The isotropic material is assumed to have Young's modulus of $E^0 = 1,000$ and Poisson's ratio of $\nu = 0.3$. A cube of edge length $L = 24$ is divided into 12×12×12 B8/n125/d125 MTOP elements. The minimum length scale $r_{\min} = L/10$, and penalization parameter $p = 3$ are employed. The structure is subjected to three random loads applied at five locations as shown in

Figure 5.9. F_1 denotes the magnitude of the force at the center while F_2 and F_3 represent the loads at the midpoints between the center and the four corner points of the top face. F_1, F_2 and F_3 are assumed to be normal random variables with the mean values 100, 0 and 0, and with the standard deviations 10, 30 and 40, respectively.

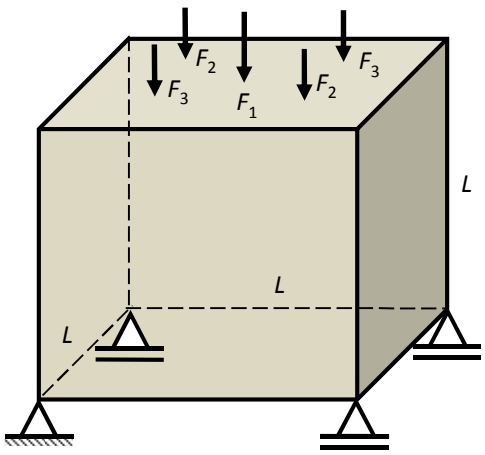

Figure 5.9: Three-dimensional topology optimization of a cube.

Limit-states are defined on the compliances caused by two load combinations $\overline{\mathbf{F}}_1 = (F_1, F_2)$ and $\overline{\mathbf{F}}_2 = (F_1, F_3)$ as follows

$$g_i(\boldsymbol{\rho}, \overline{\mathbf{F}}_i) = C_i^t - C_i(\boldsymbol{\rho}, \overline{\mathbf{F}}_i) = C_i^t - \mathbf{u}^{\mathrm{T}}\mathbf{F}_i, \;\; i = 1, 2 \tag{5.20}$$

where $C_i^t (= 120)$ is the constraint on the compliance; $C_i(\boldsymbol{\rho}, \overline{\mathbf{F}}_i)$ is the compliance corresponding to the load case $\overline{\mathbf{F}}_i$; and $\mathbf{F}_i$ is the global force vector assembled based on the load case $\overline{\mathbf{F}}_i$. The following three topology optimization methods are investigated: (1) Deterministic Topology Optimization (DTO) using the mean values of the loads with deterministic constraints $g_i(\boldsymbol{\rho}, \overline{\mathbf{F}}_i) \geq 0$; (2) CRBTO with probability constraints $P_1^t = P_2^t = 0.02275$, i.e. reliability indexes $\beta_1^t = \beta_2^t = 2.0;$ and (3) SRBTO with the system limit-state $E_{sys} = \{(g_1(\boldsymbol{\rho}, \overline{\mathbf{F}}_1) \leq 0) \bigcup (g_2(\boldsymbol{\rho}, \overline{\mathbf{F}}_2) \leq 0)\}$ with $P_{sys}^t = 0.04493$, which is given so as to match the system failure probability of the optimal topology of the CRBTO.

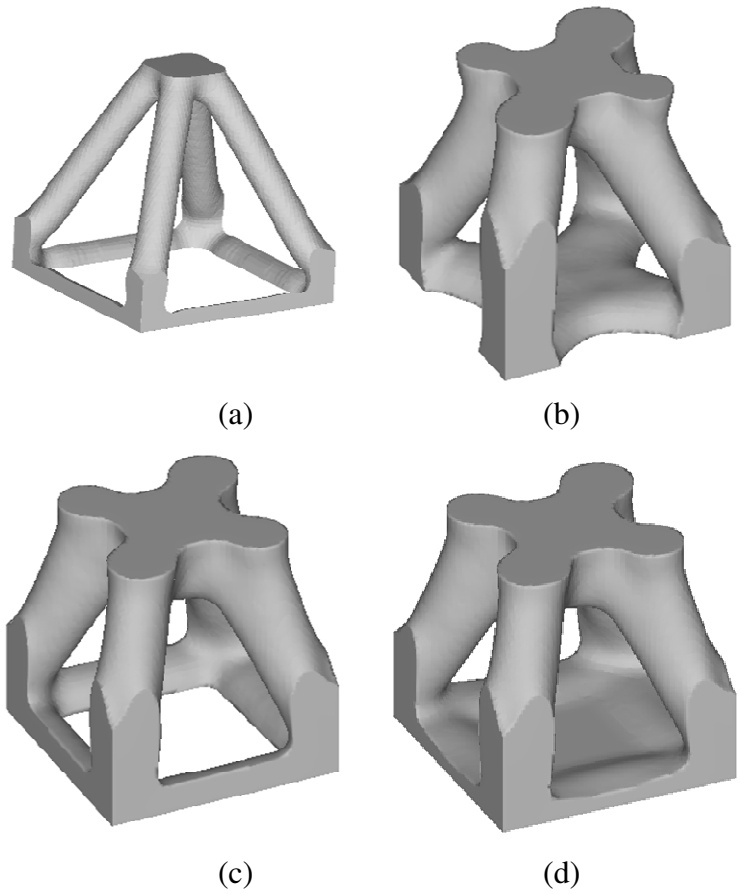

Figure 5.10: Optimal topologies by: (a) DTO (*volfrac* = 6.3%); (b) SORM-based CRBTO ($\sigma(F_1)$ = 10, *volfrac* = 24.4%); (c) SORM-based SRBTO ($\sigma(F_1)$ = 10, *volfrac* = 22.3%); and (d) SORM-based SRBTO ($\sigma(F_1)$ = 20, *volfrac* = 23.9%).

Figure 5.10 shows the optimal topologies by DTO (Figure 5.10a), SORM-based CRBTO (Figure 5.10b), and SORM-based SRBTO (Figure 5.10c). The volume fraction of DTO is lower than CRBTO and SRBTO because the risk of high compliance caused by the load uncertainties is ignored. With the same system failure probabilities, the volume fraction of CRBTO is 10% higher than SRBTO. This is because CRBTO approach (assigning fixed constraints on individual components) is generally more constrained than SRBTOs (assigning a constraint on system event, not on the individual components) at the same level of system failure probability (Nguyen et al., 2010a). Figure 5.10d shows the result of the SRBTO with the standard deviation of F_1 increased to see the impact of the load variability on the topology. In summary, it is seen from Figure 5.10

that the optimal topology is affected significantly by the load variability and the failure event definitions on the optimal topology of a structure.

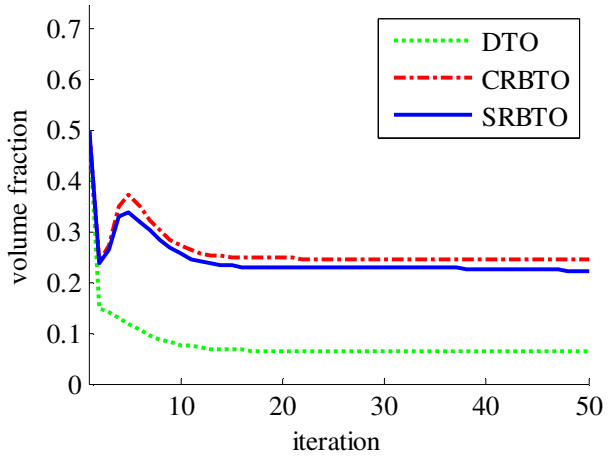

Figure 5.11: Convergence histories of topology optimizations of the cube.

The convergence histories of the optimizations are shown in Figure 5.11. The proposed single-loop SORM-based CRBTO and SRBTO show similar rates of convergence, which are also comparable to that of DTO. The system failure probability of the optimal topology found by SORM-based SRBTO/MSR, P_{sys} = 0.04493 is verified by a fairly close estimate of MCS, P_{sys} = 0.04515 (10^6 times, c.o.v = 0.005).

In order to demonstrate the improved accuracy of the SORM-based single-loop CRBTO method, the results are compared with those by the FORM-based CRBTO with the component probability targets $P_1^t = P_2^t = 0.02275$. Figure 5.12a shows the differences in the volume fractions of the optimal designs. Monte Carlo simulations (MCS: 10^6 times, c.o.v = 0.005) are performed to find the component failure probabilities of the optimal topologies by the FORM-based and SORM-based CRBTOs. The results in Figure 5.12b and Figure 5.12c show that the component probabilities of SORM-based CRBTOs are fairly close to the target probabilities while the FORM-based CRBTOs show significant errors especially when the random loads have large variability.

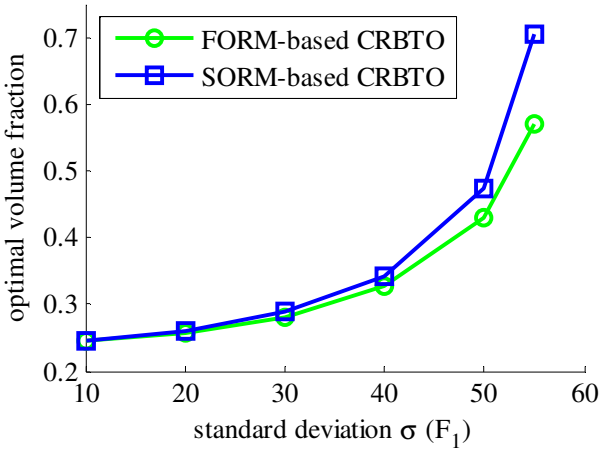

(a)

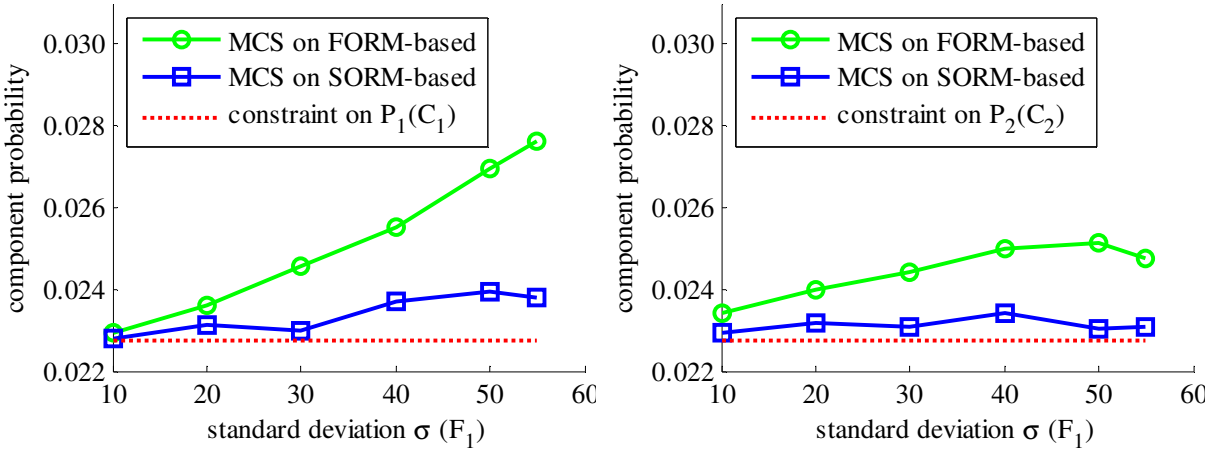

(b) (c)

Figure 5.12: CRBTOs with variation of standard deviation of load F_1: (a) volume fraction of optimal designs; (b) failure probabilities on the first limit-state; and (c) failure probabilities on the second limit-state.

The accuracy of the SORM-based single-loop SRBTO method is also investigated. The FORM-based and SORM-based SRBTO are performed with the system probability target of 0.04493 while the standard deviation of load F_1 is varied from 10 to 60. Figure 5.13a compares the volume fractions by the FORM and SORM-based SRBTOs. It is seen that the FORM-based SRBTO provides unconservative designs due to the inaccuracy in reliability calculations. The

results of Monte Carlo simulations (MCS: 10^6 times; c.o.v = 0.005) in Figure 5.13b show that the proposed SORM-based SRBTO provides improved accuracy in predicting the system failure probability.

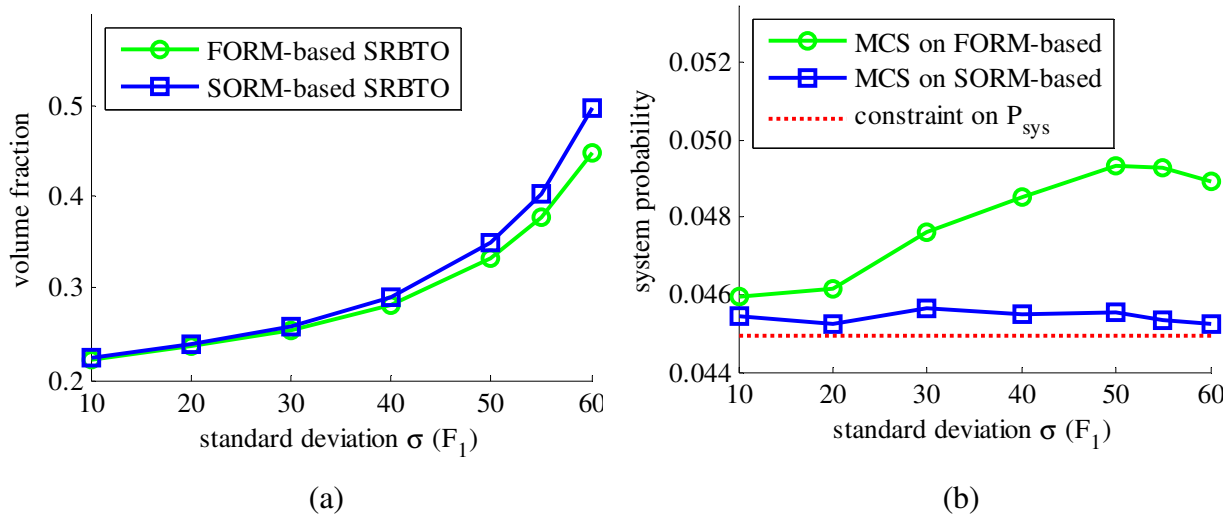

Figure 5.13: SRBTOs with variation of standard deviation of load F_1: (a) volume fractions of optimal designs; and (b) system failure probabilities.

The results in Figure 5.12a and Figure 5.13a show the volume fractions of the optimal designs increase significantly as the load variability increases. It is because the variability of random load increases the uncertainty of the compliance and thus the probability of violating given constraints.

5.5.3 Three-dimensional building

The proposed SRBTO/MSR method and the MTOP approach enable system reliability-based optimization for large-scale structural topologies. In this example, the SORM-based SRBTO employing the MTOP approach is used to design the structural topology of a building core subjected to horizontal loads. The objective of the optimization is to minimize the volume under the constraint on system failure event defined in terms of the compliances for multiple load cases. Figure 5.14a shows the domain of the topology with the dimensions of $L\times L\times 5L\times L/12$ in which $L/12$ represents the thickness of the core (L=24). The domain is divided into

12×12×60×1 B8/n125/d125 MTOP elements, which results in a total of 2,640 brick elements. The four corners of the domain are non-designable regions which are shown as black areas in Figure 5.14b. Young's modulus E^0 of 10^6, Poisson's ratio ν of 0.3, the minimum length scale $r_{\min} = L/10$, and penalization parameter $p = 4$ are employed. In this example, the building core is designed with four symmetric axes: *x*, *y* and two diagonal directions (dash-dot lines in Figure 5.14b).

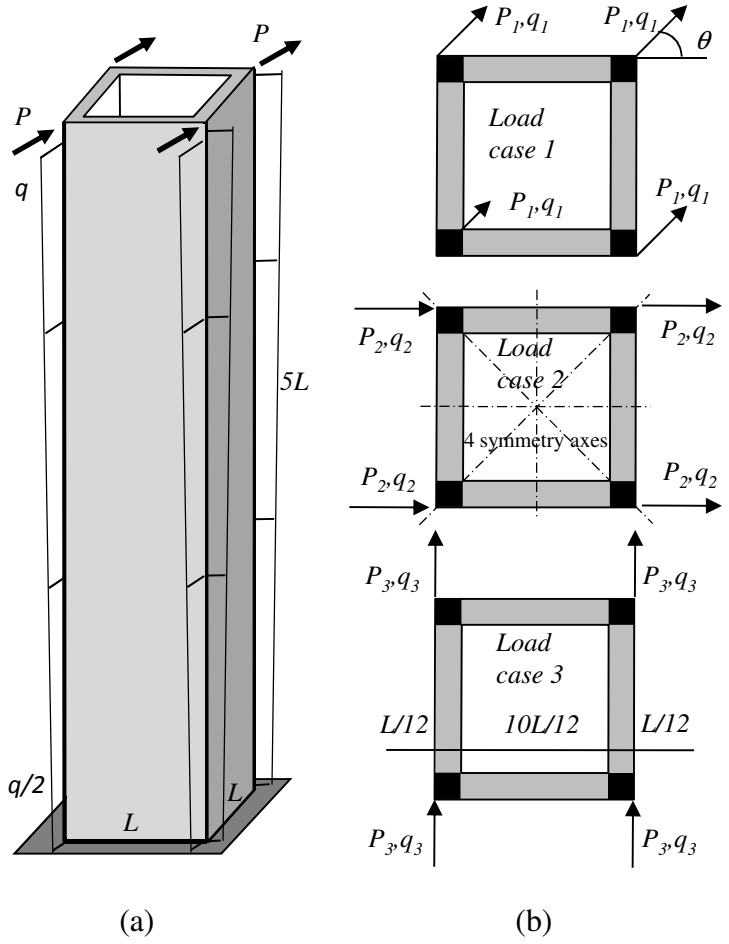

(a) (b)

Figure 5.14: Building core example: (a) domain; and (b) load cases

Three load cases as shown in Figure 5.14b are considered. In the first load case, the uncertain point loads (P_1) and the uncertain distributed loads (linearly varying from $q_1/2$ to q_1 along the height as shown in Figure 5.14a) are applied with the angle of $\theta=45^o$ (diagonal

direction). The second and third load cases have the angle of $\theta=0^o$ (x direction), and $\theta=90^o$ (y direction), respectively. During the finite element analyses, for simplicity, the distributed load is converted to the equivalent point loads applied at the finite element nodes along the height of the building. All six random variables $\{P_1,P_2, P_3, q_1, q_2, q_3\}$ are assumed to follow normal distributions. Table 5.2 provides the means and the coefficients of variation (c.o.v) of the random variables and the corresponding constraints given on the compliances of the system. These load random variables are assumed to be correlated with correlation coefficient $\rho_{same} = 0.50$ when they belong to the same load case and the correlation coefficient $\rho_{diff} = 0.25$ for the loads from different load cases.

Table 5.2: Three-dimensional building example: statistical parameters of the load random variables and constraint on the compliances

Load Cases	P		q (at top)		C_i^t
	mean	c.o.v	mean	c.o.v	
Case 1	70.71	0.30	2.82	0.15	250
Case 2	50.00	0.15	2.00	0.30	125
Case 3	50.00	0.20	2.00	0.15	125

First of all, the optimization problem is solved without pattern repetition constraints (Case I). The deterministic topology optimization is performed using the mean values of the loads (Figure 5.15a) and the SORM-based SRBTO is conducted with the target system probability $P_{sys}^t = 0.05$ on the series system event of compliance limit-states determined for the three load cases (Figure 5.15b). The DTO (*volfrac* = 21.93%) and SRBTO (*volfrac* = 28.15%) result in significantly different topologies. The higher volume fraction in the SRBTO topology implies the importance of considering the uncertainties in the loads for building structures. In addition, the topology in Figure 5.15b from SRBTO shows a better design than the design from DTO in Figure 5.15a: First, the diagonal members in Figure 5.15b are distributed more evenly along the vertical direction. Second, the diagonal members in Figure 5.15b start from the supports to transfer the load, that pattern is often found in the design practice. The component and system probabilities of the optimal topologies by SRBTO/MSR and MCS (10^6 times, c.o.v = 0.005) are shown in

Table 5.3, which confirms the accuracy of the SORM-based SRBTO. The component probabilities of 0.02731, 0.02088, and 0.00539 help identify the relative importance ranking of the three constraints as 1→2→3.

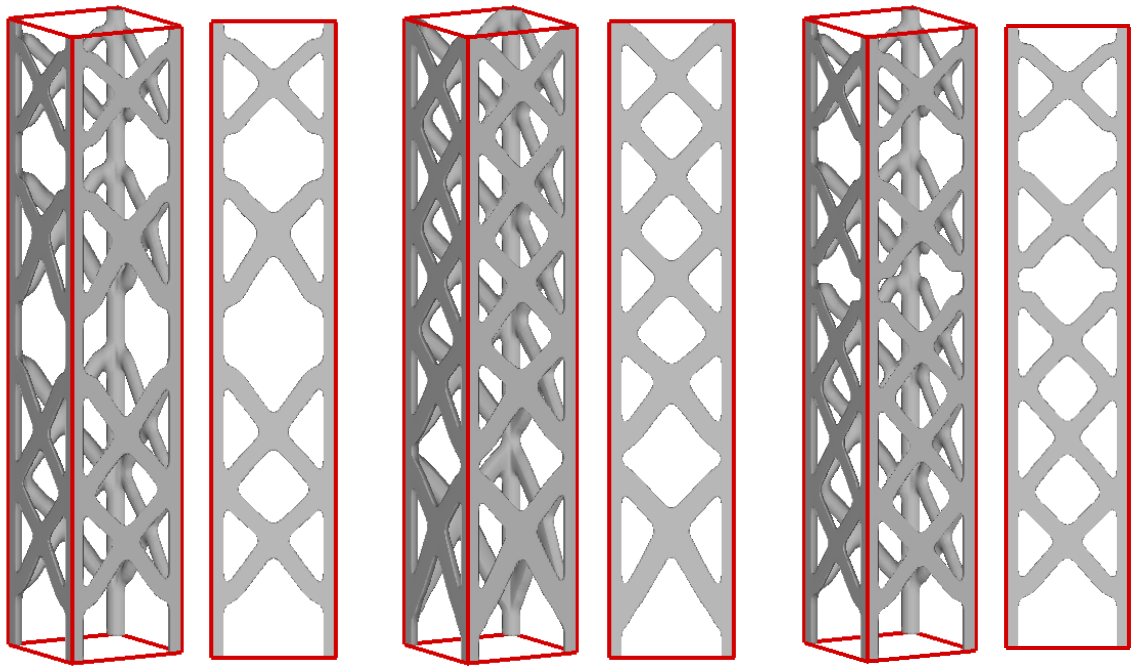

(a) (b) (c)

Figure 5.15: Building core optimal topologies (three-dimensional and side views): (a) DTO *volfrac*=21.93%; (b) SRBTO *volfrac*=28.15% ($P_{sys}^t = 0.05$); and (c) SRBTO *volfrac*=22.25% ($P_{sys}^t = 0.85$).

Next, the system probability target P_{sys}^t is varied from 0.01 to 0.85 (Case II). Figure 5.16 shows the volume fractions of the optimal designs for the range. It is seen that the decrease of the target probability (i.e. more conservative) increases the volume fractions of the optimal designs. The volume fraction of the SRBTO converges to that of DTO as the target probability increases. For example, the target system probability of 0.85 results in the volume fraction of 22.25%, which is only 1.4% different from DTO (21.93%). Even though these two optimal volume fractions are fairly close to each other, it is noteworthy that the optimal topology of SRBTO (P_{sys}=0.85) in Figure 5.15c is different from that of DTO in Figure 5.15a.

Table 5.3: Three-dimensional building example: component and system probabilities by SRBTO/MSR and MCS (10^6 times). Note: the changes from the default case are shown in bold.

		P_1	P_2	P_3	P_{sys}
ρ_{same} = 0.50 ρ_{diff} = 0.25	SRBTO/MSR	0.02731	0.02088	0.00539	0.05000
	MCS (c.o.v=0.005)	0.02747	0.021006	0.00542	0.05023
ρ_{same} = 0.50 ρ_{diff} = 0.25	SRBTO/MSR	0.26940	0.25973	0.20818	**0.50000**
	MCS (c.o.v=0.001)	0.26977	0.26006	0.20800	0.50008
ρ_{same} = **0.90** ρ_{diff} = **0.45**	SRBTO/MSR	0.02812	0.02227	0.00625	0.05000
	MCS (c.o.v=0.004)	0.02816	0.02242	0.00638	0.05017

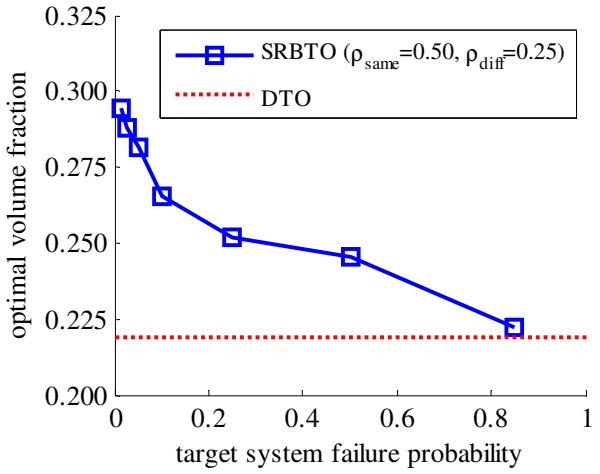

Figure 5.16: Optimal volume fractions with target system failure probability.

The problem is solved again using pattern repetition constraints. Figure 5.17 shows pattern repetitions along the vertical direction in existing buildings. This type of pattern repetition constraint is included for both DTO and SRBTO in this numerical example. The number of pattern repetitions along the vertical direction (denoted by *m*) is varied from 1 to 12 to investigate the impact of these constraints on the optimal topologies. The optimal topologies by DTO and SRBTO (with $P_{sys}^t = 0.05$) are shown in Figure 5.18a and Figure 5.18b, respectively. Figure 5.18 demonstrates significant impacts of the pattern repetition constraints on optimal topologies and topologies that are similar to those in existing buildings (e.g., Figure 5.17a and

Figure 5.17c). The effect of the correlation coefficients is also investigated by increasing the correlation coefficients (Case III). Figure 5.19 shows the optimal volume fractions versus the number of pattern repetitions, *m* by DTO, SRBTO (ρ_{same}=0.50, ρ_{diff}=0.25), and SRBTO (ρ_{same}=0.90, ρ_{diff}=0.45). A larger number of patterns result in more constrained optimization problem, and thus provide higher volume fractions. Impacts of the correlation between uncertain loads are also observed.

It is noted that the topology optimization framework in this example is based on continuum structures. After obtaining optimal continuum topologies, for example as shown in Figure 5.18, engineers may need to transform the results from continuum to discrete structures. For instance, discrete components such as beam and column elements can be used to interpret the structural components.

(a) (b) (c)

Figure 5.17: Pattern repetitions in existing building designs: (a) Jardine house – Hong Kong; (b) Taipei 101 tower – Taipei; and (c) Takshing house – Hong Kong (taken from http://dangpotter.wordpress.com, http://www.taiwan-taipei.com, and http://www.som.com).

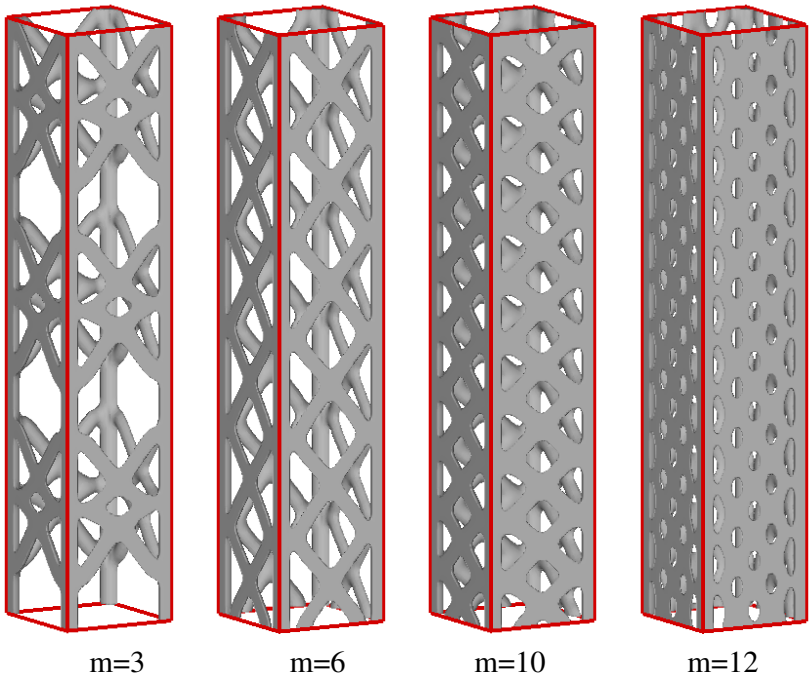

(a)

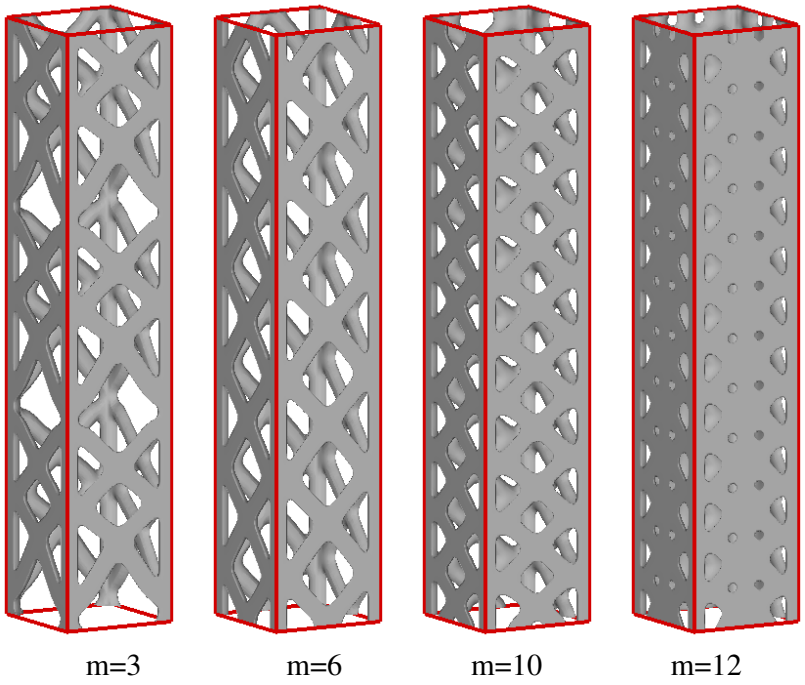

(b)

Figure 5.18: Building core optimal topologies with pattern repetition: (a) DTO; and (b) SRBTO (ρ_{same}=0.50, ρ_{diff}=0.25, $P_{sys}^{t} = 0.05$).

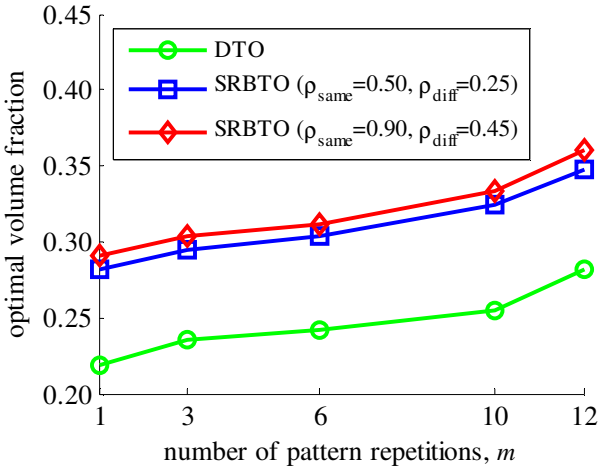

Figure 5.19: Optimal volume fraction with the number of pattern repetitions ($P_{sys}^{t} = 0.05$).

5.6 CONCLUDING REMARKS

This chapter presents three research developments for enhancing the theories and applications of component and system reliability-based topology optimization (CRBTO and SRBTO): (1) developing a single-loop SRBTO approach that employs the matrix-based system reliability (MSR) method to handle the statistical dependence between multiple limit-states; (2) developing SORM-based single-loop approaches for CRBTO and SRBTO to improve the accuracy in evaluating probabilistic constraints; and (3) incorporating multiresolution topology optimization (MTOP) approach to CRBTO and SRBTO in order to obtain high-resolution design with a relatively low computation cost with a capability of imposing pattern repetition and symmetric constraints. Three numerical examples of two- and three-dimensional structures demonstrate that (1) uncertainties in TO problems can make significant impact on optimal topologies; (2) if SRBTO problem (i.e. TO with probabilistic constraint given on a system event, not on individual limit-states) is solved by CRBTO approaches, it is hard to determine corresponding component target failure probabilities and the problem becomes more constrained in general; (3) statistical dependence between limit-states can be successfully incorporated by use of the MSR method, which may cause a significant difference in optimal topologies; (4) SORM-based RBTO approaches provide optimal designs with improved accuracy in satisfying

component and system probabilistic constraints; and (5) MTOP approach enables us to perform CRBTOs and SRBTOs of large-scale TO problems with low computational cost and is capable of imposing pattern symmetry and repetitions in large-scale RBTO problems.

CHAPTER 6 – CONCLUSIONS AND FUTURE WORK

This thesis describes the design and topology optimization problems under uncertainties. First, a multiresolution topology optimization approach is developed to overcome the issue of computational cost. Second, the single-loop system reliability-based design and topology optimization using matrix-based system reliability method is proposed and verified through numerical examples. This chapter summarizes the thesis, its contributions and provides suggestions for future work.

6.1 SUMMARY AND CONCLUDING REMARKS

The basics of topology optimization and reliability-based design optimization are described in the first chapter. The topology optimization approach is introduced in comparison with the classical size and shape optimization approaches. The well-known Solid Isotropic Material with Penalization (SIMP) model is briefly reviewed. Additionally, the reliability-based design optimization problem is introduced.

Chapter 2 presents the formulations of the topology optimization for minimum compliance. The formulations of the integration of the stiffness matrix are discussed. Next, the multiresolution topology optimization approach is proposed by using different discretizations. The MTOP elements are introduced for both 2D (Q4/n25) and 3D (B8/n125) problems, and several other element types such as hexagonal and tetrahedral using MTOP are also discussed. Chapter 3 further develops the MTOP approach in Chapter 2 by reducing the number of design variables in the MTOP approach in Chapter 2. The adaptive multiresolution topology optimization is introduced in this chapter. Also, a ratio to measure the resolution and efficiency of a model is proposed. The approaches proposed in Chapters 2 and 3 are demonstrated by

numerous numerical examples to show the features of the approaches over the conventional element-based approach.

In Chapter 4, the reliability-based design optimization approaches in the literature are reviewed. The formulations of the reliability index approach (RIA) and the performance measure approach (MPA) are compared. Also, the double-loop and single-loop approaches are discussed. Next, the component and system reliability-based design optimization problems (CRBDO/SRBDO) are described. The matrix-based system reliability (MSR) method is briefly reviewed and further developed for integration with the single-loop approach. Finally, the SRBDO/MSR procedure is proposed and demonstrated with numerical examples and verified by Monte Carlo simulation.

The RBDO approach is applied to topology optimization problem, so-called reliability-based topology optimization (RBTO) in Chapter 5. The single-loop approach is derived using the first-order reliability method (FORM) which is not accurate when the limit-state functions are highly nonlinear. Hence, the SORM-based RBTO formulations are proposed in this chapter to improve the accuracy. The RBTO frame work is integrated with the MTOP approach above to enhance the efficiency. Numerical examples are presented to demonstrate the SORM-based RBTO over the FORM-based approach.

The major contributions of this study are summarized as follows:

- A multiresolution topology optimization (MTOP) approach is proposed based on the discretizations of the density, design variable and displacement fields with distinct resolutions. The MTOP approach is first developed using the same mesh for design variables and density. MTOP elements including Q4/n25, B8/n125 are introduced in comparison to the conventional Q4/U, B8/U elements. The MTOP approach enables us to obtain high-resolution topology design with a relatively low computational cost. The MTOP approach is demonstrated by numerous two- and three-dimensional topology optimization problems. The MTOP approach developed in this study has been successfully applied in designing the optimal shape of bone replacement

structures to improve the current practice of the craniofacial reconstruction (Sutradhar et al., 2010).

- The MTOP approach is further developed by employing *fully distinct* meshes for density, design variable and displacement. In comparison to the first development of MTOP approach which uses the same mesh for design variables and density, the second development of MTOP approach employs different resolutions for design variable and density fields. Specifically, a relatively fine mesh for element density, a moderately fine mesh for design variables, and a relatively coarse mesh for finite elements are employed. This improvement further reduces the number of design variables in comparison to the original MTOP approach. New iMTOP elements including Q4/n25/d4, B8/n125/d27 are introduced.
- An adaptive multiresolution topology optimization scheme is proposed in which the MTOP or iMTOP elements are used only when and where needed. This scheme allows us to further reduce the number of density elements and the number of design variables.
- "iMTOP ratio" is introduced as a measurement of the resolution and efficiency model. It is based on the ratio of the number of finite elements, the number of density elements, and number of design variables.
- A single-loop system reliability-based design optimization approach using matrix-based system reliability method is introduced. The SRBDO/MSR approach is applicable to general system events including link-set, cut-set systems under dependence between component events.
- The reliability-based topology optimization (RBTO) problems are investigated in both component and system constraint levels. Its efficiency is enhanced by employing the proposed MTOP approach and the single-loop approach.
- To improve the accuracy of the RBTO problem for component and system levels, the second-order reliability method (SORM) is employed to enhance the accuracy of the

probability computation. The SORM-based CRBTO and SRBTO provide more accurate results than the FORM-based approaches.

- MTOP approach is further developed to include the pattern symmetry and repetition constraint to apply for practical design. These constraints are often employed in the concept design of structures such as buildings, bridges.
- The proposed approaches are demonstrated by numerical examples for the structural system of a building core in both DTO and RBTO.
- The accuracy of the developed RBDO and RBTO algorithms are confirmed by Monte Carlo simulations of the failure probabilities of the optimal designs and topologies.

6.2 SUGGESTIONS FOR FUTURE WORK

Based on the outcomes from this study, the following research topics are recommended for future work.

- This study has shown the advantages of the MTOP approach in obtaining high-resolution design over conventional topology optimization approaches. One key factor in the MTOP approach is the use of a projection scheme to compute the density from the design variables. The use of the projection scheme provides not only the minimum length scale control but also the smooth transition of the density in the domain. However, the current projection scheme results in grey areas between the solid and the void which is sometimes not preferable. Topics for further investigation include the development of a new projection scheme or smoothening effect to obtain more black and white designs. An example of high fidelity design is the use of the Heaviside function (Guest et al., 2004; Guest and Genut, 2009) or morphology-based black and white filter (Sigmund, 2007).
- The MTOP approach employs a number of density elements and design variables per finite element. For example, the element B8/n125/d27 implies 125 density elements and 27 design variables per B8 element. This study has shown the features of the

MTOP element over conventional topology optimization element such as B8/U which has one density per B8 element. However, in this study, the number of density elements and design variables per finite element are chosen heuristically. The study can further explore the optimal number and locations of the density elements and design variables. The optimal number and location of the density elements and design variables can lead to better performance of the multiresolution approach such as higher resolution design or less computational cost. Additionally, the adaptive multiresolution scheme introduced in this study is focusing on a heuristic selective adjustment of the design space. Further study should use multiresolution approach in conjunction with other adaptive schemes (Maute and Ramm, 1995; Ainsworth and Oden; Costa Jr and Alves, 2003; Stainko, 2006; de Sturler et al., 2008).

- The multiresolution approach in this study has been applied to the minimum compliance and compliant mechanism problems. Topics for further investigation include the applications of the multiresolution topology optimization to other fields such as multiphysics and multi-scale problems (Carbonari et al., 2009), material design (Paulino et al., 2009), multifunctional material systems (Rubio et al., 2009), and energy harvesting devices (Silva and Paulino, 2008). Moreover, the current study is limited to linear elastic static problems, the future work should investigate the performance of the multiresolution approach in nonlinear (Jung and Cho, 2004) or dynamic problems (Rubio et al., 2009).
- The multiresolution approach can be combined with fast iterative solvers to handle very large-scale problems. For example, Wang et al. (2007) introduced Krylov subspace methods with recycling to solve relatively large-scale topology optimization problems using conventional elements. The future work can consider the MTOP approach using Krylov subspace methods with recycling technique.
- The system reliability-based design optimization (SRBDO) in the current study uses the matrix-based system reliability (MSR) method for computation of the system probability and its sensitivities. When the number of component events increases, the

number of basic MECE events increase exponentially, therefore, the sizes of the event vector $\mathbf{c}$ and "probability" vector $\mathbf{p}$ increase exponentially as and may exceed the computer memory capacity. Therefore, in such cases, it may need to employ other system reliability methods which are able to handle large-scale general system event and the dependence between component events. For example, the sequential compounding approach (Kang and Song, 2010) can be considered. Further study may tailor the MSR method to SRBDO such as multi-scale approach (Song and Ok, 2010) to overcome the limitation of the size vectors.

- Challenging SRBDO problems such as those with mixed continuous-discrete random variables and time variant reliability (Gunawan and Papalambros, 2007; McDonald and Mahadevan, 2008) need to be addressed as well.
- A comprehensive study on impacts of the structural redundancy on the reliability is needed by use of design/topology optimization algorithms. For example, when a structural system may consist of a number of redundant members, the ultimate capacity of structure is highly dependent on the degree of the structural redundancy (Tsompanakis et al., 2008). One might need to explore the possibility of including the system reliability in the objective function during the investigation.
- The current study considers the displacement, compliance or volume fraction as design constraints. These are domain-wide quantities or a quantity at a pre-determined location. Problems with local constraints such as stress-based optimization in the context of reliability-based optimization should be addressed.

REFERENCES

Ainsworth, M., Oden, J. T., (2000). A posteriori error estimation in finite element analysis. New York, Wiley and Sons.

Allen, M., Raulli, M., Maute, K., Frangopol, D. M., (2004). "Reliability-based analysis and design optimization of electrostatically actuated MEMS." *Computers and Structures* **82**(13-14): 1007-1020.

Almeida, S. R. M., Paulino, G. H., Silva, E. C. N., (2009). "A simple and effective inverse projection scheme for void distribution control in topology optimization." *Structural and Multidisciplinary Optimization* **39**(4): 359-371.

Almeida, S. R. M., Paulino, G. H., Silva, E. C. N., (2010). "Material gradation and layout in topology optimization of functionally graded structures: a global-local approach." *Structural and Multidisciplinary Optimization*.

Amir, O., Bendsoe, M. P., Sigmund, O., (2009). "Approximate reanalysis in topology optimization." *International Journal for Numerical Methods in Engineering* **78**(12): 1474-1491.

Amir, O., Stolpe, M., Sigmund, O., (2010). "Efficient use of iterative solvers in nested topology optimization." *Structural and Multidisciplinary Optimization* **42**(1): 55-72.

Aoues, Y., Chateauneuf, A., (2008). "Reliability-based optimization of structural systems by adaptive target safety-application to rc frames." *Structural Safety* **30**(2): 144-161.

Ba-Abbad, M. A., Nikolaidis, E., Kapania, R. K., (2006). "New approach for system reliability-based design optimization." *AIAA journal* **44**(5): 1087-1096.

Bae, K., Wang, S., Choi, K. K., (2002). "Reliability-based topology optimization." In: AIAA 2002-5542, 9th AIAA/ISSMO Symposium on Multidisciplinary Analysis and Optimization, 4–6 September 2002, Atlanta.

Bendsøe, M. P., (1989). "Optimal shape design as a material distribution problem." *Structural and Multidisciplinary Optimization* **1**(4): 193-202.

Bendsøe, M. P., Kikuchi, N., (1988). "Generating optimal topologies in structural design using a homogenization method." *Computer Methods in Applied Mechanics and Engineering* **71**(2): 197-224.

Bendsøe, M. P., Sigmund, O., (1999). "Material interpolation schemes in topology optimization." *Archive of Applied Mechanics* **69**(9): 635-654.

Bendsøe, M. P., Sigmund, O., (2003). Topology optimization: theory, methods, and applications, Springer Verlag.

Bjerager, P., Krenk, S., (1989). "Parametric sensitivity in first order reliability theory." *Journal of Engineering Mechanics* **115**(7): 1577-1582.

Borrvall, T., Petersson, J., (2001). "Large-scale topology optimization in 3D using parallel computing." *Computer Methods in Applied Mechanics and Engineering* **190**(46-47): 6201-6229.

Carbonari, R. C., Silva, E. C. N., Paulino, G. H., (2009). "Multi-actuated functionally graded piezoelectric micro-tools design: a multiphysics topology optimization approach." *International Journal for Numerical Methods in Engineering* **77**(3): 301-336.

Chan, K. Y., Skerlos, S. J., Papalambros, P., (2007). "An adaptive sequential linear programming algorithm for optimal design problems with probabilistic constraints." *Journal of Mechanical Design* **129**: 140.

Chen, S., Chen, W., Lee, S., (2010). "Level set based robust shape and topology optimization under random field uncertainties." *Structural and Multidisciplinary Optimization* **41**(4): 507-524.

Cook, R. D., Malkus, D. S., Plesha, M. E., Witt, R. J., (2002). Concepts and applications of finite element analysis, John Wiley & Sons: New York.

Costa Jr, J. C. A., Alves, M. K., (2003). "Layout optimization with h-adaptivity of structures." *International Journal for Numerical Methods in Engineering* **58**(1): 83-102.

de Ruiter, M. J., van Keulen, F., (2004). "Topology optimization using a topology description function." *Structural and Multidisciplinary Optimization* **26**(6): 406-416.

de Sturler, E., Paulino, G. H., Wang, S. (2008). "Topology optimization with adaptive mesh refinement." Proceedings of the 6th International Conference on Computation of Shell and Spatial Structures IASS-IACM 2008:‘Spanning Nano to Mega'.

Der Kiureghian, A. (2005). First-and second-order reliability methods. Engineering Design Reliability Handbook. CH 14. Florida, CRC, Boca Raton.

Diaz, A., Sigmund, O., (1995). "Checkerboard patterns in layout optimization." *Structural and Multidisciplinary Optimization* **10**(1): 40-45.

Ditlevsen, O., (1979). "Narrow reliability bounds for structural systems." *Mechanics Based Design of Structures and Machines* **7**(4): 453-472.

Du, X., Sudjianto, A., Chen, W., (2004). "An integrated framework for optimization under uncertainty using inverse reliability strategy." *Journal of Mechanical Design* **126**: 562.

Du, X. P., Chen, W., (2000). "Towards a better understanding of modeling feasibility robustness in engineering design." *Journal of Mechanical Design* **122**(4): 385-394.

Du, X. P., Chen, W., (2004). "Sequential optimization and reliability assessment method for efficient probabilistic design." *Journal of Mechanical Design* **126**(2): 225-233.

Dunnett, C. W., Sobel, M., (1955). "Approximations to the probability integral and certain percentage points of a multivariate analogue of student's t-distribution." *Biometrika* **42**(1-2): 258-260.

Enevoldsen, I., Sørensen, J. D., (1994). "Reliability-based optimization in structural engineering." *Structural Safety* **15**(3): 169-196.

Eschenauer, H. A., Olhoff, N., (2001). "Topology optimization of continuum structures: a review." *Applied Mechanics Reviews* **54**(4): 331-389.

Evgrafov, A., Rupp, C. J., Maute, K., Dunn, M. L., (2008). "Large-scale parallel topology optimization using a dual-primal substructuring solver." *Structural and Multidisciplinary Optimization* **36**(4): 329-345.

Frangopol, D. M., Maute, K. (2005). Reliability-based optimization of civil and aerospace structural systems. Engineering Design Reliability Handbook. CH 24. Florida, CRC, Boca Raton.

Guest, J. K., Genut, L. C. S., (2009). "Reducing dimensionality in topology optimization using adaptive design variable fields." *International Journal for Numerical Methods in Engineering* **81**(8): 1019 - 1045.

Guest, J. K., Igusa, T., (2008). "Structural optimization under uncertain loads and nodal locations." *Computer Methods in Applied Mechanics and Engineering* **198**(1): 116-124.

Guest, J. K., Prévost, J. H., Belytschko, T., (2004). "Achieving minimum length scale in topology optimization using nodal design variables and projection functions." *International Journal for Numerical Methods in Engineering* **61**(2): 238-254.

Gunawan, S., Papalambros, P. Y., (2007). "Reliability optimization with mixed continuous-discrete random variables and parameters." *Journal of Mechanical Design* **129**: 158.

Jung, H. S., Cho, S., (2004). "Reliability-based topology optimization of geometrically nonlinear structures with loading and material uncertainties." *Finite Elements in Analysis & Design* **41**(3): 311-331.

Kang, J., Kim, C., Wang, S., (2004). "Reliability-based topology optimization for electromagnetic systems." *Compel-the International Journal for Computation and Mathematics in Electrical and Electronic Engineering* **23**(3): 715-723.

Kang, W. H., Lee, Y. J., Song, J., (2010). "Further development of matrix-based system reliability method and applications to structural systems." *Structural and Infrastructure Engineering: Maintenance, Management, Life-cycle Design and Performance*.

Kang, W. H., Song, J. (2008). "Evaluation of multinormal integral and sensitivity by matrix-based system reliability method." Proceedings of the 10th AIAA Nondeterministic Approaches Conference, 7–10 April, Schaumburg, Illinois.

Kang, W. H., Song, J., (2010). "Evaluation of multivariate normal integrals for general systems by sequential compounding." *Structural Safety* **32**(1): 35-41.

Kang, W. H., Song, J., Gardoni, P., (2008). "Matrix-based system reliability method and applications to bridge networks." *Reliability Engineering and System Safety* **93**: 1584-1593.

Kharmanda, G., Olhoff, N., Mohamed, A., Lemaire, M., (2004). "Reliability-based topology optimization." *Structural and Multidisciplinary Optimization* **26**(5): 295-307.

Kim, C., Wang, S., Rae, K., Moon, H., Choi, K. K., (2006). "Reliability-based topology optimization with uncertainties." *Journal of Mechanical Science and Technology* **20**(4): 494-504.

Kim, J. E., Jang, G. W., Kim, Y. Y., (2003). "Adaptive multiscale wavelet-Galerkin analysis for plane elasticity problems and its applications to multiscale topology design optimization." *International Journal of Solids and Structures* **40**(23): 6473-6496.

Kim, Y. Y., Yoon, G. H., (2000). "Multi-resolution multi-scale topology optimization – a new paradigm." *International Journal of Solids and Structures* **37**(39): 5529-5559.

Krog, L., Tucker, A., Kemp, M., Boyd, R. (2004). "Topology optimization of aircraft wing box ribs." Proceedings of the 10th AIAA/ISSMO Multidisciplinary Analysis and Optimization Conference, 30 August – 1 September, Albany, New York.

Kuschel, N., Rackwitz, R., (2000). "Optimal design under time-variant reliability constraints." *Structural Safety* **22**(2): 113-127.

Lee, I., Choi, K. K., Gorsich, D., (2010a). "System reliability-based design optimization using the MPP-based dimension reduction method." *Structural and Multidisciplinary Optimization* **41**(6): 823-839.

Lee, Y. J., Song, J., Gardoni, P., Lim, H. W., (2010b). "Post-hazard flow capacity of bridge transportation network considering structural deterioration of bridges." *Structural and Infrastructure Engineering: Maintenance, Management, Life-cycle Design and Performance*.

Liang, J., Mourelatos, Z. P., Nikolaidis, E., (2007). "A single-loop approach for system reliability-based design optimization." *Journal of Mechanical Design* **129**(12): 1215-1224.

Liang, J., Mourelatos, Z. P., Tu, J., (2008). "A single-loop method for reliability-based design optimisation." *International Journal of Product Development* **5**(1): 76-92.

Lin, C. Y., Chou, J. N., (1999). "A two-stage approach for structural topology optimization." *Advances in Engineering Software* **30**(4): 261-271.

Lógó, J., Ghaemi, M., Rad, M. M., (2009). "Optimal topologies in case of probabilistic loading: the influence of load correlation." *Mechanics Based Design of Structures and Machines* **37**(3): 327-348.

Luo, Y., Kang, Z., Luo, Z., Li, A., (2009). "Continuum topology optimization with non-probabilistic reliability constraints based on multi-ellipsoid convex model." *Structural and Multidisciplinary Optimization* **39**(3): 297-310.

Matsui, K., Terada, K., (2004). "Continuous approximation of material distribution for topology optimization." *International Journal for Numerical Methods in Engineering* **59**(14): 1925-1944.

Maute, K., Frangopol, D. M., (2003). "Reliability-based design of MEMS mechanisms by topology optimization." *Computers and Structures* **81**(8-11): 813-824.

Maute, K., Ramm, E., (1995). "Adaptive topology optimization." *Structural and Multidisciplinary Optimization* **10**(2): 100-112.

McAllister, C. D., Simpson, T. W., (2003). "Multidisciplinary robust design optimization of an internal combustion engine." *Journal of Mechanical Design(1990)* **125**(1): 124-130.

McDonald, M., Mahadevan, S., (2008). "Design optimization with system-level reliability constraints." *Journal of Mechanical Design* **130**(2): 021403.

McDonald, M., Mahadevan, S., (2008). "Reliability-based optimization with discrete and continuous decision and random variables." *Journal of Mechanical Design* **130**: 061401.

Mlejnek, H. P., Schirrmacher, R., (1993). "An engineer's approach to optimal material distribution and shape finding." *Computer Methods in Applied Mechanics and Engineering* **106**(1-2): 1-26.

Mogami, K., Nishiwaki, S., Izui, K., Yoshimura, M., Kogiso, N., (2006). "Reliability-based structural optimization of frame structures for multiple failure criteria using topology optimization techniques." *Structural and Multidisciplinary Optimization* **32**(4): 299-311.

Nguyen, T. H., Paulino, G. H., Song, J., Le, C. H., (2010b). "A computational paradigm for multiresolution topology optimization (MTOP)." *Structural and Multidisciplinary Optimization* **41**(4): 525-539.

Nguyen, T. H., Paulino, G. H., Song, J., Le, C. H., (2010d). "Improving multiresolution topology optimization via multiple discretizations." *International Journal for Numerical Methods in Engineering* (submitted).

Nguyen, T. H., Song, J., Paulino, G. H. (2006). "Probabilistic fracture analysis of functional graded materials: implementation and numerical examples." Multiscale and Functionally

Graded Materials Conference (MFGM2006), AIP Conference Proceedings, American Institute of Physics **973**: 159-164.

Nguyen, T. H., Song, J., Paulino, G. H. (2009). "Single-loop system reliability-based design optimization (SRBDO) using matrix-based system reliability (MSR) method." Proceeding of the 10th International Conference on Structural Safety and Reliability (ICOSSAR10), Osaka, Japan, 1534-1541.

Nguyen, T. H., Song, J., Paulino, G. H., (2010a). "Single-loop system reliability-based design optimization using matrix-based system reliability method: theory and applications." *Journal of Mechanical Design* **132**(1): 011005-1~11.

Nguyen, T. H., Song, J., Paulino, G. H. (2010c). "Challenges and advances in system reliability based optimization of structural topology." Proceedings of the 19th Analysis and Computation Specialty Conference, ASCE, Orlando, Florida, 480-491.

Nguyen, T. H., Song, J., Paulino, G. H., (2010e). "Single-loop system reliability-based topology optimization considering statistical dependence between limit states." *Structural and Multidisciplinary Optimization* (submitted).

Nguyen, T. H., Song, J., Paulino, G. H. (2010f). "Enhancing single-loop approach for component and system reliability-based topology optimization." Proceedings of the 13th AIAA/ISSMO Multidisciplinary Analysis and Optimization Conference, 13–15 September, Fort Worth, Texas.

Pandey, M. D., (1998). "An effective approximation to evaluate multinormal integrals." *Structural Safety* **20**(1): 51-67.

Paulino, G. H., Le, C. H., (2009). "A modified Q4/Q4 element for topology optimization." *Structural and Multidisciplinary Optimization* **37**(3): 255-264.

Paulino, G. H., Pereira, A., Talischi, C., Menezes, I. F. M., Celes, W. (2008). "Embedding of superelements for three-dimensional topology optimization." Proceedings of Iberian Latin American Congress on Computational Methods in Engineering (CILAMCE).

Paulino, G. H., Silva, E. C. N., Le, C. H., (2009). "Optimal design of periodic functionally graded composites with prescribed properties." *Structural and Multidisciplinary Optimization* **38**(5): 469-489.

Pomezanski, V., Querin, O. M., Rozvany, G. I. N., (2005). "CO-SIMP: extended SIMP algorithm with direct corner contact control." *Structural and Multidisciplinary Optimization* **30**(2): 164-168.

Poulsen, T. A., (2002a). "Topology optimization in wavelet space." *International Journal for Numerical Methods in Engineering* **53**(3): 567-582.

Poulsen, T. A., (2002b). "A simple scheme to prevent checkerboard patterns and one-node connected hinges in topology optimization." *Structural and Multidisciplinary Optimization* **24**(5): 396-399.

Rahman, S., Wei, D., (2008). "Design sensitivity and reliability-based structural optimization by univariate decomposition." *Structural and Multidisciplinary Optimization* **35**(3): 245-261.

Rahmatalla, S. F., Swan, C. C., (2004). "A Q4/Q4 continuum structural topology optimization implementation." *Structural and Multidisciplinary Optimization* **27**(1): 130-135.

Royset, J. O., Der Kiureghian, A., Polak, E., (2001). "Reliability-based optimal design of series structural systems." *Journal of Engineering Mechanics* **127**(6): 607-614.

Royset, J. O., Der Kiureghian, A., Polak, E., (2001). "Reliability-based optimal structural design by the decoupling approach." *Reliability Engineering and System Safety* **73**(3): 213-221.

Royset, J. O., Der Kiureghian, A., Polak, E., (2006). "Optimal design with probabilistic objective and constraints." *Journal of Engineering Mechanics* **132**(1): 107-118.

Rozvany, G. I. N., (1996). "Some shortcomings in Michell's truss theory." *Structural and Multidisciplinary Optimization* **12**(4): 244-250.

Rozvany, G. I. N., (2001). "Aims, scope, methods, history and unified terminology of computer-aided topology optimization in structural mechanics." *Structural and Multidisciplinary Optimization* **21**(2): 90-108.

Rozvany, G. I. N. (2008). "Exact analytical solutions for benchmark problems in probabilistic topology optimization." EngOpt 2008—International Conference on Engineering Optimization, Rio de Janeiro

Rozvany, G. I. N., (2009). "A critical review of established methods of structural topology optimization." *Structural and Multidisciplinary Optimization* **37**(3): 217-237.

Rozvany, G. I. N., Zhou, M., Birker, T., (1992). "Generalized shape optimization without homogenization." *Structural and Multidisciplinary Optimization* **4**(3): 250-252.

Rubio, W. M., Silva, E. C. N., Paulino, G. H., (2009). "Toward optimal design of piezoelectric transducers based on multifunctional and smoothly graded hybrid material systems." *Journal of Intelligent Material Systems and Structures* **20**(14): 1725-1746.

Shan, S., Wang, G. G., (2008). "Reliable design space and complete single-loop reliability-based design optimization." *Reliability Engineering and System Safety* **93**(8): 1218-1230.

Sigmund, O., (2000). "Topology optimization: a tool for the tailoring of structures and materials." *Philosophical Transactions: Mathematical, Physical and Engineering Sciences* **358**(1765): 211-227.

Sigmund, O., (2001). "A 99 line topology optimization code written in Matlab." *Structural and Multidisciplinary Optimization* **21**(2): 120-127.

Sigmund, O., (2007). "Morphology-based black and white filters for topology optimization." *Structural and Multidisciplinary Optimization* **33**(4): 401-424.

Sigmund, O., Petersson, J., (1998). "Numerical instabilities in topology optimization: a survey on procedures dealing with checkerboards, mesh-dependencies and local minima." *Structural and Multidisciplinary Optimization* **16**(1): 68-75.

Silva, E. C. N., Paulino, G. H. (2008). "Toward topology optimization of energy harvesting devices using hybrid materials." Proceedings of the Brazil AFOSR Workshop – Advanced Structural Mechanics and Computational Mathematics. Campinas.

Silva, M., Tortorelli, D. A., Norato, J. A., Ha, C., Bae, H. R., (2010). "Component and system reliability-based topology optimization using a single-loop method." *Structural and Multidisciplinary Optimization* **41**(1): 87-106.

Song, J., Der Kiureghian, A., (2003). "Bounds on system reliability by linear programming." *Journal of Engineering Mechanics* **129**(6): 627-636.

Song, J., Der Kiureghian, A. (2005). "Component importance measures by linear programming bounds on system reliability." Proceedings of the 9th International Conference on Structural Safety and Reliability (ICOSSAR9), Rome, Italy.

Song, J., Kang, W.-H. (2008). "Estimation of structural robustness against progressive collapse based on system reliability." Proceeding of the Inaugural International Conference of the Engineering Mechanics Institute, 18-21May, Minneapolis, Minnesota.

Song, J., Kang, W. H., (2009). "System reliability and sensitivity under statistical dependence by matrix-based system reliability method." *Structural Safety* **31**(2): 148-156.

Song, J., Nguyen, T. H., Paulino, G. H. (2006). "Probabilistic fracture analysis of functional graded materials: uncertainties and probabilistic analysis method." Multiscale and Functionally Graded Materials Conference (MFGM2006), AIP Conference Proceedings, American Institute of Physics **973**: 153-158.

Song, J., Ok, S. Y., (2010). "Multi-scale system reliability analysis of lifeline networks under earthquake hazards." *Earthquake Engineering & Structural Dynamics* **39**(3): 259-279.

Stainko, R., (2006). "An adaptive multilevel approach to the minimal compliance problem in topology optimization." *Communications in Numerical Methods in Engineering* **22**(2): 109-118.

Streicher, H., Rackwitz, R., (2004). "Time-variant reliability-oriented structural optimization and a renewal model for life-cycle costing." *Probabilistic Engineering Mechanics* **19**(1-2): 171-183.

Sutradhar, A., Paulino, G. H., Miller, M. J., Nguyen, T. H., (2010). "Topological optimization for designing patient-specific large craniofacial segmental bone replacements." *Proceedings of the National Academy of Sciences* **107**(30): 13222-13227.

Suzuki, K., Kikuchi, N., (1991). "A homogenization method for shape and topology optimization." *Computer Methods in Applied Mechanics and Engineering* **93**(3): 291-318.

Svanberg, K., (1987). "The method of moving asymptotes- a new method for structural optimization." *International Journal for Numerical Methods in Engineering* **24**(2): 359-373.

Talischi, C., Paulino, G. H., Le, C. H., (2009). "Honeycomb Wachspress finite elements for structural topology optimization." *Structural and Multidisciplinary Optimization* **37**(6): 569-583.

Talischi, C., Paulino, G. H., Pereira, A., Menezes, I. F. M., Celes, W., (2010). "Polygonal finite elements for topology optimization: a unifying paradigm." *International Journal for Numerical Methods in Engineering* **82**(6): 671-698.

Thanedar, P. B., Kodiyalam, S., (1992). "Structural optimization using probabilistic constraints." *Structural and Multidisciplinary Optimization* **4**(3): 236-240.

Tsompanakis, Y., Lagaros, N. D., Papadrakakis, M., (2008). Structural design optimization considering uncertainties, Taylor & Francis.

Tu, J., Choi, K. K., Park, Y. H., (1999). "A new study on reliability-based design optimization." *Journal of Mechanical Design* **121**(4): 557-564.

Valdebenito, M. A., Schuëller, G. I., (2010). "A survey on approaches for reliability-based optimization." *Structural and Multidisciplinary Optimization*.

Wang, S., de Sturler, E., Paulino, G. H., (2007). "Large-scale topology optimization using preconditioned Krylov subspace methods with recycling." *International Journal for Numerical Methods in Engineering* **69**(12): 2441-2468.

Wu, Y. T., Wang, W., (1998). "Efficient probabilistic design by converting reliability constraints to approximately equivalent deterministic constraints." *Journal of Integrated Design and Process Sciences* **2**(4): 13-21.

Xu, H., Rahman, S., (2005). "Decomposition methods for structural reliability analysis." *Probabilistic Engineering Mechanics* **20**(3): 239-250.

Yang, R. J., Chuang, C., Gu, L., Li, G., (2005). "Experience with approximate reliability-based optimization methods II: an exhaust system problem." *Structural and Multidisciplinary Optimization* **29**(6): 488-497.

Youn, B. D., Choi, K. K., Du, L., (2005). "Enriched performance measure approach for reliability-based design optimization." *AIAA journal* **43**(4): 874-884.

Youn, B. D., Choi, K. K., Park, Y. H., (2003). "Hybrid analysis method for reliability-based design optimization." *Journal of Mechanical Design* **125**(2): 221-232.

Zhou, M., Rozvany, G. I. N., (1991). "The COC algorithm, Part II: Topological, geometrical and generalized shape optimization." *Computer Methods in Applied Mechanics and Engineering* **89**(1-3): 309-336.

APPENDIX A - METHOD OF MOVING ASYMPTOTES

Topology optimization employs a large number of design variables, therefore, large-scale first order-optimizer is expected. The Method of Moving Asymptotes (MMA) is a mathematical programming algorithm well suited for the structural topology optimization (Svanberg, 1987; Bendsøe and Sigmund, 2003). Because of the merits, the MMA approach is employed as the optimizer throughout this thesis.

The MMA algorithm is especially useful for solving smooth, nonlinear optimization problems via a sequence of simpler approximate sub-problems of given type. These sub-problems are constructed based on the sensitivity information of the current and several previous iterations. Additionally, these sub-problems are separable and convex (Svanberg, 1987; Bendsøe and Sigmund, 2003). In the MMA approach, a function F of n real variables $x = (x_1, \ldots, x_n)$ is approximated around a given iteration point $\mathbf{x}^0$ as follows

$$F(\mathbf{x}) \approx F(\mathbf{x}^0) + \sum_{i=1}^{n} \left(\frac{r_i}{U_i - x_i} + \frac{s_i}{x_i - L_i} \right) \tag{A.1}$$

where the numbers r_i, s_i are chosen as

$$\text{if } \frac{\partial F}{\partial x_i}(x^0) > 0 \text{ then } r_i = \left(U_i - x_i^0\right)^2 \frac{\partial F}{\partial x_i}(x^0) \text{ and } s_i = 0 \tag{A.2}$$

$$\text{if } \frac{\partial F}{\partial x_i}(x^0) < 0 \text{ then } r_i = 0 \text{ and } s_i = -\left(x_i^0 - L_i\right)^2 \frac{\partial F}{\partial x_i}(x^0) \tag{A.3}$$

The parameters U_i , L_i give the vertical asymptotes for the approximations of the function F, thus the algorithm is named as Method of Moving Asymptotes (MMA). The parameters U_i , L_i for each function are updated at each iteration. The details and merits of the algorithm are given in (Svanberg, 1987; Bendsøe and Sigmund, 2003).

APPENDIX B - ILLUSTRATIVE EXAMPLE OF MSR METHOD

Consider three system events, each of which consists of five component events, E_i, $i = 1,...,5$:

$$\begin{aligned} E_{sys} &= E_1 \cup E_2 \cup E_3 \cup E_4 \cup E_5 \quad \text{(series)} \\ E_{sys} &= E_1 \cap E_2 \cap E_3 \cap E_4 \cap E_5 \quad \text{(parallel)} \\ E_{sys} &= (E_1 \cup E_2 \cup E_3) \cap (E_2 \cup E_3 \cup E_4) \cap (E_3 \cup E_4 \cup E_5) \quad \text{(link-set)} \end{aligned} \tag{B.1}$$

In this illustrative example, the probabilities of the system events, $P(E_{sys})$ are computed by the MSR method based on the results of the component reliability analyses by first-order reliability method (FORM). After FORM analysis, each component event is approximately described by

$$E_i : Z_i \le -\beta_i, \quad i = 1,...,5 \tag{B.2}$$

and where Z_i is correlated standard normal random variable; and β_i is the FORM reliability index of E_i, $i = 1,...,5$. The correlation coefficient between Z_i and Z_j, $i \neq j$ are computed by the inner-product of the negative normalized gradient vectors at the corresponding MPPs (Der Kiureghian, 2005). In this example, suppose $\beta_i = 3$, $i = 1,...,5$ and the inner products give the correlation coefficient matrix

$$\mathbf{R} = \begin{bmatrix} 1 & 0.89 & 0.88 & 0.87 & 0.86 \\ 0.89 & 1 & 0.90 & 0.90 & 0.90 \\ 0.88 & 0.99 & 1 & 0.90 & 0.90 \\ 0.87 & 0.90 & 0.90 & 1 & 0.90 \\ 0.86 & 0.90 & 0.90 & 0.90 & 1 \end{bmatrix} \tag{B.3}$$

The MSR method computes the probabilities of the system events in (B.1) by the matrix formulation in (4.16). The numerical integration requires three tasks: (a) describing **R** approximately by use of a generalized DS model and identifying common source random

variables (CSRVs) $\mathbf{S}$, (b) constructing the event vector $\mathbf{c}$, and (c) computing the conditional probability vector $\mathbf{p}(\mathbf{s})$.

First, the correlation coefficients in $\mathbf{R}$ are fitted by those constructed by a generalized DS model, i.e. $\rho_{ij} = \sum_{k=1}^{m} (r_{ik} . r_{jk})$ with the minimum error. When one CSRV is used, the coefficients in the generalized DS model in (4.22) are

$$r_{11} = 0.9223,\ r_{21} = 0.9539,\ r_{31} = 0.9541,\ r_{41} = 0.9432,\ r_{51} = 0.9435. \tag{B.4}$$

When two CSRVs are used for improved accuracy, the coefficients are obtained as

$$\begin{aligned} &r_{11} = 0.9262,\ r_{21} = 0.6989,\ r_{31} = 0.6801,\ r_{41} = 0.6632,\ r_{51} = 0.6427 \\ &r_{12} = 0.3769,\ r_{22} = 0.6436,\ r_{32} = 0.6614,\ r_{42} = 0.6782,\ r_{52} = 0.6998 \end{aligned} \tag{B.5}$$

The joint PDF of CSRVs in (4.16), i.e. $f_{\mathbf{S}}(\mathbf{s})$ is $\varphi(s_1)$ and $\varphi(s_1)\varphi(s_2)$ for one- and two-CSRV cases, respectively, in which $\varphi(\cdot)$ denotes the PDF of the standard normal distribution.

Second, the event vector $\mathbf{c}$ is constructed for each of the system events. The event vectors for the five component events are first constructed by the sequential matrix-based procedures proposed in (Song and Kang, 2008).

$$\mathbf{C}_{[1]} = \begin{bmatrix} 1 \\ 0 \end{bmatrix},\ \mathbf{C}_{[i]} = \begin{bmatrix} \mathbf{C}_{[i-1]} & \mathbf{1} \\ \mathbf{C}_{[i-1]} & \mathbf{0} \end{bmatrix} \text{ for } i = 2,...,5 \tag{B.6}$$

where $\mathbf{0}$ and $\mathbf{1}$ denote the column vectors of 2^{i-1} zeros and ones, respectively. When the iterative procedure is completed, the i-th column of $\mathbf{C}_{[5]}$ is the event vector of the i-th component event E_i, $i = 1,...,5$. As a result, the event vectors of the five components are obtained as

$$\begin{aligned} \mathbf{c}^{E_1} &= [1\ 0\ 1\ 0\ 1\ 0\ 1\ 0\ 1\ 0\ 1\ 0\ 1\ 0\ 1\ 0\ 1\ 0\ 1\ 0\ 1\ 0\ 1\ 0\ 1\ 0\ 1\ 0]^{\mathrm{T}} \\ \mathbf{c}^{E_2} &= [1\ 1\ 0\ 0\ 1\ 1\ 0\ 0\ 1\ 1\ 0\ 0\ 1\ 1\ 0\ 0\ 1\ 1\ 0\ 0\ 1\ 1\ 0\ 0\ 1\ 1\ 0\ 0\ 1\ 1\ 0\ 0]^{\mathrm{T}} \\ \mathbf{c}^{E_3} &= [1\ 1\ 1\ 1\ 0\ 0\ 0\ 0\ 1\ 1\ 1\ 1\ 0\ 0\ 0\ 0\ 1\ 1\ 1\ 1\ 0\ 0\ 0\ 0\ 1\ 1\ 1\ 1\ 0\ 0\ 0\ 0]^{\mathrm{T}} \\ \mathbf{c}^{E_4} &= [1\ 1\ 1\ 1\ 1\ 1\ 1\ 1\ 0\ 0\ 0\ 0\ 0\ 0\ 0\ 0\ 1\ 1\ 1\ 1\ 1\ 1\ 1\ 1\ 0\ 0\ 0\ 0\ 0\ 0\ 0\ 0]^{\mathrm{T}} \\ \mathbf{c}^{E_5} &= [1\ 1\ 1\ 1\ 1\ 1\ 1\ 1\ 1\ 1\ 1\ 1\ 1\ 1\ 1\ 1\ 0\ 0\ 0\ 0\ 0\ 0\ 0\ 0\ 0\ 0\ 0\ 0\ 0\ 0\ 0\ 0]^{\mathrm{T}} \end{aligned} \tag{B.7}$$

Then, the event vector of the system event E_{sys} is obtained by matrix-based procedures employing the event vectors of the components. For example, the event vector for the

complementary event of E, the intersection and the union of the component events are obtained as follows

$$\begin{aligned}
&\mathbf{c}^{\bar{E}} = \mathbf{1} - \mathbf{c}^{E} \\
&\mathbf{c}^{E_1 \cdots E_n} = \mathbf{c}^{E_1} .* \mathbf{c}^{E_2} .* \cdots .* \mathbf{c}^{E_n} \\
&\mathbf{c}^{E_1 \cup \cdots \cup E_n} = \mathbf{1} - (\mathbf{1} - \mathbf{c}^{E_1}) .* (\mathbf{1} - \mathbf{c}^{E_2}) .* \cdots .* (\mathbf{1} - \mathbf{c}^{E_n})
\end{aligned} \tag{B.8}$$

where $.*$ denotes the element-wise multiplication of two vectors.

Finally, the conditional probability vector $\mathbf{p}(\mathbf{s})$ is constructed by the following matrix-based procedure:

$$\begin{aligned}
&\mathbf{p}_{[1]}(\mathbf{s}) = [P_1(\mathbf{s}) \;\; 1 - P_1(\mathbf{s})]^{\mathrm{T}} \\
&\mathbf{p}_{[i]}(\mathbf{s}) = \begin{bmatrix} \mathbf{p}_{[i-1]}(\mathbf{s}) \cdot P_i(\mathbf{s}) \\ \mathbf{p}_{[i-1]}(\mathbf{s}) \cdot [1 - P_i(\mathbf{s})] \end{bmatrix} \;\; \text{for } i = 2, ..., 5
\end{aligned} . \tag{B.9}$$

where $P_i(\mathbf{s})$ is the conditional probability of the i-th component given $\mathbf{S} = \mathbf{s}$, which is computed by (4.22) employing the reliability indexes $\beta_i = 3$ and the generalized DS model coefficients in (B.4) or (B.5). When the sequential matrix-based procedure in (B.9) is completed, $\mathbf{p}_{[5]}(\mathbf{s})$ is used as $\mathbf{p}(\mathbf{s})$ in (4.16).

Table B.1: System probabilities computed by MSR, MCS and bounding formula ($\times 10^{-3}$)

System Events	Bi-component bounds		MSR: No. of CSRVs		MCS (N=10^7 times)	
	Lower bound	Upper bound	1	2	$P(E_{sys})$	c.o.v
Series	2.309	4.338	3.528	3.526	3.532	0.005
Parallel	N/A	N/A	0.2314	0.2318	0.2329	0.021
Link-set	N/A	N/A	1.738	1.739	1.764	0.008

Table B.1 shows the results of the system reliability analysis by the MSR method, MCS and the bi-component bounding formula (Ditlevsen, 1979). Close agreements between the results by MSR method and those by MCS confirm the accuracy of the MSR method for the given example while the bi-component bounds show significant width for the series system.

APPENDIX C - NOMENCLATURE

$\mathbf{d}$	= vector of design variables
C	= compliance
V_s	= prescribed volume
V	= volume
$\boldsymbol{\psi}$	= position of a point in the domain, coordinate vector
volfrac	= volume fraction
$N_i(.)$	= shape function
$\mathbf{D}^0$	= constitutive matrix corresponds to the solid material
$\mathbf{D}$	= constitutive matrix
$\mathbf{B}$	= strain-displacement matrix of shape function derivatives
$\mathbf{K}$	= global stiffness matrix
$\mathbf{K}_e$	= stiffness matrix of displacement element *e*
$\mathbf{K}_e^0$	= stiffness matrix of element *e* corresponding to the solid material
n	= number of density elements per displacement element
E	= Young's modulus
E^0	= Young's modulus corresponding to solid material
ρ_i	= density of element *i*
d_n	= design variable *n*
$r_{\min}$	= minimum length scale
p	= penalization parameter
$f_p(.)$	= projection function
$\mathbf{u}$	= global displacement vector
$\mathbf{f}$	= global load vector
A_i	= area (or volume) of the density element *i* in the initial domain

A_i^0 = area (or volume) of the density element i in the reference domain

$w(.)$ = weight function in the projection scheme

Q4/n25 = MTOP Q4 element with 25 density elements and 25 design variables

Q4/n25/d4 = iMTOP Q4 element with 25 density elements and 4 design variables

B8/n125 = MTOP B8 element with 125 density elements and 125 design variables

B8/n125/d8 = iMTOP B8 element with 125 density elements and 8 design variables

$\mathbf{c}$ = "event" vector

$f(\cdot)$ = objective function

$g_i(\mathbf{d}, \mathbf{X})$ = limit-state (or performance) function of the i-th failure mode

$\mathbf{p}$ = "probability" vector

P_i = actual failure probability of the i-th mode

P_i^t = target failure probability of the i-th mode

P_{sys} = actual system failure probability

P_{sys}^t = target system failure probability

$\mathbf{S}$ = common source random variables

$\mathbf{U}_i^*$ = most probable failure point of the i-th mode

$\mathbf{X}$ = random variables

$\hat{\boldsymbol{\alpha}}_i$ = negative normalized gradient vector

β_i = reliability index

β_i^t = target reliability index

$\boldsymbol{\mu}_{\mathbf{X}}$ = vector of means of $\mathbf{X}$

APPENDIX D - ABBREVIATIONS

CAMD	= continuous approximation of material distribution
CRBDO	= component reliability-based design optimization
CRBTO	= component reliability-based topology optimization
CSRV	= common source random variable
DTO	= deterministic topology optimization
FORM	= first-order reliability method
iMTOP	= improving multiresolution topology optimization
MCS	= Monte Carlo simulation
MECE	= mutually exclusive and collective exhaustive
MMA	= method of moving asymptotes
MSR	= matrix-based system reliability
MTOP	= multiresolution topology optimization
PDF	= probability density function
PMA	= performance measure approach
RBDO	= reliability-based design optimization
RBTO	= reliability-based topology optimization
RIA	= reliability index approach
SIMP	= solid isotropic material with penalization
SORM	= second-order reliability method
SRBDO	= system reliability-based design optimization
SRBDO/MSR	= SRBDO using MSR
SRBTO	= system reliability-based topology optimization
SRBTO/MSR	= SRBTO using MSR